

**POTENTIAL AND ELECTRIC FIELD DISTRIBUTION  
ASSOCIATED WITH HVDC INSULATORS UNDER  
DIFFERENT POLLUTION CONDITIONS**

BY

**TAISIR H. TUFFAHA**

A Thesis Presented to the  
DEANSHIP OF GRADUATE STUDIES

**KING FAHD UNIVERSITY OF PETROLEUM & MINERALS**

DHAHRAN, SAUDI ARABIA

In Partial Fulfillment of the  
Requirements for the Degree of

**MASTER OF SCIENCE**

In

**ELECTRICAL ENGINEERING**

December 2015

KING FAHD UNIVERSITY OF PETROLEUM & MINERALS

DHAHRAN- 31261, SAUDI ARABIA

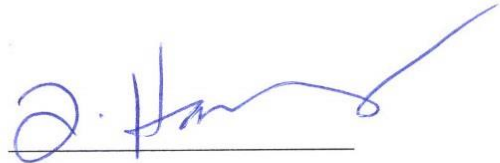
**DEANSHIP OF GRADUATE STUDIES**

This Thesis, written by **TAISIR HUSAM TUFFAHA** under the direction of his Thesis advisor and approved by his Thesis committee, has been presented and accepted by the Dean of Graduate Studies, in partial fulfillment of the requirements for the degree of **MASTER OF SCIENCE IN ELECTRICAL ENGINEERING.**



Thesis Committee



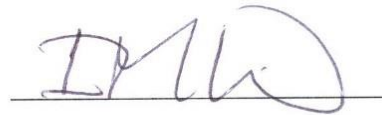
Dr. ALI A. AL-SHAIKHI  
Department Chairman



Prof. ZAKARIYA M. AL-HAMOZ  
(Advisor)

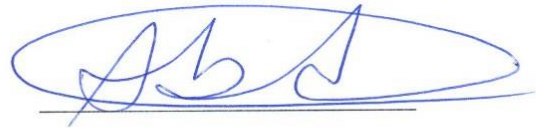


Dr. SALAM A. ZUMMO  
Dean of Graduate Studies



Prof. IBRAHIM M. EL-AMIN  
(Member)

31/12/15  
Date



Prof. MOHAMMAD A. ABIDO  
(Member)

© TAISIR H. TUFFAHA

2015

Dedicated to my beloved Father, Mother, Brothers and Sisters

## ACKNOWLEDGMENTS

My deepest gratitude to the majesty of Allah the most merciful, the most beneficent who gave me the ability and strength to begin and end my Master degree journey.

Acknowledgement also go to King Fahd University of Petroleum and Minerals for the great opportunity to pursue my degree. I would like to express my sincere appreciation to my advisor **Prof. Zakariya Al-Hamouz** for giving me the opportunity of becoming one of his students. I thank him for the enormous amount of effort, time and support he gave me during the completion of my Master study and related research. His wide knowledge, continuous motivation, and immense, helped me in all the time of writing my Thesis in its best form. I could not imagine of having a better mentor who I would work with and gave me the same passion of his. To that generous and countless hours, in that office, where we met, discussed and accomplished the work. I say thank you. In addition to my advisor, I also would like to thank my thesis committee: **Prof. Ibrahim El-Amin** and **Prof Mohammad Abido**, for their insightful comments and encouragement, but also for the fruitful questions which incented me to widen my research from various perspectives. My sincere thanks also goes to the department chairman **Dr. Ali Al-Shaikhi** and the dean of graduate studies **Dr. Salam Zummo**. To my dear friends, **Maad Alowaifeer**, **Abdurrahman Hamad**, **Mo'men Ghazi**, **Abdullah Alshaer** and **Khaled Ashmawi** for their massive help and support until the completion of my Thesis. Finally, I would like to thank my Father, Mother, brothers and sisters who keep supporting me physically, mentally and spiritually during writing this Thesis and my life as well.

# TABLE OF CONTENTS

<b>ACKNOWLEDGMENTS</b> .....	V
<b>TABLE OF CONTENTS</b> .....	VI
<b>LIST OF TABLES</b> .....	IX
<b>LIST OF FIGURES</b> .....	X
<b>LIST OF ABBREVIATIONS</b> .....	XV
<b>ABSTRACT</b> .....	XVI
<b>ملخص الرسالة</b> .....	XVIII
<b>CHAPTER ONE: INTRODUCTION</b> .....	1
1.1 Background .....	1
1.2 Thesis Motivations .....	2
1.3 Thesis Objectives .....	3
1.4 Thesis Organization .....	4
<b>CHAPTER TWO: LITERATURE REVIEW</b> .....	5
2.1 Overview .....	5
2.2 Types of HV insulators .....	6
2.2.1 Porcelain Insulators .....	6
2.2.2 Glass Insulators .....	7
2.2.3 SiR Insulators .....	7
2.3 Experimental Work .....	9
2.4 Simulation work .....	13
2.4.1 Custom made models .....	13

2.4.2 Electric field modeling using (FEM) .....	13
2.4.3 Electric field modeling using Boundary element method and charge simulation method....	14
2.5 Conclusion.....	15
<b>CHAPTER THREE: RESEARCH METHODOLOGY .....</b>	<b>16</b>
3.1 Governing Equations.....	16
3.2 Finite Element Method (FEM).....	18
3.3 Particle Swarm Optimization Technique .....	20
3.3.1 Introduction .....	20
3.3.2 Basic PSO Algorithm.....	21
<b>CHAPTER FOUR: PROPOSED ALGORITHM OF ELECTRIC FIELD CONTROL .....</b>	<b>24</b>
4.1 Introduction .....	24
4.2 Proposed Algorithm .....	25
<b>CHAPTER FIVE: INSULATOR TESTING AND STUDY CASES.....</b>	<b>31</b>
5.1 Insulator Models.....	31
5.2 Case Studies .....	34
<b>CHAPTER SIX: RESULTS AND DISCUSSIONS.....</b>	<b>36</b>
6.1 AC and DC electric field comparison .....	36
6.2 Performance under contaminated conditions and DC stress .....	37
6.2.1 Porcelain insulator (A) – Single unit.....	38
6.2.2 Porcelain insulator (A) – 15 units string .....	41
6.2.3 Glass insulator (B) -15 units string .....	49
6.2.4 SiR insulators (C-E) .....	51
6.3 Enhancement of electric field profiles using control devices.....	57
6.3.1 Porcelain insulator (A- 15 units).....	58

6.3.2 Glass insulator (B- 15 units).....	68
6.3.3 Comparison between Porcelain (A-15) and Glass (B-15) insulators .....	74
6.3.4 SiR insulator (D) .....	76
6.3.5 Insulator (E) 500 kVDC .....	85
6.4 Effect of using corona ring device on AC and DC electric fields .....	87
<b>CHAPTER SEVEN: CONCLUSIONS AND RECOMMENDATIONS.....</b>	<b>89</b>
7.1 Conclusions .....	89
7.2 Future work .....	91
<b>REFERENCES.....</b>	<b>92</b>
<b>APPENDIX.....</b>	<b>97</b>
A.1 Insulator (A) Contours .....	97
A.2 Insulator (B) Contours.....	99
A.3 Insulators (E) Contours .....	101
<b>VITAE.....</b>	<b>103</b>

## LIST OF TABLES

Table 5.1. Dimensions of porcelain and glass insulators .....	33
Table 5.2. Dimensions of SiR insulators.....	33
Table 5.3. Materials properties .....	33
Table 5.4. Contamination severity and respective conductivities .....	34
Table 5.5. Pollution scenarios .....	34
Table 6.1. Upper and lower limits of optimized corona ring parameters.....	58
Table 6.2. Upper and lower limits of optimized Arc Horn parameters.....	58
Table 6.3. Summary of insulator's string efficiencies .....	74
Table 6.4. Percentage Reduction in the maximum electric field Along PATH 2 for both insulators .....	75
Table 6.5. upper and lower limits of optimized paprametrns of insulaotr (D).....	78
Table 6.6. Optimal positions of electric field control devices .....	79

## LIST OF FIGURES

Figure 2.1. Cap and Pin Porcelain Insulator [13].....	6
Figure 2.2. Cap and Pin Glass Insulator [14].....	7
Figure 2.3. SiR insulator [15] .....	8
Figure 3.1. Example of a discretized domain ‘D’ .....	19
Figure 3.2. flow chart of PSO algorithm.....	23
Figure 4.1. Main workflow of the thesis.....	24
Figure 4.2. Electric field control devices configuration, [SiR : a) Corona Ring. b) Arc Horn] [Porcelain and glass: c) Corona Ring d) Arc horn] .....	26
Figure 4.3. MATLAB™ and ANSYS™ interface.....	27
Figure 4.4. Using the MACRO file in the interfacing process.....	29
Figure 4.5. Flow chart of solution process.....	30
Figure 5.1. Configurations of insulators, a) porcelain insulator (A) b) glass insulator (B) .....	31
Figure 5.2. Configurations of insulators a) 15kV SiR (C), b) 300 kV SiR (D), c) 500 kV SiR (E).....	32
Figure 6.1. AC and DC electric field comparison.....	37
Figure 6.2. a) Non-uniform pollution (S2). b) Non-uniform water droplet (S3) c) Non- uniform water droplet + pollution (S4). .....	39
Figure 6.3. Corresponding electric fields of contamination scenarios.....	40
Figure 6.4. Fifteen units string of insulator (A). a) Complete string. b) Considered paths.....	41
Figure 6.5. Pollution profile along the first insulator (A) .....	42
Figure 6.6. Electric field of PATH 1 along the string (A-15).....	43
Figure 6.7. Electric field of PATH 2 along the string (A-15).....	43
Figure 6.8. Electric field of PATH 3 along the string (A-15).....	44
Figure 6.9. Voltage distribution of PATH 1 along the string (A-15).....	44
Figure 6.10. Voltage distribution of PATH 2 along the string (A-15).....	45

Figure 6.11. Voltage distribution of PATH 3 along the string (A-15).....	45
Figure 6.12. Electric field along the surface of the first insulator (A) .....	46
Figure 6.13. Voltage distribution along the surface of the first insulator (A).....	47
Figure 6.14. Maximum electric field comparison of the three paths. a) clean. b) contaminated .	47
Figure 6.15. Percentage change in maximum electric field due contamination .....	48
Figure 6.16. Fifteen units string of insulator (B). a) Complete string. b) Considered paths .....	49
Figure 6.17. Maximum electric field comparison of the three paths. a) clean. b) contaminated .	50
Figure 6.18. Percentage change in maximum electric field due contamination .....	51
Figure 6.19. SiR insulator (C). a) non-uniform pollution (S2). b) non uniform water droplet (S3). c) non-uniform water+pollution (S4).....	52
Figure 6.20. Electric field distribution of insulator (C) under non-uniform pollution.....	52
Figure 6.21. Electric field distribution of insulator (C) under non-uniform water droplets .....	53
Figure 6.22. Electric field distribution of insulator (C) under combined pollution .....	53
Figure 6.23. Voltage distribution of insulator (C) .....	53
Figure 6.24. Electric field distribution along insulator's (D) surface.....	54
Figure 6.25. Voltage distribution along insulator's (D) surface.....	55
Figure 6.26. Electric field distribution along insulator's (E) surface .....	56
Figure 6.27. Voltage distribution along insulator's (E) surface .....	56
Figure 6.28. Variation of J with Iteration number .....	59
Figure 6.29. Electric field of PATH 1 along the string (A-15) with control devices under contaminated conditions.....	60
Figure 6.30. Voltage distribution of PATH 1 along the string (A-15) with control devices under contaminated conditions.....	61
Figure 6.31. Electric field of PATH 2 along the string (A-15) with control devices under contaminated conditions.....	61

Figure 6.32.	Voltage Distribution of PATH 2 along the string (A-15) with control devices under contaminated conditions.....	62
Figure 6.33.	Electric field of PATH 3 along the string (A-15) with control devices under contaminated conditions.....	62
Figure 6.34.	Voltage Distribution of PATH 3 along the string (A-15) with control devices under contaminated conditions.....	63
Figure 6.35.	Electric field along the surface of the first insulator (A) with control devices under contaminated conditions.....	64
Figure 6.36.	Voltage Distribution along the surface of the first insulator (A) with control devices under contaminated conditions.....	64
Figure 6.37.	Maximum electric field comparison along PATH 1, when using control devices under contaminated conditions.....	66
Figure 6.38.	Maximum electric field comparison along PATH 2, when using control devices under contaminated conditions.....	66
Figure 6.39.	Maximum electric field comparison along PATH 3, when using control devices under contaminated conditions.....	67
Figure 6.40.	Percentage change in the maximum electric field due to Arc Horn for insulator (A) under contaminated conditions.....	67
Figure 6.41.	Percentage change in the maximum electric field due to corona ring for insulator (A) under contaminated conditions.....	68
Figure 6.42.	Electric field along the surface of the first insulator (B) with control devices under contaminated conditions.....	69
Figure 6.43.	Voltage distribution along the surface of the first insulator (B) with control devices under contaminated conditions.....	69
Figure 6.44.	Maximum electric field comparison of PATH 1 with control devices under contaminated conditions.....	71

Figure 6.45. Maximum electric field comparison of PATH 2 with control devices under contaminated conditions.....	72
Figure 6.46. Maximum electric field comparison of PATH 3 with control devices under contaminated conditions.....	72
Figure 6.47. Percentage change in the maximum electric field due to Arc horn for insulator (B). .....	73
Figure 6.48. Percentage change in the maximum electric field due to corona ring for insulator (B). .....	73
Figure 6.49. Comparing Glass and Porcelain Insulators.....	75
Figure 6.50. Electric field distribution along insulator's (D) surface with corona ring .....	76
Figure 6.51. Voltage distribution along insulator's (D) surface, in the presence of corona ring.	77
Figure 6.52. Electric field distribution along insulator's (D) surface with corona ring (Selected points).....	77
Figure 6.53. Objective function J versus Iteration number for double arc horns devices.....	78
Figure 6.54. Different electric field control devices configurations, a) single corona ring, b) single arc horn, c) double corona rings, d) double arc horns, e) corona and arc horn .....	79
Figure 6.55. Insulator (D) Electric field contours; a) without control, b) with single arc horn, c) with double arc horns, d) with single corona ring, e) with double corona ring f) with combined corona ring and arc horn.....	81
Figure 6.56. Insulator (D) Voltage contours; a) without control,b) with single arc horn, c) with double arc horns,d) with single corona ring, e) with double corona ring, f) with combined corona ring and arc horn.....	82
Figure 6.57. Electric field distributions for different control devices.....	83
Figure 6.58. Maximum electric field comparison for different control devices .....	84
Figure 6.59. Percentage reduction in Maximum electric field for different control devices .....	84

Figure 6.60. Electric field distribution along insulator's (E) surface with corona ring .....	85
Figure 6.61. Voltage distribution along insulator's (E) surface, in the presence of corona ring .	86
Figure 6.62. Electric field distribution along insulator's (E) surface with corona ring (Selected points).....	86
Figure 6.63. AC and DC electric field comparison along PATH 2 .....	87
Figure 6.64. Percentage change comparison between AC and DC electric fields in the presence of corona ring .....	88
Figure A. 1. Insulator (A- 15 units) Electric field contours; a) without control, b) with Arc horn, c) with corona ring.....	97
Figure A. 2. Insulator (A- 15 units) Voltage contours; a) without control, b) with Arc horn, c) with corona ring .....	98
Figure A. 3. Insulator (B- 15 units) Electric field contours; a) without control, b) with Arc horn, c) with corona ring.....	99
Figure A. 4. Insulator (B- 15 units) Voltage contours; a) without control, b) with corona ring.....	100
Figure A. 5. Insulator (E) Electric field contours; a) without control, b) with corona ring .....	101
Figure A. 6. Insulator (E) Voltage contours; a) without control, b) with corona ring .....	102

## LIST OF ABBREVIATIONS

<b>AC</b>	:	Alternating current
<b>DC</b>	:	Direct current
<b>EPDM</b>	:	Ethylene Propylene Diene Monomer
<b>ESDD</b>	:	Equivalent Salt Deposit Density
<b>FEM</b>	:	Finite Element
<b>FOV</b>	:	Flash over Voltage
<b>HVDC</b>	:	High Voltage Direct Current
<b>IEC</b>	:	International Electro-Technical Commission
<b>IEEE</b>	:	Institute of Electrical and Electronics Engineers
<b>NSDD</b>	:	Non Soluble Deposit Density
<b>PSO</b>	:	Particle Swarm Optimization
<b>RTV</b>	:	Room Temperature Vulcanized
<b>SiR</b>	:	Silicon Rubber

## **ABSTRACT**

Full Name : TAISIR HUSAM TAISIR TUFFAHA  
Thesis Title : POTENTIAL AND ELECTRIC FIELD DISTRIBUTION  
ASSOCIATED WITH HVDC INSULATORS UNDER DIFFERENT  
POLLUTION CONDITIONS  
Major Field : Electrical Engineering  
Date of Degree : December 2015

High voltage insulators play a major role in energy transmission systems. The main role of these insulators is to ensure and maintain high level of line-tower insulation which may be affected by different environmental factors such as humidity, dust, heat and chemical contaminations. Such contamination in the presence of high electric field may lead to insulator flashover which affects the transmission system reliability. HV insulators were widely studied under AC voltage. However, under DC voltage, investigations are still premature. In this Thesis work, the electric field and voltage profiles of different types of HV insulators were investigated under clean and contaminated conditions stressed with DC voltages. Moreover, the effect of different electric field control devices such as Corona ring and Arc Horns on the electric field and voltage profiles, has been investigated under clean and polluted conditions.

The electric field has been formulated as an optimization problem. An optimization algorithm has been developed using ANSYS<sup>TM</sup> MACRO script and MATLAB<sup>TM</sup> Particle Swarm Optimization toolbox. The studied insulators include porcelain, glass and silicon rubber operating at voltage level ranging from 15 to 500 kVDC. The results show that under HVDC, the worst electric field profile was found at a combination of water droplets

and non-uniform pollution. For fifteen unit string insulator including porcelain and glass, the most affected region by contamination was found to be near the pollution junction. In addition, the Arc horn control device provides lower electric field profiles as compared to corona ring's. For the case of long rod SiR insulator, the best control scheme is given by double Arc Horns, where the maximum electric field has been reduced 80%. Finally, under DC voltage, the results show that the electric field control device (corona ring) has performed just as good as or even better than under AC voltage.

## ملخص الرسالة

الاسم الكامل: تيسير حسام تيسير تفاحة

عنوان الرسالة: توزيع المجال والجهد الكهربائي المرافقين لعوازل التيار الدائم تحت ظروف مختلفة من التلوث

التخصص: الهندسة الكهربائية

تاريخ الدرجة العلمية: ديسمبر 2015

لعوازل الضغط العالي أهمية كبيرة في عملية نقل الطاقة الكهربائية. و الدور الاساسي لهذه العوازل هو ضمانه واستمرارية أعلى مستوى من العزل الكهربائي بين الخط الحي والبرج المؤرض، والتي قد تتأثر بعدة عوامل بيئية منها: الرطوبة والأترية والحرارة و الملوثات الكيميائية. هذه الملوثات تحت تأثير المجال الكهربائي العالي، قد تؤدي إلى انهيار العازل كهربائيا والتي تؤثر سلبا على اعتمادية نظام نقل الطاقة. مثل هذه العوازل قد تمت دراستها بشكل مكثف تحت تأثير التيار المتردد. و في المقابل لا تزال الدراسات غير مكتملة تحت تأثير التيار الدائم. في هذه الأطروحة، قد تمت دراسة توزيع المجال والجهد الكهربائيين لعدد من عوازل الضغط العالي المختلفة تحت تأثير التيار الدائم، مأخوذاً بالاعتبار ظروف التلوث المختلفة. كما وتمت دراسة تأثير أجهزة التحكم بالمجال الكهربائي كـ (Corona ring) و (Arc Horn) على توزيع المجال والجهد الكهربائي تحت الظروف النظيفة و الملوثة. بالإضافة إلى صياغة المجال الكهربائي كمعادلة للتمثيل. فقد تم تطوير خوارزمية خاصة لإيجاد القيم المثلى لأبعاد أجهزة التحكم بالمجال الكهربائي وبالتالي التقليل من شدة المجال بالإستعانة بنص الـ MACRO الخاص ببرنامج الـ ANSYS<sup>TM</sup> و أداة التمثيل PSO الموجودة في برنامج الـ MATLAB<sup>TM</sup>. وكانت العوازل المطروحة متألفة من : العوازل الزخرفية والعوازل الزجاجية بالإضافة إلى عوازل السليكون المطاطي، تحت جهود كهربية مختلفة تتراوح بين 15 الى 500 kVDC. وقد أظهرت النتائج تحت تأثير التيار المستمر أن أسوأ توزيع للمجال الكهربائي قد وجد تحت تأثير التلوث غير المنتظم مصحوبا بقطرات الماء المتفرقة. وفي حالة الخمسة عشر وحدة متصلة من العازلين : الزخرفي والزجاجي، فقد وجدت المنطقة الأكثر تأثرا بالتلوث تقع بالقرب من نقطة التقاء الضغط العالي مع التلوث. وفي حالة السلسلة الملوثة من العوازل، فقد وجد أن استخدام جهاز الـ Arc Horn قد تفوق على أداء جهاز الـ Corona ring في تخفيض المجال الكهربائي. وفي حالة عازل السليكون المطاطي الطويل، فقد وجد أن استخدام Double Arc Horn كأداة تحكم بالمجال، قد نتج عنه أفضل شكل للمجال الكهربائي، حيث تم تخفيض القيمة القصوى للمجال الكهربائي بنسبة تصل إلى 80%. و أخيرا، فقد وجد أن أداء جهاز التحكم (corona ring)، تحت تأثير ضغط التيار المستمر، لا يقل عن أو ربما يتفوق عن أداء نفس الجهاز تحت تأثير التيار المتردد.

# CHAPTER ONE

## INTRODUCTION

### 1.1 Background

The main purpose of high voltage (HV) insulators is to provide isolation between the transmission line and the grounded tower. The insulators are either ceramic, glass or composite (Silicon Rubber). Ceramic insulators are known for their durability and long-life, while SiR insulators are light weighted and possess a better hydrophobicity property than ceramic insulators. Many studies have been carried out in the literature that investigated different aspects of HVAC insulators problem such as: electric field and potential distribution, effect of contamination level on flashover voltage (FOV), contamination level monitoring, the effect of electric field control devices such as corona rings and arc horns, etc [1-9] are documented. Nowadays as the load penetration is increasing rapidly, HVDC transmission becomes much more effective alternative, technically and economically, owing to the many advantages of HVDC transmission such as, lack of the reactive power problems and stability issues [10]. Unfortunately, studies of potential and electric field distribution associated with insulators under HVDC are still immature.

In the Kingdom of Saudi Arabia, after deciding to interconnect the Central region network with the West Region over 800km distance, the interest in DC transmission was heightened

for its superior potential when it comes to long distances. However, the performance of HVDC insulators have not been well investigated under the kingdom's environment. The environment of Saudi Arabia is known for its challenging contamination conditions including high levels of humidity (in coastal regions), dust and heat. Thus, exquisite researches needed to be done in this area.

Given the brief background, this Thesis proposes an electric field and a potential distribution evaluation on the surface of composite, porcelain and glass insulators using the FEM software ANSYS<sup>TM</sup> under combined HVDC and contaminated conditions. Moreover, a MATLAB<sup>TM</sup> based particle swarm optimization (PSO) tool was used to provide an optimal selection of electric field control device parameters in order to minimize the electric field distribution on these insulators under contaminated conditions.

## **1.2 Thesis Motivations**

As mentioned earlier, no detailed work has been conducted on evaluating the electric field and potential distribution on the surface of insulators under combined polluted conditions and control devices stressed by HVDC. Thus, the motivation of investigating the problem can be summarized in the following points:

- It will help the designers of HV insulators to take care of the regions where the electric field is expected to have high values especially under contamination. Thus preventing any catastrophic damages, and increasing the overall reliability of the power system in general.
- The proposed dimensions of electric field control devices may help the electric utilities in choosing the suitable device dimensions for specific types of insulators.

- Since the contaminations profiles were taken from a real data in the eastern province of Saudi Arabia, The outcome of this Thesis is expected to enrich electric utilities in the kingdom of Saudi Arabia about the performance of HV insulators under DC stress.

### **1.3 Thesis Objectives**

The main objectives of this Thesis is to evaluate the electric field and voltage distributions of HV insulators stressed by DC voltage, under clean and contaminated conditions. Ceramic, glass and SiR insulators will be tested. Different methods of minimizing the maximum electric field on HVDC insulators will be discussed. The effect of using corona ring on AC and DC electric fields will be studied. Therefore, the objectives are:

**Objective 1:** Numerical evaluation of electric stress and potential along the surface of porcelain, glass and SiR insulators under HVDC.

**Objective 2:** Investigating the effect of different pollution levels and distribution on the studied insulators.

**Objective 3:** Proposing an optimal dimensions of electric field control device for insulators operating under DC voltage.

**Objective 4:** Studying the effect of using corona ring device on AC and DC electric fields.

## **1.4 Thesis Organization**

In addition to the introduction, the Thesis has six more chapters organized as the following: chapter two contains a comprehensive literature review describing HVDC insulator problems and pointing the gaps in this field of research by surveying both experimental and simulation based works. Followed by the Thesis Methodology in chapter three which includes, the used governing equations, FEM method and PSO technique. The proposed optimization algorithm is shown in chapter four. Insulator models and case studies are presented in chapter five. Discussion and analysis on the obtained results will be in chapter six. Finally, conclusion and recommendations regarding future works are pointed in chapter seven.

# CHAPTER TWO

## LITERATURE REVIEW

### 2.1 Overview

Overhead line insulators are used to support the line conductors and separate them electrically from each other. Therefore, an insulator should meet the following requirements [11]:

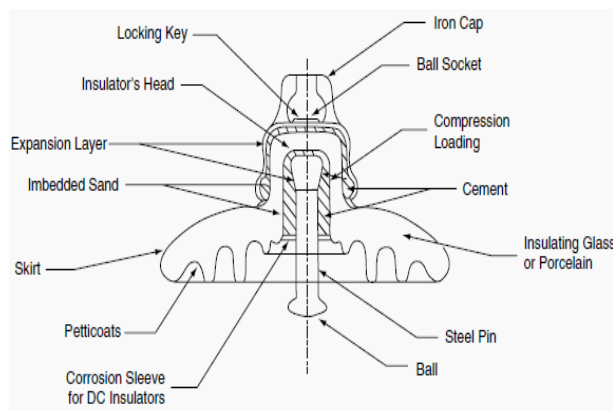
- i. The dielectric strength should be high so that it can withstand the normal operating voltage and overvoltage due to lightning and switching.
- ii. It should possess high mechanical strength to bear the conductor under the worst weather conditions such as wind, ice, etc.
- iii. It should have a high resistance due to thermal stress.
- iv. The leakage current to ground should be at very minimum.
- v. It should also be very smooth and free of any sharp edges, in addition to self-cleaning against rain and dust.

As a result, the HV insulator should be carefully designed, especially under DC stress in order to meet the requirements of an acceptable insulating criteria. In this chapter, a quick overview will be given regarding the most common types of insulators, followed by an extensive literature survey on the work done (experimentally and numerically) on HVDC insulators.

## 2.2 Types of HV insulators

### 2.2.1 Porcelain Insulators

Porcelain insulators which are also known as ceramic insulators are made of fine homogenous mix of wet plastic clay which is shaped, covered with glaze and then fired in a kiln. Glazing is necessary to obtain a surface which can be kept relatively free from dust and other contamination. Porcelain insulators are usually made in three types: Pin type insulators, cap and pin insulator and strain type insulators [12]. The most common type is the cap and pin type presented in Figure 2.1. The name cap and pin, is given because these insulators are fitted with (bell) shaped galvanized, malleable iron cast or forged steel caps and galvanized forged steel pins, then these pieces are cemented together to form the cap and pin type. These insulators are connected to form a string which can withstand higher voltages based on the string's length. Porcelain is mechanically stronger than glass, gives less trouble from leakage and is less affected by the changes of temperature. Due to these reasons, porcelain is the most commonly used material for manufacture of insulators.



(a) Cross section of cap and pin insulator



(b) The product of cap and pin insulator

**Figure 2.1. Cap and Pin Porcelain Insulator [13]**

### 2.2.2 Glass Insulators

Toughness glass is the other material normally used for insulators. Glass is cheaper than porcelain in the simpler shapes, owing to its transparency, flaws in the material can be detected easily by visual examination. However, moisture readily condenses on its surface which causes high surface leakage currents. Another disadvantage is that in high voltage insulators, the larger mass of the material combined with the irregular shape may result in internal strain after cooling thus reducing the reliability of insulator. As a result, the glass insulators are less frequently used than the porcelain. Similar to porcelain insulators, glass insulators are divided into three types: pin and cap, Figure 2.2, pin type and strain type insulators [12].

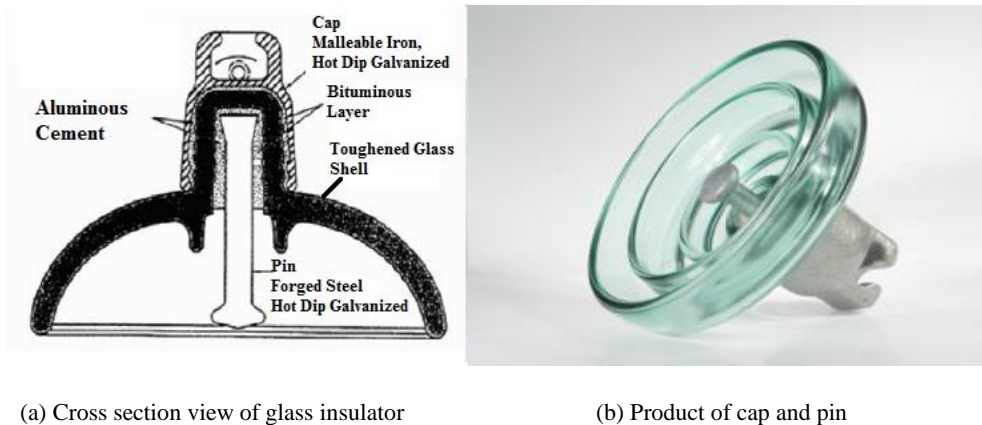
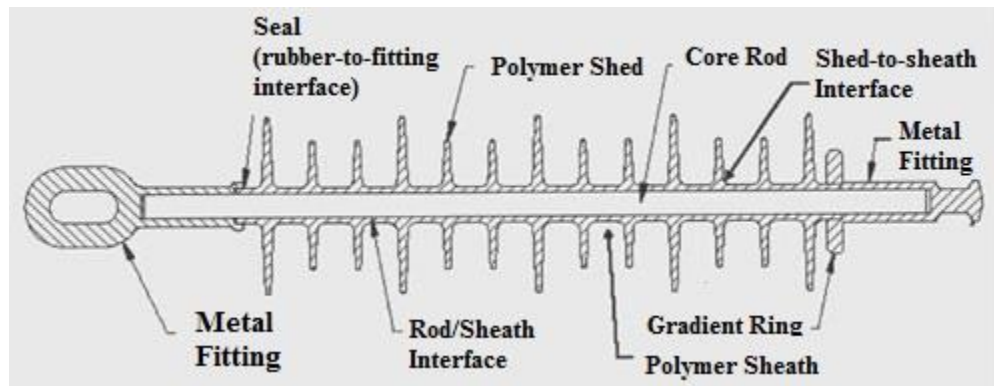


Figure 2.2. Cap and Pin Glass Insulator [14]

### 2.2.3 SiR Insulators

Since the early sixties of past century, alternative materials, namely composite (polymers) have emerged, and presently they are being used extensively for a variety of outdoor insulator applications. Composite insulators are commonly made of silicone rubber (SiR) and ethylene propylene rubber EPR. The main advantages of composite insulators are its

light weight, superior vandal resistance and the possession of good anti-pollution properties [12]. On the other hand, many difficulties have been countered during first two decades of operation. The typical of these were: tracking and erosion of polymer sheds; chalking and crazing of sheds which lead to increased contamination collection. However, through continuous effort and research in polymeric material development, much improved version of SiR insulators have been introduced. The basic construction of SiR insulators consists of three main materials which are: Fiber glass (core), Silicon Rubber (water sheds) and the metal end fittings as shown in Figure 2.3.



(a) Cross section view



(b) Product of SiR insulator

**Figure 2.3. SiR insulator [15]**

## 2.3 Experimental Work

In this section, different setups will be discussed based on their applications and desired outputs. The literature work is arranged chronologically from 1991 to 2014. The main objective of this section is to summarize the different approaches followed to test various types of HVDC insulators under normal and contaminated conditions, and recording their findings.

The research conducted in 1991 by Qisheng, Li, et al [16], had investigated two years of natural contamination tests on six types of insulators. The specimens were four types of five units suspension Ceramic disc insulators, in addition to two station post insulators. The specimens were subjected to 90 kVDC continuously. The specimens were mounted on 12 m above the ground and with two meters of separation between each tested subjects. The authors stated that, the insulator subjected to DC voltage attracts 20% more pollution than in AC.

Meanwhile the team of Ishikawa et.al in Japan [17] investigated single unit FOV phenomena in suspension string subjected to HVDC. They've related the sensitivity of geometry on HVDC insulator performance. They've used different number of suspension insulator string; between 29 and 46 units were tested. The insulator units were two DC fog disc Ceramic insulator. The applied voltage was between  $\pm 500$  and  $\pm 250$  kVDC. Two main operating conditions were considered, the first condition was with non-soluble deposit density (NSDD) of  $0.1 \text{ mg/cm}^2$  and fog density ranging between  $[0.3-0.5 \text{ g/m}^3]$ , and the other condition was with fog density of  $[3-5 \text{ g/m}^3]$  under the same NSDD level. They

suggested to have larger shed diameters and room temperature vulcanized (RTV) coated units to eliminate that phenomena.

On the other hand, A.Karn et.al [18] made a behavioral comparison of corona inception and FOV between HVAC and HVDC insulators. They've used ordinary coated and non-coated disc type Ceramic insulators. The voltage levels ranged between 0-90 kVDC. The test was carried out according to ANS c29.1 standard. They have reported that, the corona inception voltage is higher for RTV coated units than the non-coated.

In 2007, J.M, Seifert et.al [19] have conducted a comparison of the pollution performance between long rod and disc type Ceramic insulators. Two types of disc insulators were used. The first was HVAC type, and the other one was HVDC. The voltage level was around  $\pm 533$  kVDC induced by voltage doubler circuit. The test procedure was done according to IEC TC36 (SC) 75, and IEC 61425. They've stated that, if the insulators were designed properly, similar pollution performance can be reached from both insulators.

In the same subject of performance comparison, Xingliane et.al [20] have performed a DC pollution FOV performance comparison between ceramic, glass and composite insulators. The specimens used were single disc type AC Ceramic insulator, and two disc types (ceramic and glass) DC insulators. In addition to five SiR insulators. The voltage level used was  $\pm 600$  kVDC. All the tests were performed inside a climate test chamber of 7.8m diameter and height of 11m. Then the tests were carried out according to the standards IEEE std-4 and IEC 1245. They've agreed with Qisheng study that DC voltage attracts more contamination than AC.

The researchers in [21] applied the thermal runaway test on ceramic, glass and SiR Insulators. The procedure was followed as in IEC-61325. They've stated that the higher temperature, the lower insulating resistance becomes.

For high altitude applications, Z.Zhang et.al [22] have studied the FOV performance of various types of long string insulators; including Ceramic, glass and SiR long rod insulators. The applied voltage was  $\pm 600$  kVDC. The test was carried out in an artificial pollution climate chamber of 7.8m in diameter and height of 11.6m. The test procedure was according to the following standards: IEC 1245, Electra No.136, CIGRE Elcectra no 140, IEC 60-1 and IEEE std-4. Their results agreed with Seifert and Xingliane [19] [20] on the linearity between pollution FOV and the string length. They've also recommended the composite insulator under heavy polluted conditions.

Heger, G., et al [23], conducted a comparison between AC & DC surface discharge of insulator materials. The materials were Ceramic RTV coated, HTV- Silicon rubber and EPDM rubber. They have found that EPDM rubber insulator performs better under DC than SiR material. The test voltages were  $\pm 2.5, 3.5, 4.5$  kVDC and 7.5kVAC. The tests were done according to IEC 60587. The insulator samples were mounted on a support stand in angle of  $45^\circ$  as for the "inclined plane test apparatus".

Under 500kVDC, Seo, I. J., et al [24] investigated the DC break down voltage of polymeric insulators. The used samples were polymeric composite material, prepared in different ways by mixing silicon and Alumina Trihydrate (ATH) respectively. Their results say that when ATH is used as a filler material, the breakdown voltage is twice higher than under

AC. Furthermore, Jeong, et al [25] performed similar tests on SiR Insulators and got the same conclusion.

In addition to the research in [21], another pollution FOV performance comparison was conducted under UHVDC at high altitudes by team Lin Yang et.al [26]. The specimens used were Ceramic long rod, disc type and SiR Insulators. The voltage level was  $\pm 250\text{kVDC}$ . The test was performed in  $10 \times 10 \times 10 \text{ m}^3$  artificial pollution chamber that can control the air pressure, temperature and rain inside it. The tests were done according to IEC 61245 and GB/T 22707 standards. The results also confirm with Xingliane [20] that under low air pressure, the effect of pollution becomes more on FOV than under normal air pressure.

Recently, an Iranian team [27] [28], performed an extensive study on SiR insulators under HVDC heavy polluted conditions, and came with results that agree with most of the literature. All the samples were SiR insulators of different leakage distances and lengths. The test chamber was  $2 \times 2 \times 2 \text{ m}^3$ . The voltage used was  $100 \text{ kVDC}$ . The tests were according to IEC 1245 standard.

Z.Zhang et.al [29] studied the Fan shaped non-uniform pollution FOV performance of various types of disc suspension insulators. The specimens used were Ceramic and glass disc insulators forming a string of 7 units. All the tests were carried out in a test chamber of  $7.8\text{m}$  diameter and  $11.6\text{m}$  high. The authors used similar equipments as those in research [22]. They've stated that, larger diameter doesn't improve performance especially under Fan shaped contamination.

## **2.4 Simulation work**

In this section, the recent attempts of numerically evaluating the electric field and voltage distributions along HVDC insulators have been summarized. The general approach to solve this particular problem, is by solving the Laplacian field, when considering zero space charge, or solving the Poisson's equation in case of space charge existence. One of the most common approaches to solve either of these two equations is by using the finite element method (FEM). In the following literature, different attempts were recorded based on their methods.

### **2.4.1 Custom made models**

Sundararajan and Gorur [30] [31], proposed a dynamic arc model to study the effect of insulator profiles on DC FOV under polluted conditions. The simulation subjects were Ceramic disc insulators of different geometries, under both contamination and non-contamination conditions. The model agrees with the practical results which makes it reliable. However, the model is complex to adapt, and only evaluates the FOV possibilities as a function of contamination level, rather than the complete electric field and voltage distributions profiles.

### **2.4.2 Electric field modeling using (FEM)**

In electric field modeling using FEM, Yan et al [32] have done a numerical calculation of electric field and voltage distribution for HVDC SiR insulators. The simulation was carried out using ANSYS<sup>TM</sup> software to solve 2-D axisymmetric electric field governed by the Laplace equation. They've used far field unit and artificial truncation boundary to solve

the open field problem. Their results show that the calculated domain size has no effect on the accuracy of the results when using far field unit boundaries. In recent work, Yan et.al [33] have computed the electric field of HVDC insulator considering surface charges, and compared to the case when not considering it. They've also used the FEM to solve the Poisson's equation of the potential field. The insulator unit was SiR stressed by DC voltage. In order to calculate the electric field in presence of space charge, an iterative approach has been followed to update the surface charge at each cycle of calculation till the solution converges. Their results indicate the observable difference between the two cases. The study does not include porcelain and glass insulators strings, as well as the effect of contamination and electric field control devices.

Pretorius et al [34], have used electric field modeling to confirm their experimental results on investigating the effect of cracked glass insulator unit, on the complete string, under HVDC. They have found that the string's performance was very much affected when including cracked units.

### **2.4.3 Electric field modeling using Boundary element method and charge simulation method**

One of the used methods of calculating the electric field and voltage distributions are Boundary element method (BEM) and Charge simulation method (CSM). By using 3-d COULOMB<sup>TM</sup> software which solves the electric field problem using BEM, the researchers Kumar and Gorayan [35] have studied the effect of increasing the pollution (severity) level on the Ceramic insulator surface under HVDC. They have found that the maximum electric field proportionally increases with the severity level.

The CSM method was used by Jiahong and Gorur [36] to calculate the electric field and voltage distribution of composite insulator under HVDC. The electric field profile was evaluated under both clean and wet conditions, then compared to AC insulators. They've stated that under the same nominal voltage, the electric field under HVDC is higher than in AC near HV end fitting, thereby the necessity of adding corona and grading rings rises to the transmission lines. However, the studied geometry problem was simple. Moreover, this specific method requires a high computational capability as compared to FEM.

## **2.5 Conclusion**

Based on the previous literature survey, and to the author's knowledge, no work has been conducted to investigate the electric field and voltage distribution profiles along different types of HV insulators subjected to DC voltage under dry and different contaminated surface conditions. Moreover, the effect of optimized control devices on controlling the electric field profile, will be introduced for the first time under combined HVDC and contaminated conditions.

## CHAPTER THREE

### RESEARCH METHODOLOGY

This chapter discusses the governing equations, the finite element technique and particle swarm optimization method that have been used to achieve the Thesis objectives.

#### 3.1 Governing Equations

In order to investigate the insulator performance under HVDC, the electric field and voltage profiles need to be calculated first. The electrostatic field distribution ( $E$ ) is obtained by calculating the voltage ( $V$ ), then directly taking its gradient ( $-\nabla$ ). Thus, the electric field is given by:

$$E = -\nabla V \quad (3.1)$$

From Maxwell's equation, the divergence of the electric flux density  $D$  ( $C/m^2$ ) from closed surface will give the charge density  $\rho$  ( $C/m^2$ ) enclosed by that surface:

$$\nabla \cdot E = \nabla \cdot (-\nabla V) = \rho/\epsilon \quad (3.2)$$

Where,  $\epsilon$  is the dielectric constant of the material, given by  $\epsilon = \epsilon_o \epsilon_r$ , where  $\epsilon_o$  is the permittivity of air ( $8.854 \times 10^{-12}$  F/m) and  $\epsilon_r$  is the relative permittivity of the insulator material [37].

Equation (3.2) can be written as Poisson's equation given by:

$$\nabla^2 V = -\rho/\varepsilon \quad (3.3)$$

If the space charge was neglected, the Poisson's equation becomes the Laplace equation given in (3.4)

$$\nabla^2 V = 0 \quad (3.4)$$

However, to evaluate the electric field distribution along the insulator's contaminated surface, the continuity equation has to be considered [38].

$$\nabla \cdot \left( J + \frac{\partial D}{\partial t} \right) = 0 \quad (3.5)$$

Where,  $J$  is the current density ( $A/m^2$ ).

Since,  $J = \sigma E$  and  $D = \varepsilon E$ , where  $\sigma$  is the electric conductivity (S/m), equation (3.5) becomes

$$-\nabla(\sigma \nabla V) - \nabla \cdot \left( \varepsilon \nabla \frac{\partial D}{\partial t} \right) = 0 \quad (3.6)$$

In case of DC, the partial derivative term of equation (3.6) will become zero and yield to (3.7) which clearly indicates that surface conductivity  $\sigma$ , will decide the electric field distribution under contamination condition.

$$-\nabla \cdot (\sigma \nabla V) = 0 \quad (3.7)$$

Eventually for a 2-D problem, (3.7) and a Cartesian form of (3.8) given in (3.8) will be solved together. It is worth mentioning that only positive voltage polarity is considered due to the software limitations.

$$\nabla^2 V = \frac{\partial^2 V}{\partial x^2} + \frac{\partial^2 V}{\partial y^2} = 0 \quad (3.8)$$

### 3.2 Finite Element Method (FEM)

To solve equations (3.7) and (3.8) which are coupled partial differential equations, finite element method (FEM) will be used. This technique has been proven to be a good numerical solution alternative for complicated geometries.

The general solution steps for solving (3.7) and (3.8) are given below:

- 1) Domain discretization: where the problem is divided into finite number of elements to be solved [39]

$$F(u) = \frac{1}{2} \int_D \sigma \left[ \left( \frac{du}{dx} \right)^2 + \left( \frac{du}{dy} \right)^2 \right] \quad (3.9)$$

Where,  $u$  is the potential in Domain  $D$  shown in Figure 3.1 and  $\sigma$  is the conductivity.

- 2) Developing a simple linear equation to approximate the solution for each element inside the domain  $D$ .

$$u_i(x, y) = \alpha_{i1} + \alpha_{i2} x + \alpha_{i3} y ; \quad i = 1, 2, 3, \dots, n \quad (3.10)$$

Where,

$u_i(x, y)$  is the electric potential of any arbitrary point inside each subdomain  $D_i$ .  $\alpha_{i1}$ ,  $\alpha_{i2}$  and  $\alpha_{i3}$  are the coefficients for the triangular element  $i$ .  $n$  is the total number of elements [40].

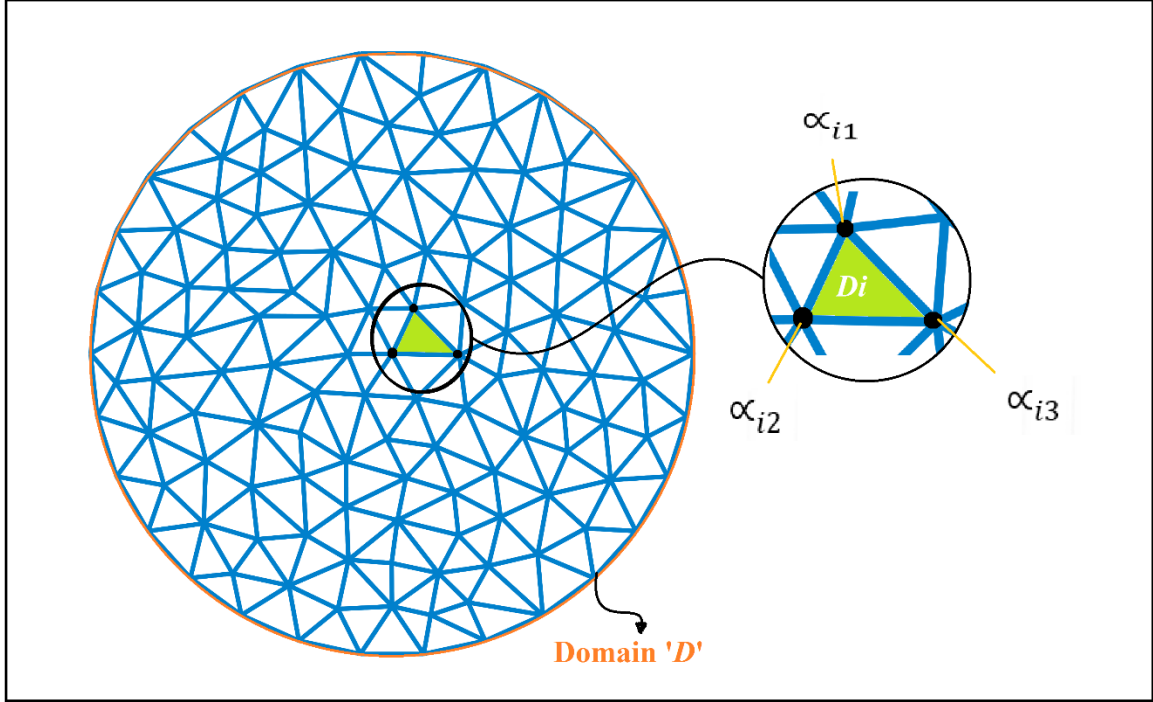


Figure 3.1 Example of a discretized domain 'D'

- 3) Assembling all the linear element equations and applying the boundary conditions

$$[S_{ji}]\{u_i\} = \{T_j\} \quad i,j=1,2,\dots,nd \quad (3.11)$$

Where  $[S_{ji}]$  is the coefficient matrix,  $\{u_i\}$  the potential vector at any node  $i$ ,  $\{T_j\}$  is the vector of free terms and  $nd$  is the number of nodes.

- 4) Finally, after solving (3.8), the potential distribution at each node is known and the electric field can be calculated accordingly [6].

$$\mathbf{E}_X = -\frac{\delta u}{\delta x}, \quad \mathbf{E}_Y = -\frac{\delta u}{\delta y} \quad (3.12)$$

By the help of ANSYS<sup>TM</sup> (FEM software), all of the previous steps have been implemented and calculated internally.

### **3.3 Particle Swarm Optimization Technique**

#### **3.3.1 Introduction**

Particle swarm is a population-based algorithm, originally developed by the social psychologist James Kennedy and the electrical engineer professor Russell C. Eberhart [41].

PSO algorithm was inspired from the behaviour of animal's societies such as bird flocking that don't have any leader in their group. Naturally, finding food by a flock of animals that have no leaders will happen randomly by following one of the members of the group that has reached the closest position with a food source (potential solution). Simultaneously, the flocks will achieve their best condition by communicating with members who already have a better (closest) position. The member which has a better condition will inform it to its flocks and the others will move to that place simultaneously. This process will keep happening repeatedly until the best conditions or a food source discovered. The criteria of PSO algorithm in finding the optimal values follows the work behaviour of this animal society [42].

The algorithm is widely used and rapidly developing for its easy implementation and the few particles required for optimization process. Moreover, the method can be applied to optimization problems which have large dimensions, and has no overlapping and mutation

calculation as in (genetic algorithm). On the other hand, the stochastic variability of the PSO results is very high for some problems [43]. Based on the previous argument and owing to the many advantages of PSO, this method was chosen to solve the optimization problem.

### 3.3.2 Basic PSO Algorithm

The algorithm starts by forming a random group of individuals called particles move in steps all over a certain region. At each step, the algorithm evaluates the objective function for each individual (particle). After this evaluation, the algorithm calculates the velocity of each particle, and generates the new particles accordingly. Finally, the algorithm will redo the same process until the stopping criteria is met. These steps can be summarized as follows [41] :

#### Symbols:

- $k$  - Iteration number
- $i$  - Particle number
- $g$  - Global particle
- $x_k^i$  - Particle position.
- $v_k^i$  - Particle velocity.
- $v_0^{max}$  - Initial maximum limit of particle velocity .
- $P_k^i$  - Best position of particle  $i$
- $P_k^g$  - Global best position in the swarm.
- $c_1, c_2$  - cognitive and social parameters.
- $w$  - weight parameter.

- $r_1, r_2$  - random numbers between 0 and 1.

The position of each individual particles will be updated from:

$$\mathbf{x}_{k+1}^i = \mathbf{x}_k^i + \mathbf{v}_{k+1}^i \quad (3.13)$$

With velocity updated as follows:

$$\mathbf{v}_{k+1}^i = w \cdot \mathbf{v}_k^i + c_1 r_1 (\mathbf{P}_k^i - \mathbf{x}_k^i) + c_2 r_2 (\mathbf{P}_k^g - \mathbf{x}_k^i) \quad (3.14)$$

### 1) Initialization

- Set the maximum iteration number  $k_{max}$ , and the constants  $c_1$  and  $c_2$ .
- Randomly initialize particle position  $\mathbf{x}_0^i \in D$  in  $R^n$  for  $i = 1, \dots, p$
- Randomly initialize particle velocity  $0 \leq \mathbf{v}_0^i \leq \mathbf{v}_0^{max}$  for  $i = 1, \dots, p$
- Set the iteration number  $k=1$ .

### 2) Optimization

- Evaluate the objective function value  $f_k^i$  using desired space coordinate  $\mathbf{x}_k^i$ .
- If  $f_k^i \leq f_{best}^i$  then  $f_{best}^i = f_k^i$  and  $\mathbf{P}_k^i = \mathbf{x}_k^i$ .
- If  $f_k^i \leq f_{best}^g$  then  $f_{best}^g = f_k^i$  and  $\mathbf{P}_k^g = \mathbf{x}_k^i$ .
- If stopping criteria was met, Terminate the process, if not
- Update the particle velocity  $\mathbf{v}_k^i$  for  $i = 1, \dots, p$
- Update the particle position  $\mathbf{x}_k^i$  for  $i = 1, \dots, p$
- Increment  $k = k + 1$ .
- Go to step (2.i)

The flow chart of Figure 3.2 includes all the mentioned steps of PSO algorithm.

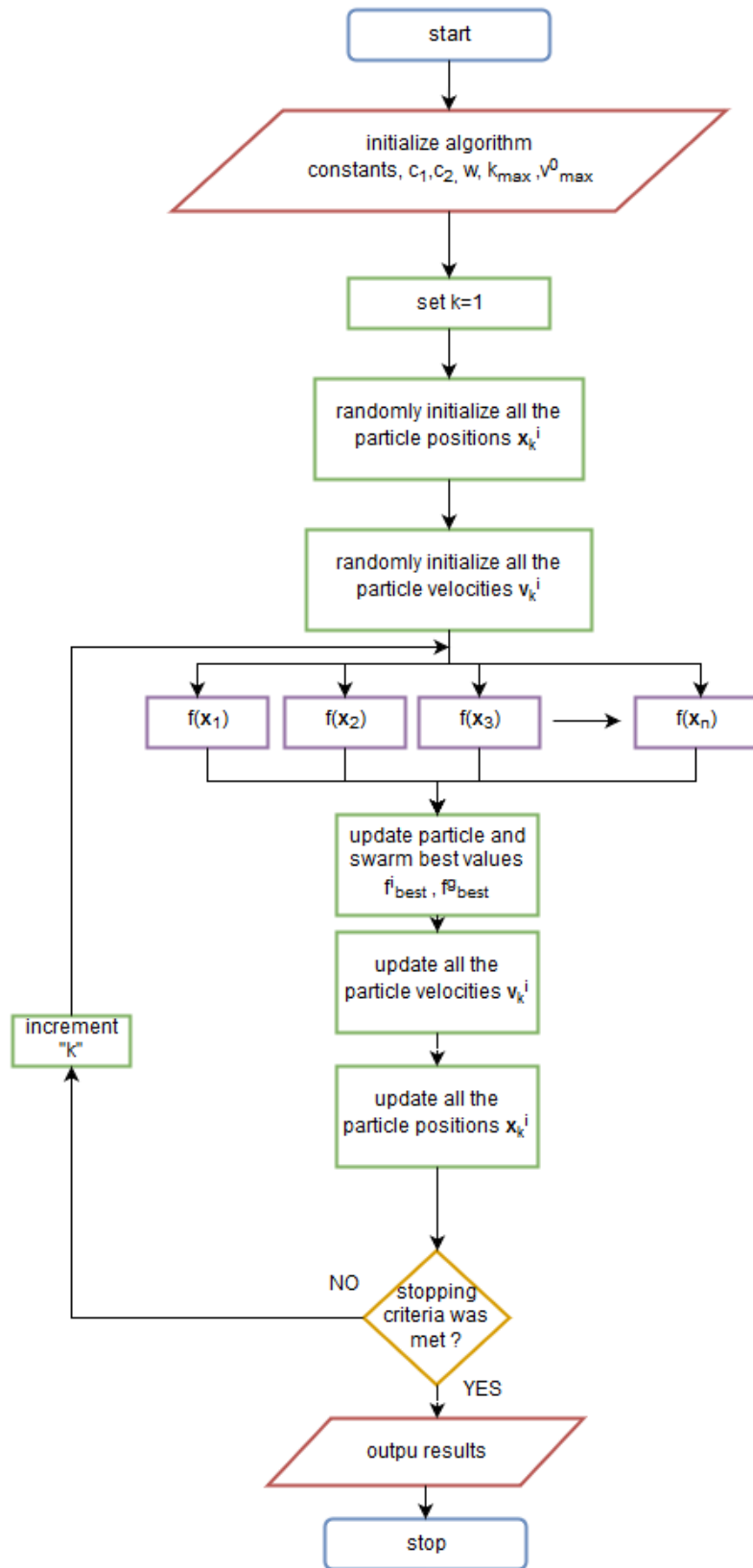


Figure 3.2. flow chart of PSO algorithm

# CHAPTER FOUR

## PROPOSED ALGORITHM OF ELECTRIC FIELD

### CONTROL

#### 4.1 Introduction

After introducing the main aspects in the research methodology chapter, these aspects can be combined together to form the main workflow of this thesis as shown in Figure 4.1

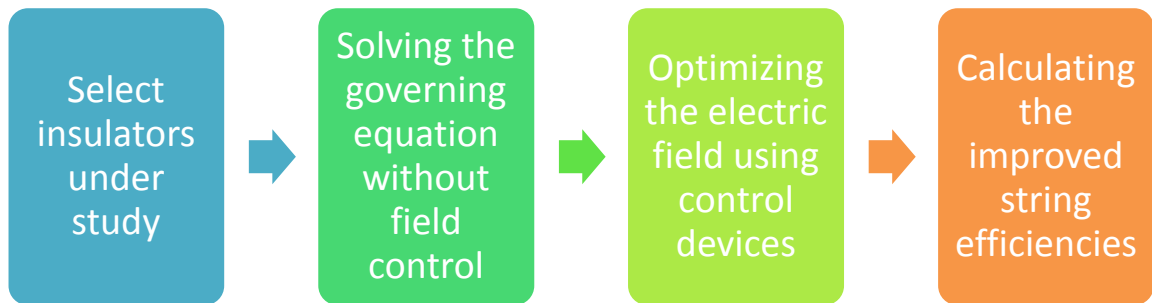


Figure 4.1. Main workflow of the thesis

The work flow starts by selecting the insulators, these insulators are porcelain, glass and SiR. However, detailed discussions about these insulators will be given in the next chapter. The next step is to evaluate the electric field problem without any electric field control under contamination using (FEM) by ANSYS<sup>TM</sup>. After that, based on the obtained electric field profiles, two electric field control devices will be used to minimize the maximum

electric field around these insulators. In order to optimize these devices, PSO algorithm provided by MATLAB<sup>TM</sup> is used. However, to do such optimization, an interface between ANSYS<sup>TM</sup> and MATLAB<sup>TM</sup> softwares is needed first, which will be discussed in details in the upcoming section. Finally, the enhanced electric field profiles will be measured in terms of string efficiency and percentage of electric field reduction.

## **4.2 Proposed Algorithm**

As mentioned earlier, electric field and voltage distributions along insulator's surface were generally evaluated using finite element method (FEM) via ANSYS<sup>TM</sup> software. The electric field control devices i.e (corona ring and arc horn) were optimized based on their own parameters. The optimization parameters for corona ring include: the ring radius (R), distance from high voltage end (H) and ring thickness radius (D). On the other hand, the Arc horn has only two parameters i.e x-position (X) and y-position (Y), as shown in Figure 4.2 (a, b, c and d).

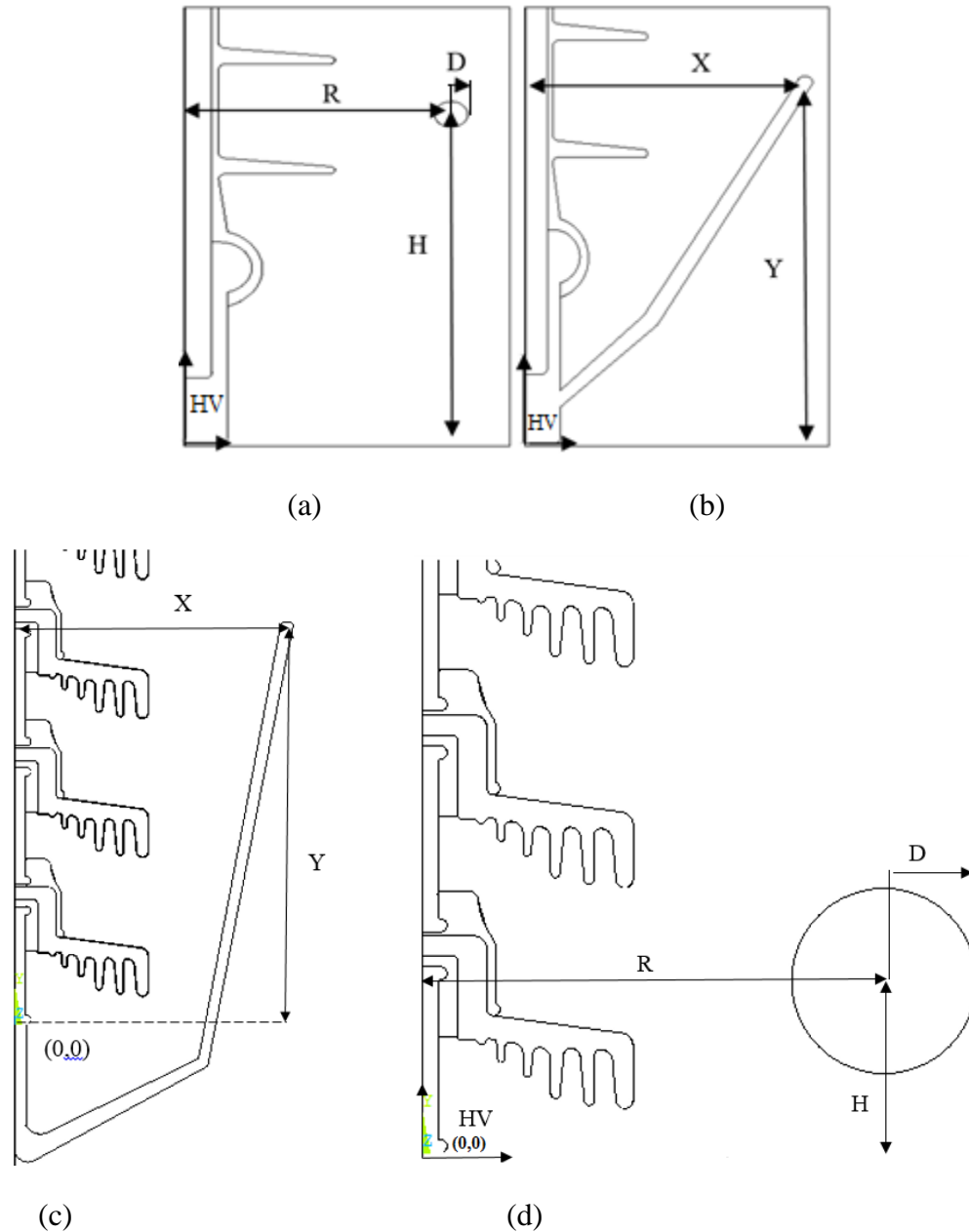


**Figure 4.2. Electric field control devices configuration, [SiR : a) Corona Ring. b) Arc Horn.] [Porcelain and glass: c) Corona Ring d) Arc horn]**

The optimal goal is to find the positions or/and dimensions which give the optimal reduction of the electric field. The optimization process is based on mutual data communication between ANSYS<sup>TM</sup> and MATLAB<sup>TM</sup> softwares, as shown in Figure 4.3.

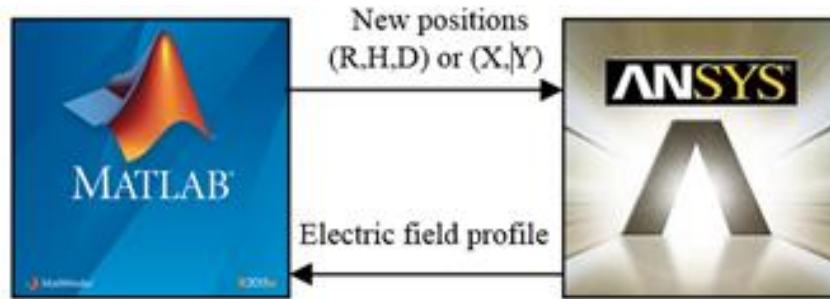


Figure 4.3. MATLAB™ and ANSYS™ interface

ANSYS™ is used to evaluate the electric field governing equations while MATLAB™ is used to run the Particle Swarm optimization algorithm.

The objective function ( $J$ ) is to minimize the maximum electric field ( $E_{max}$ ) along the insulator's surface as shown in (4.1).

$$J = \text{Min} \{ E_{max} \} \quad (4.1)$$

Subject to:

$$X_{min} \text{ or } R_{min} \leq X \text{ or } R \leq X_{max} \text{ or } R_{max}$$

$$Y_{min} \text{ or } H_{min} \leq Y \text{ or } H \leq Y_{max} \text{ or } H_{max}$$

$$D_{min} \leq D \leq D_{max} \quad (4.2)$$

Mutating between MATLAB™ and ANSYS™ softwares is accomplished according to the block diagram shown in Figure 4.4. The key element to make such interconnection possible was by using (MACRO) file. The (MACRO) file contains the set of commands generated by ANSYS™ user interface in order to do specific tasks namely; reading the parameters generated by the optimization process, importing the insulator model, assign the proper

materials attribute, meshing, setting the boundary conditions and finally solving and exporting the results to MATLAB™.

Thus, the main steps of the proposed algorithm for electric field control can be given as:

1. Deciding which control device to be used, Arc horn or Corona ring.
2. Based on the previous choice, the parameters will be decided and the simulation can start.
3. In the beginning, MATLAB™ will start the PSO algorithm and generate the initial set of solutions.
4. MATLAB™ will export these solutions in the format of “*variable.var*”.
5. MATLAB™ will run the MACRO file to drive and communicate with ANSYS™.
6. MACRO file will command ANSYS™ to read the new set of variables generated by MATLAB™ and then solve and export the electric field in “.txt” file.
7. MATLAB™ will call the electric field “.txt” file and evaluates the fitness value of the generated set of solution.
8. MATLAB™ will generate the new set of solutions based on the previous results.
9. The steps from 4 to 8 will be repeated until the solution converges.
10. Finally, the optimal parameters will be provided as [R, H, D] in the case of Corona ring and [X, Y] in the case of Arc horn.

The detailed flow chart including the optimization process is also shown in Figure 4.5.

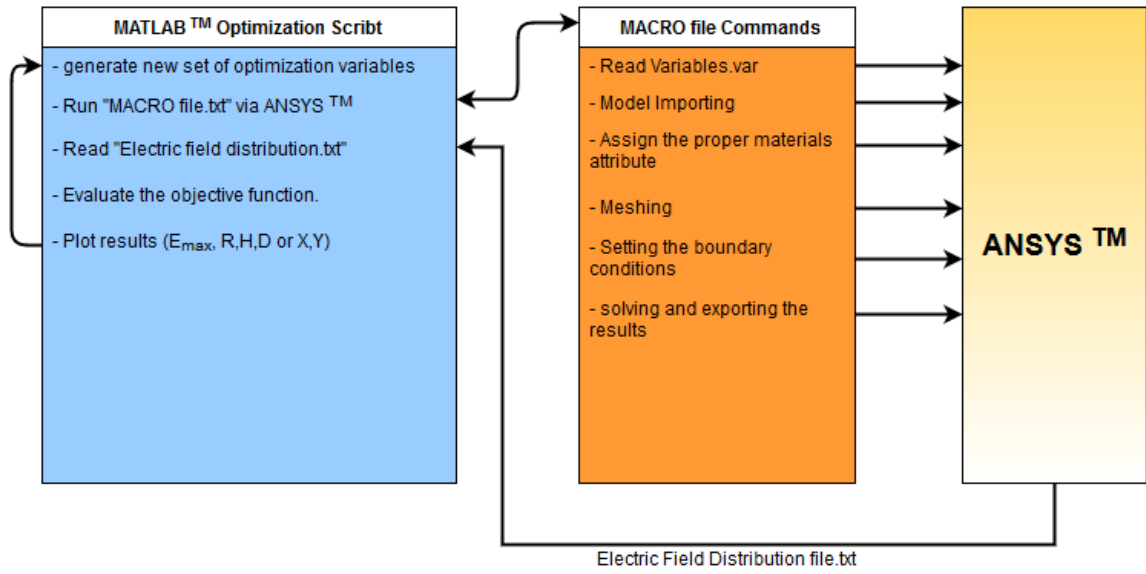


**Figure 4.4. Using the MACRO file in the interfacing process**

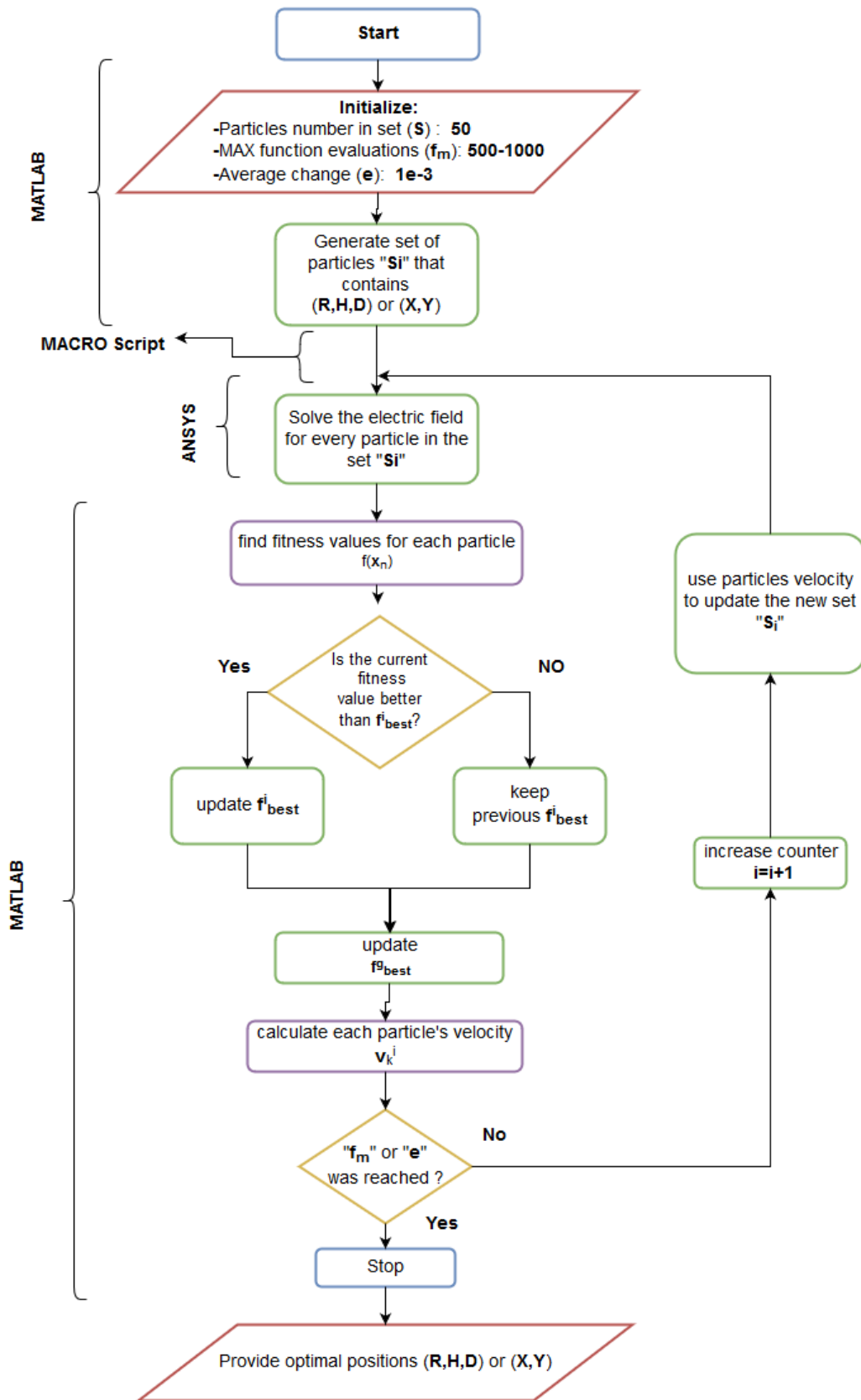


Figure 4.5. Flow chart of solution process

# CHAPTER FIVE

## INSULATOR TESTING AND STUDY CASES

### 5.1 Insulator Models

In order to study the performance of insulators under HVDC and to include as many cases as possible, different designs of porcelain, glass and SiR insulators were chosen based on what has been used in the kingdom of Saudi Arabia, as well as the available drawings from the literature, as shown in Figure 5.1 and Figure 5.2. The insulators design parameters are summarized in Table 5.1 and Table 5.2. The material properties including the relative permittivity and electric conductivity are shown in Table 5.3. For contamination material's properties, the considered ESDD levels with their corresponding conductivities were taken from actual measurements made in the eastern province of the kingdom of Saudi Arabia [44], and listed in Table 5.4.

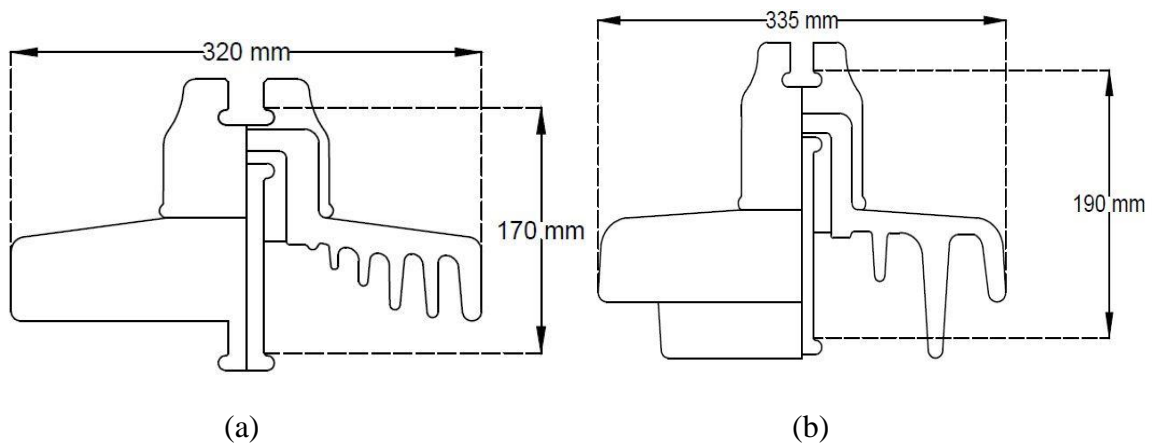
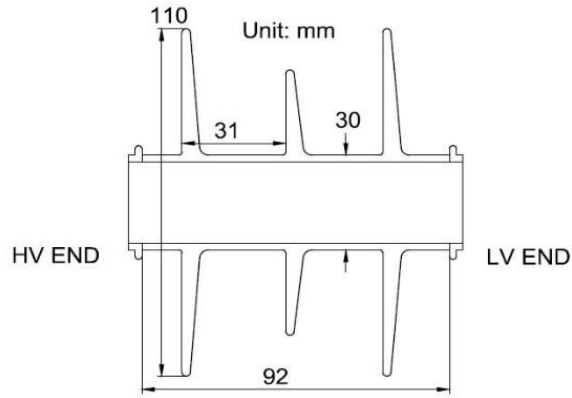
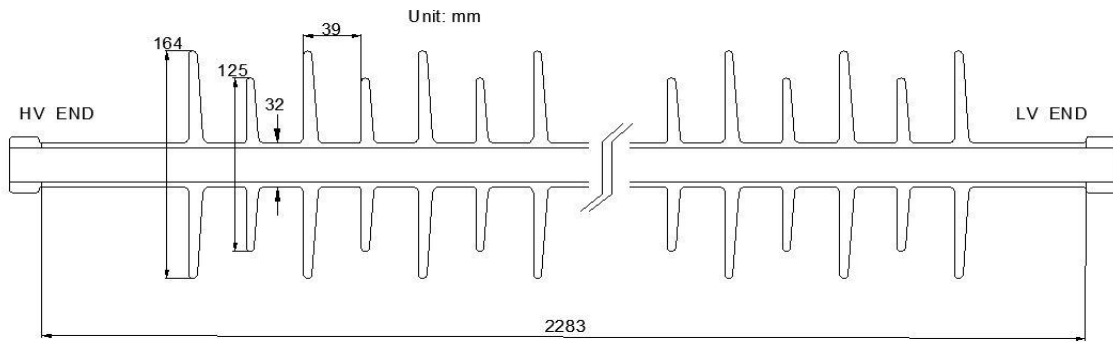


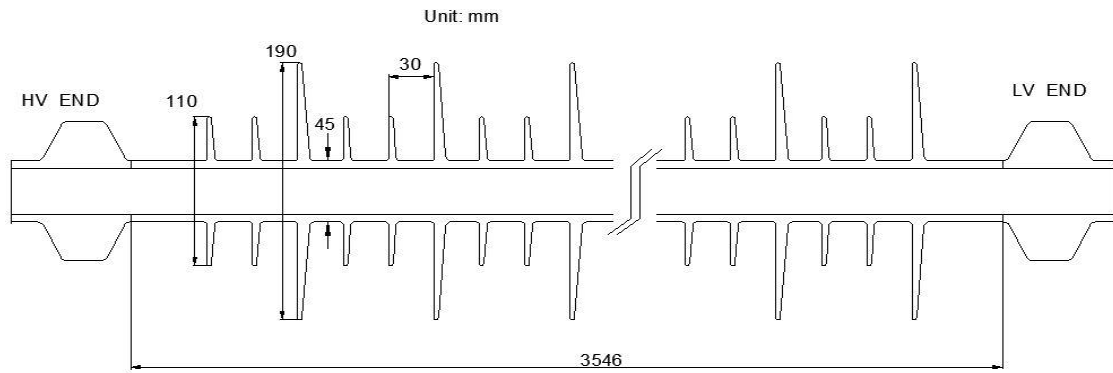
Figure 5.1. Configurations of insulators, a) porcelain insulator (A) b) glass insulator (B)



(1)



(2)



(3)

Figure 5.2. Configurations of insulators 1) 15kV SiR (C), 2) 300 kV SiR (D), 3) 500 kV SiR (E)

**Table 5.1. Dimensions of porcelain and glass insulators**

Insulator Number	Insulator name	material	Configuration height (mm)	diameter (mm)	Leakage distance (mm)
A	160KN	Porcelain	170	320	533
B	F 16 P 13/160	Glass	190	335	560

**Table 5.2. Dimensions of SiR insulators**

Insulator Number	Configuration height H (mm)	Leakage Distance L (mm)	Rod diameter (mm)	Shed spacing (mm)	No. of sheds N1/N2	L/H
C	92	300	30	31	2/1	3.26
D	2283	7865	32	39	28/27	3.44
E	3546	13546	45	30	39/78	3.82

**Table 5.3. Materials properties**

Material	Relative Permittivity $\epsilon_r$	Conductivity $\sigma$ s/cm
Air	1	1 e-16
Porcelain	5.7	1 e-15
Glass	7.5	1 e-15
Forged steel	1000	5.9 e05
Silicone rubber	4.3	1 e-15
Fiberglass	7.1	1 e-15
Arc Horn	1000	5.9 e05
Corona Ring	1000	5.9 e05
Water droplet	80	1 e-04

**Table 5.4. Contamination severity and respective conductivities**

Conductivity ( $\mu\text{S}/\text{cm}$ )	ESDD $\text{mg}/\text{cm}^2$	$\Omega \cdot \text{cm}$	Severity level as for IEC 815 [44]
130.7	0.0133	7651.109411	Very light
183.2	0.019	5458.515284	light
1390	0.1449	719.4244604	medium
3605	0.399	277.3925104	heavy

## 5.2 Case Studies

In order to study the impact of contamination as well as the electric field control devices on electric field and voltage distributions associated with HVDC insulators, different case studies have been considered, arranged as follow:

To begin with, single unit of porcelain insulator (A) was subjected to three different contamination scenarios given in Table 5.5 under 15 kV DC.

**Table 5.5. Pollution scenarios**

Pollution scenario	Description
Scenario 1 “S1”	Clean surface
Scenario 2 “S2”	Non- uniform (heavy) polluted layer
Scenario 3 “S3”	Non- uniform water droplet
Scenario 4 “S4”	Non- uniform (heavy) polluted layer + non-uniform water droplet

After that, for both porcelain and glass insulators (A & B), fifteen units string were considered and subjected to 200 kV. For each string, the electric field and voltage

distribution profiles were evaluated for clean and contaminated conditions, and the electric field control devices were introduced under contaminated conditions.

For the case of silicon rubber insulators, the same contamination scenarios in Table 5.5 were also applied into insulator (C) under 15 kV stress.

As for insulator (D), a continuous contamination profile was considered on the first 300 mm creepage distance with resistivity of  $277.3 \Omega \text{ cm}$  under 300 kV. This contamination scenario was inspired by the fact that insulators under HVDC attracts more contamination near the HV end fitting. Moreover, for this particular insulator, five different electric field control schemes namely; single corona ring, single arc horn, double corona rings, double arc horns and a combination between corona ring and arc horn, were tested and compared with each other under the same contamination condition.

Finally, the longest rod insulator (E) was subjected to a continuous contamination for the first 700 mm creepage distance with resistivity of  $277.3 \Omega \text{ cm}$  and stressed by 500 kV, with and without corona ring control.

## CHAPTER SIX

### RESULTS AND DISCUSSIONS

#### 6.1 AC and DC electric field comparison

It has been found from the literature [16] that insulators subjected to direct current voltage attract 20% more contamination than under AC. This phenomena is due to the fact that DC voltage produces a steady monopole electric field which continuously attracts the ions and other surrounding particles. On the other hand in the case of AC voltage, electric field keeps alternating which makes the attraction process less effective than under DC voltage. To have a fair comparison between AC and DC electric fields associated with the insulators, the pollution level of single unit of insulator (A) subjected to 15 kVDC voltage was increased by 20% as compared to the contamination level under AC. Figure 6.1 shows clearly that there is a noticeable difference between AC and DC electric fields. In addition, under pollution condition, insulator (A) appears to have higher electric field under DC voltage near HV and LV ends than under AC. This agrees with Gorur's findings [36]. Thus, more attention should be given to the insulators subjected to HVDC. As such, the following sections investigate the performance of HV insulators under contaminated conditions subjected to DC stress and possible ways to control its electric field.

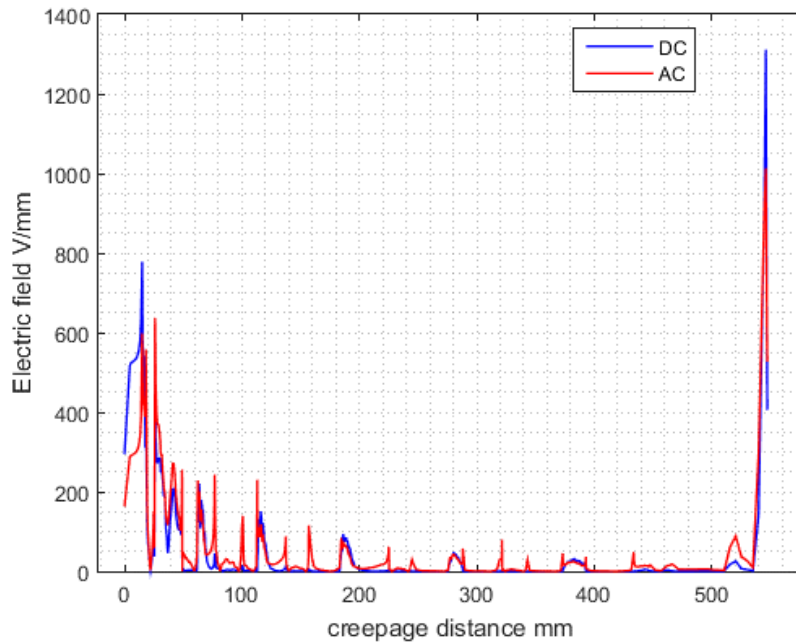


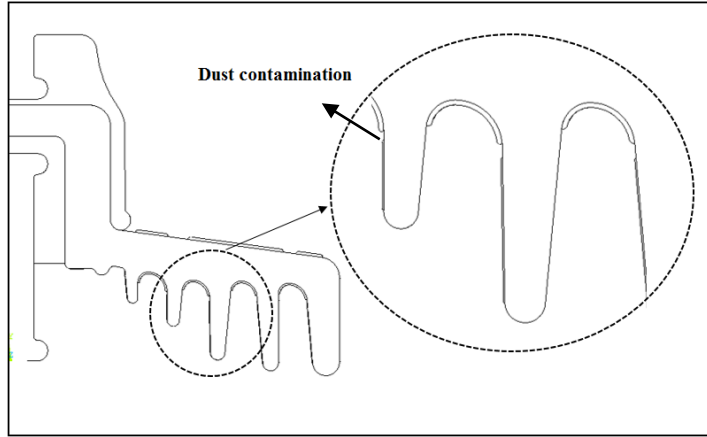
**Figure 6.1. AC and DC electric field comparison**

## **6.2 Performance under contaminated conditions and DC stress**

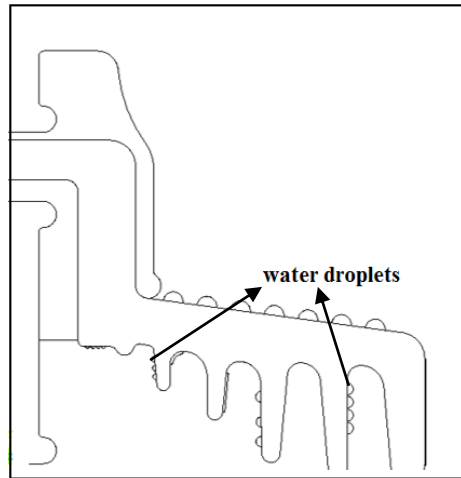
In this section onwards, the electric field governing equations given in (3.7) and (3.8), are solved using FEM. The boundary conditions at HV end were starting from 15 kV for single unit insulator and 200 kV for fifteen unit string, and zero volt at LV end. For SiR insulators, three different classes of voltage were considered i.e 15, 300 and 500 kV at HV end and zero volt at LV end. For each insulator type, the electric field and voltage profiles were evaluated under clean and contaminated conditions.

### **6.2.1 Porcelain insulator (A) – Single unit**

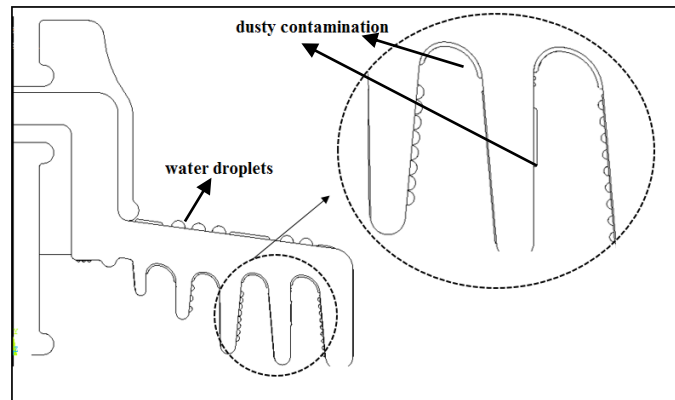
Figure 6.2 illustrates the four different pollution scenarios listed in Table 5.5. As it can be seen from Figure 6.3, combined contamination as well as non-uniform pollution scenarios, have shown an observable effect on the electric field profile. This effect appears as an increase in the maximum electric field value near HV and LV ends. On the other hand, water droplets case has slightly affected the maximum as compared to previous cases, together with some oscillation disturbances in certain areas.



(a)



(b)



(c)

Figure 6.2. a) Non-uniform pollution (S2). b) Non-uniform water droplet (S3) c) Non-uniform water droplet + pollution (S4).

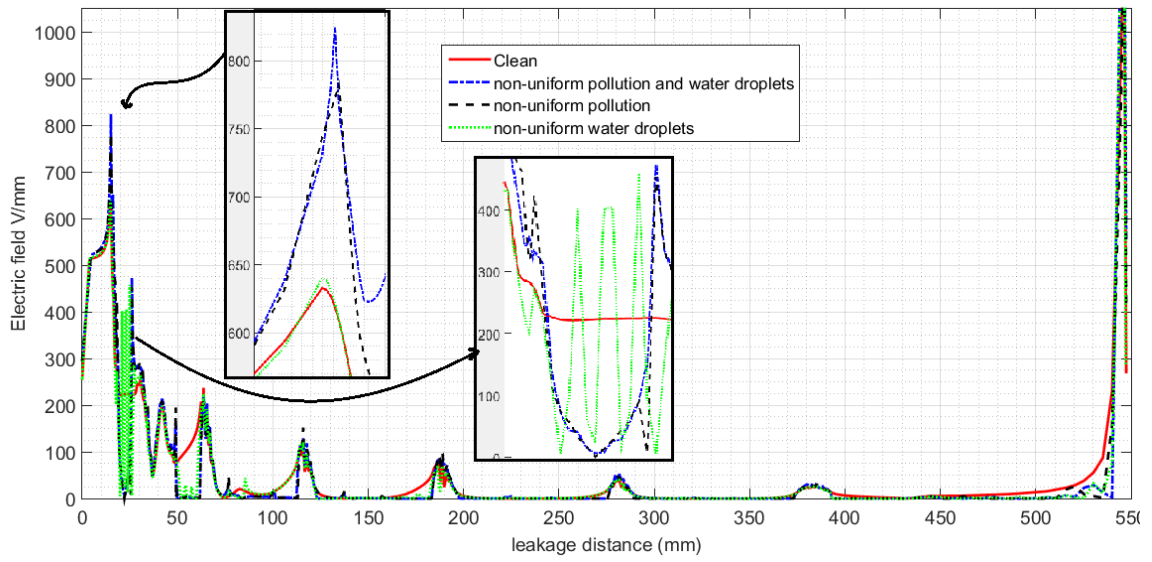


Figure 6.3. Corresponding electric fields of contamination scenarios

### 6.2.2 Porcelain insulator (A) – 15 units string

In order to investigate the electric field and voltage distribution profiles along multi-units insulator, a porcelain string consisting of fifteen units was assembled as shown in Figure 6.4 (a). The electric field and voltage profiles were obtained on three different paths as shown in Figure 6.4 (b). These paths were taken at the string's central ax (PATH 1), at the pollution junction (PATH 2) and at insulator's tangential edge (PATH 3).

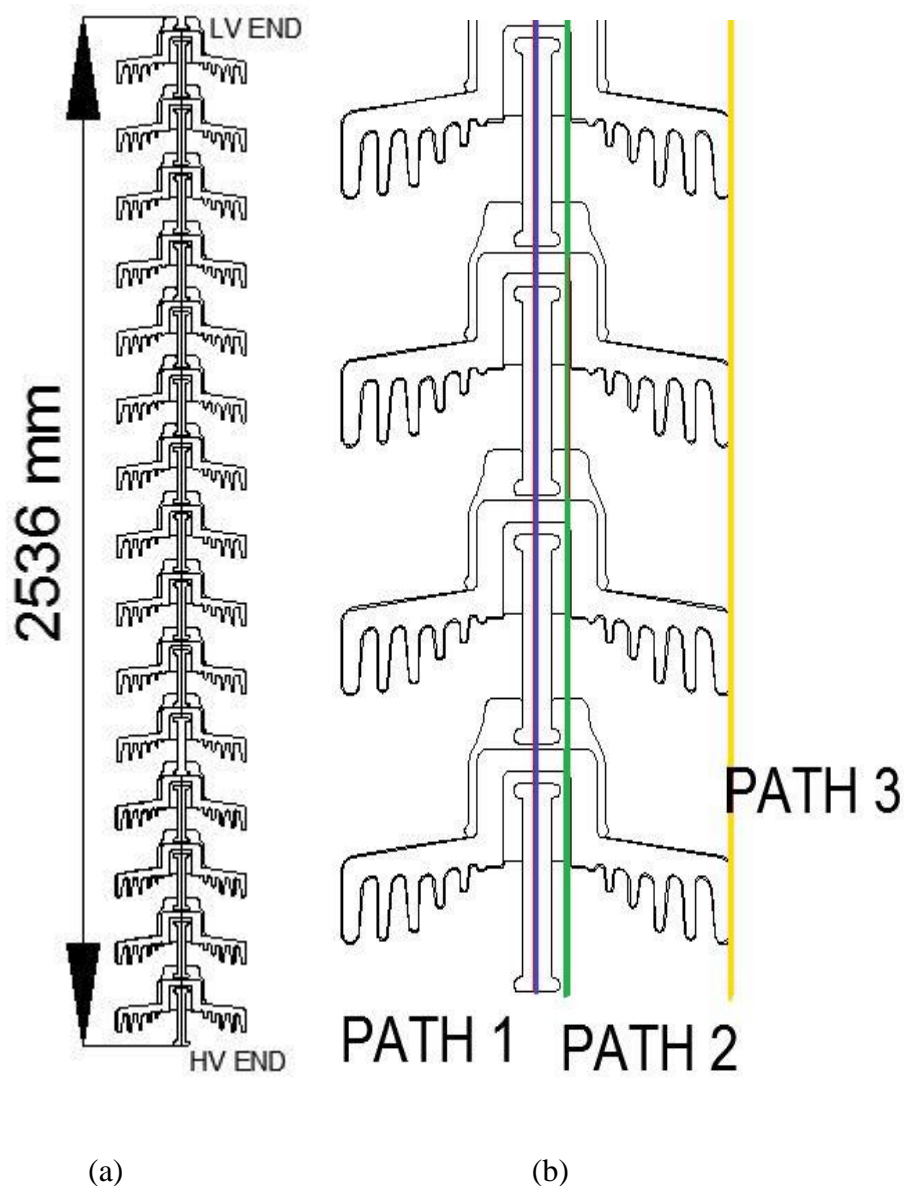
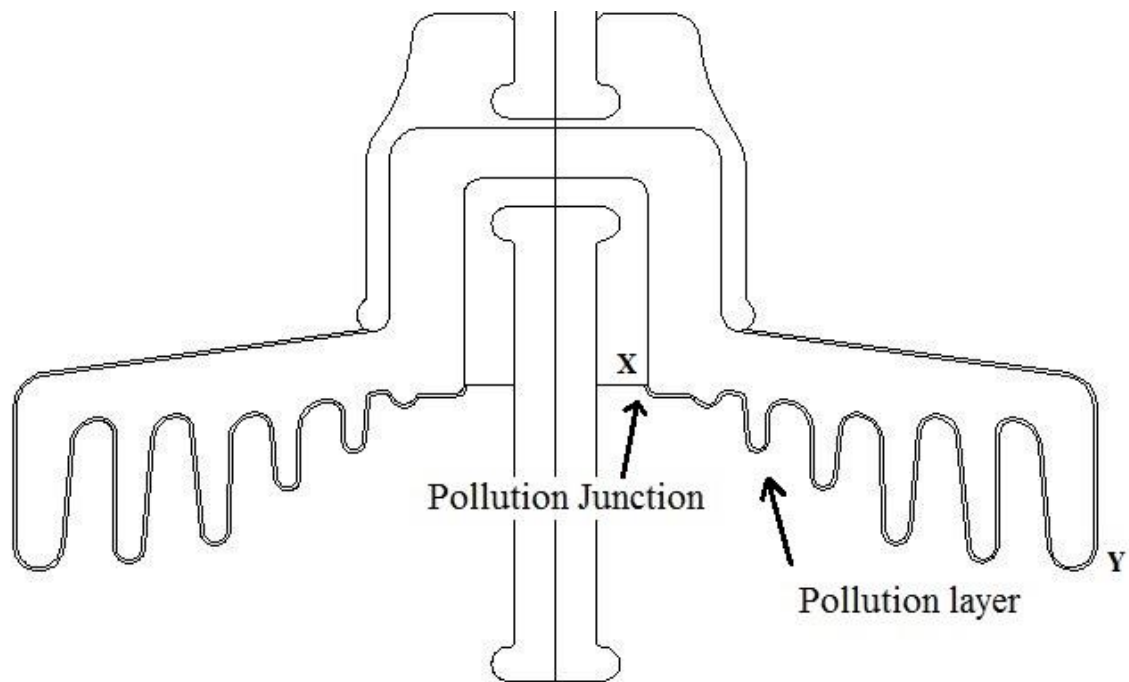


Figure 6.4. Fifteen units string of insulator (A). a) Complete string. b) Considered paths

In order to simulate the practical situation of pollution distribution under DC voltage, Porcelain and glass insulators were subjected to different contamination levels as given in Table 5.4. The first, second, third and fourth units are heavy, medium, light and very light polluted, respectively each with thickness of 1 mm, Figure 6.5. This pollution profile matches to a good extent the practical pollution situation in eastern province of Saudi Arabia.



**Figure 6.5. Pollution profile along the first insulator (A)**

Figures (6.6 - 6.8) show the electric field along PATHs 1, 2 and 3, respectively. It is clear that the highest electric field is along PATH 2. This shows that when designing and selecting insulators, one has to take care of the highest electric field it may encounter. For completeness, the voltage profiles associated with these PATHs are shown in Figures (6.9 - 6.11). Where the non-uniformity clearly appears near polluted insulators as compared to clean case.

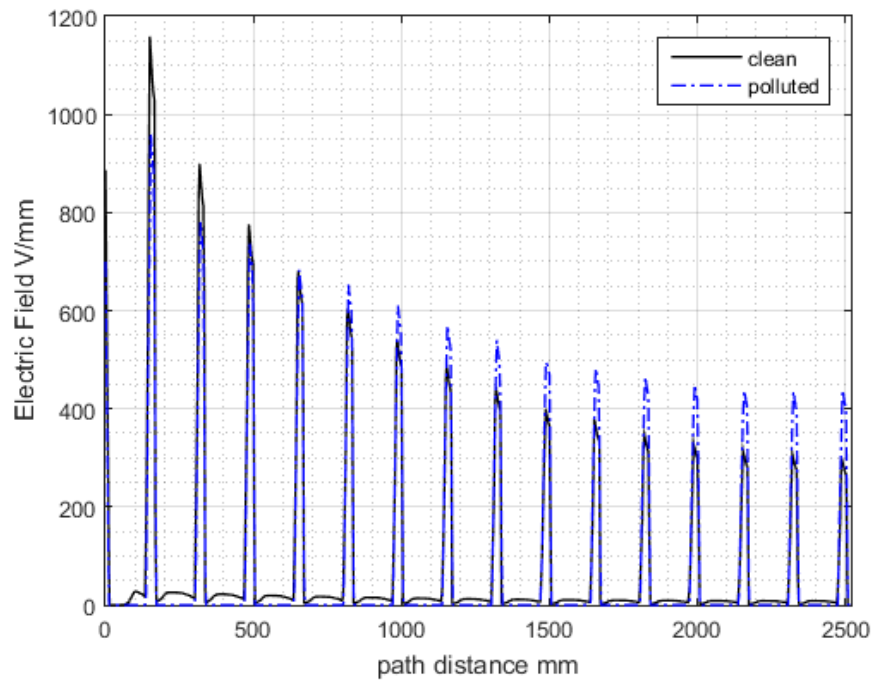


Figure 6.6. Electric field of PATH 1 along the string (A-15)

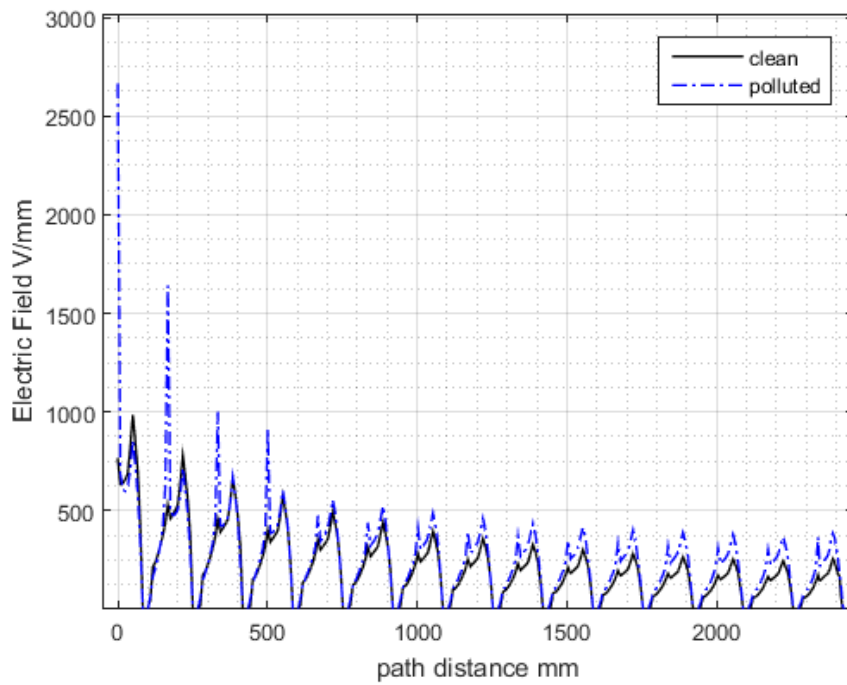


Figure 6.7. Electric field of PATH 2 along the string (A-15)

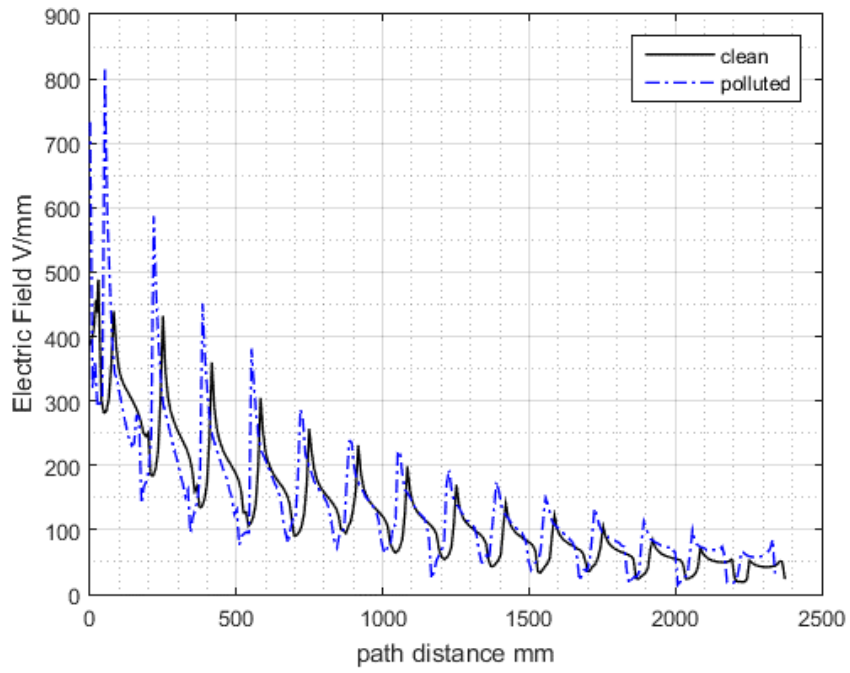


Figure 6.8. Electric field of PATH 3 along the string (A-15)

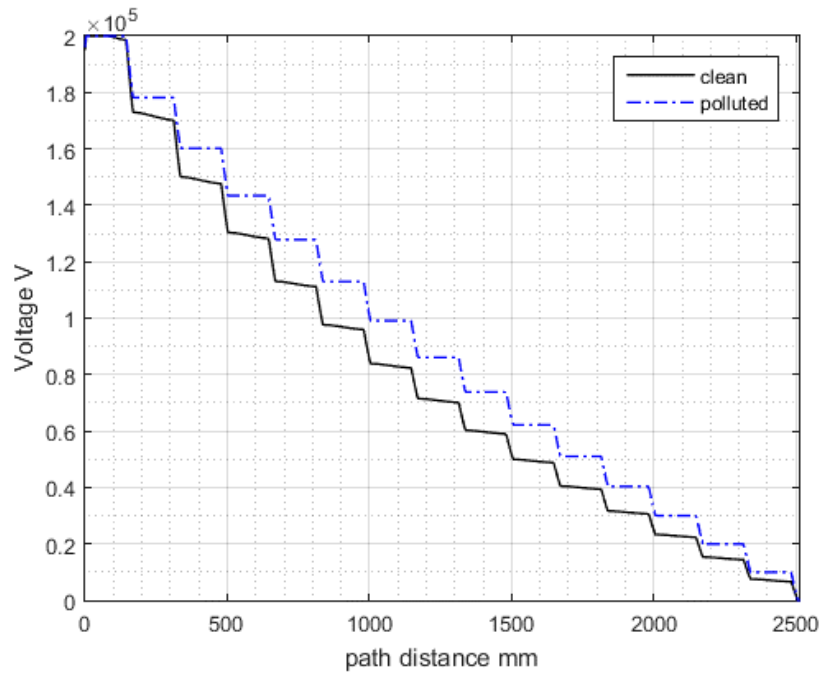
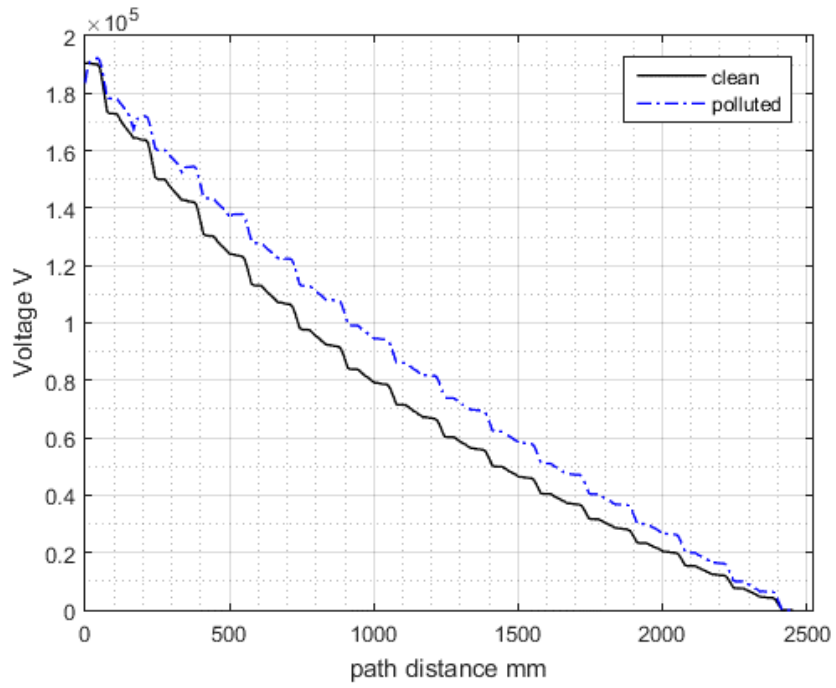
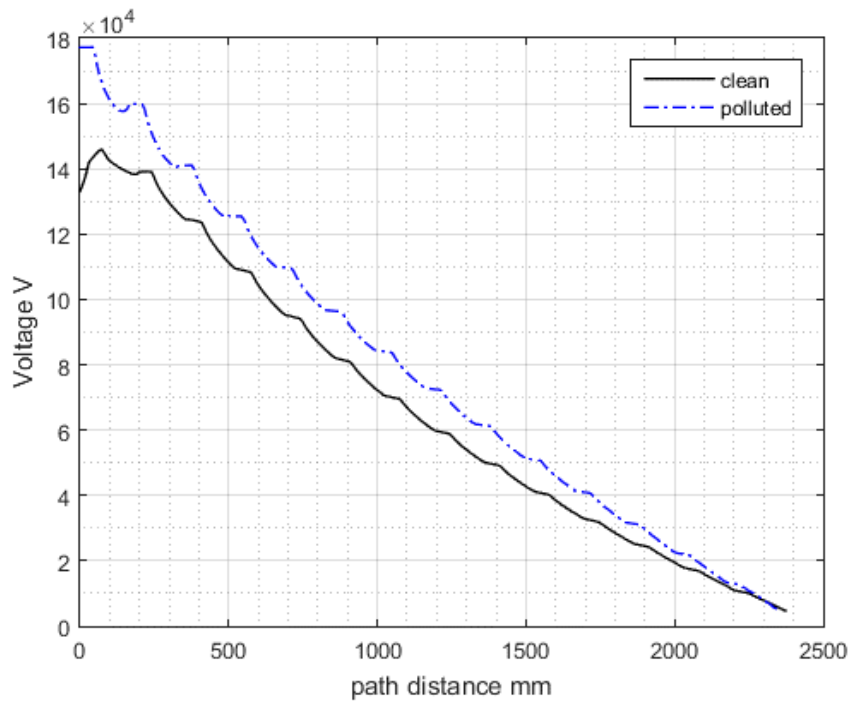


Figure 6.9. Voltage distribution of PATH 1 along the string (A-15)



**Figure 6.10. Voltage distribution of PATH 2 along the string (A-15)**



**Figure 6.11. Voltage distribution of PATH 3 along the string (A-15)**

Additionally, all figures show that units close to HV source have the highest electric field. Therefore, zooming of electric field and potential distribution profiles on the first unit are shown in Figure 6.12 and Figure 6.13, respectively. Two electric field peaks are clear in Figure 6.12 at points **X** and **Y** of Figure 6.5. The first peak of electric field can be attributed to the fact that the pollution is distributed uniformly along insulator's surface, hence it acts as a conduction layer with a uniform voltage profile. The rapid change of voltage causes that spark increase in electric field at point **X**.

On the other hand, the second electric field increase at point **Y**, is due to contact of two different mediums i.e insulator edge and air which will affect the voltage distribution hence electric field profile.

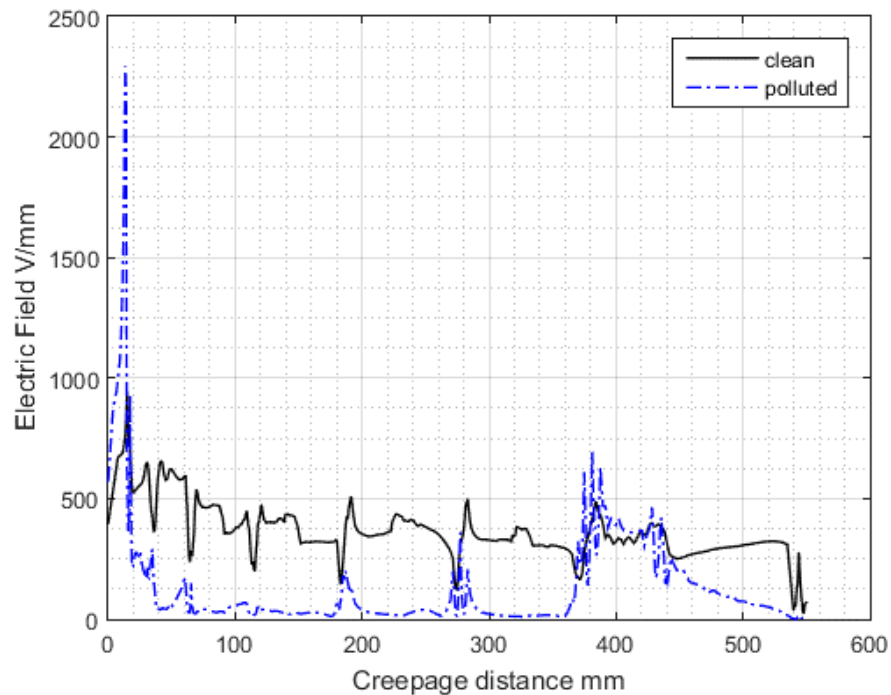


Figure 6.12. Electric field along the surface of the first insulator (A)

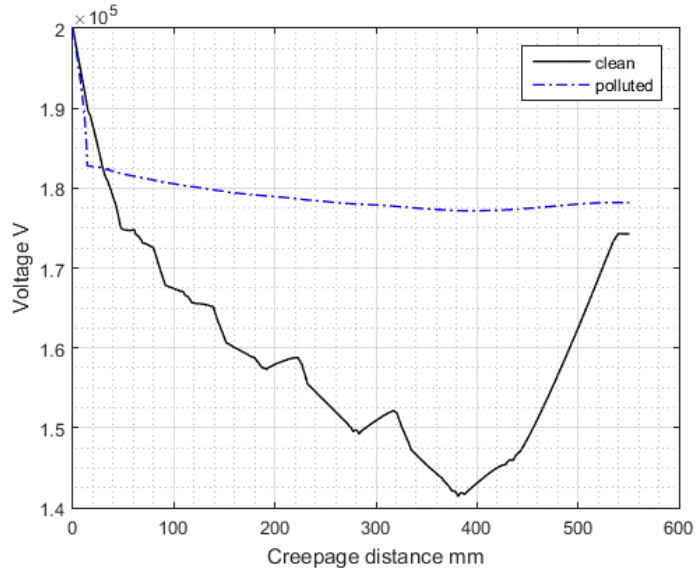


Figure 6.13. Voltage distribution along the surface of the first insulator (A)

For a better comparison, the bar charts in Figure 6.14 (a and b) show the maximum electric field at each unit, under clean and contaminated conditions. It is quite clear from Figure 6.14 (b), that each insulator has been affected by the given pollution profile. Especially, at the first four contaminated insulators along (PATH 2).

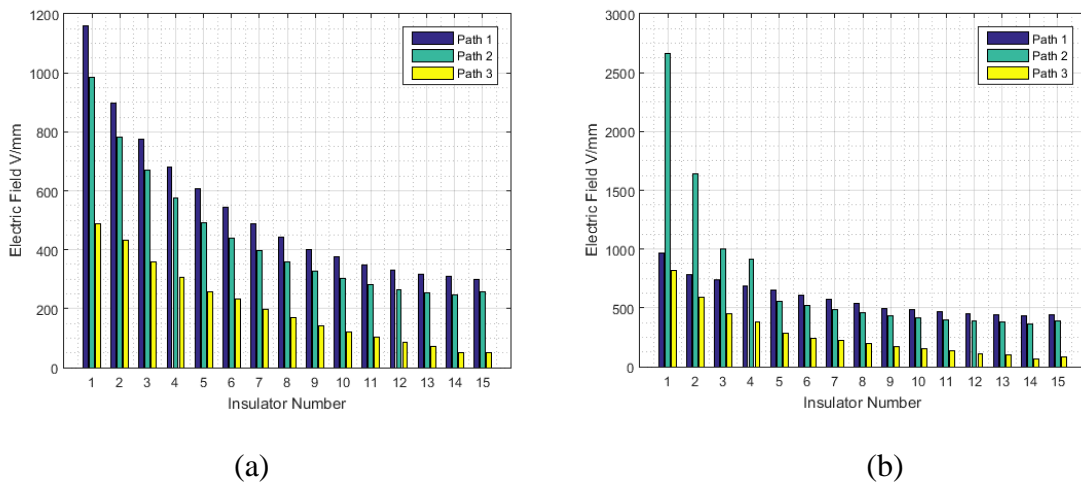


Figure 6.14. Maximum electric field comparison of the three paths. a) clean. b) contaminated

Figure 6.15 was calculated according to equation (6.1). It shows the percentage change in maximum electric field due to contaminated conditions ( $E_C$ ) as compared to clean conditions ( $E_{NC}$ ).

$$\% \text{ Percentage change in } E_{max} = \frac{E_C - E_{NC}}{E_{NC}} * 100 \quad (6.1)$$

The results show that all insulator units have suffered from an increase in the electric field. However, PATH 2 has shown the highest values at first, second, third and fourth insulators, with percentages of 170%, 110%, 50% and 59% respectively. Whereas rest of the string has increased between 10% and 68%.

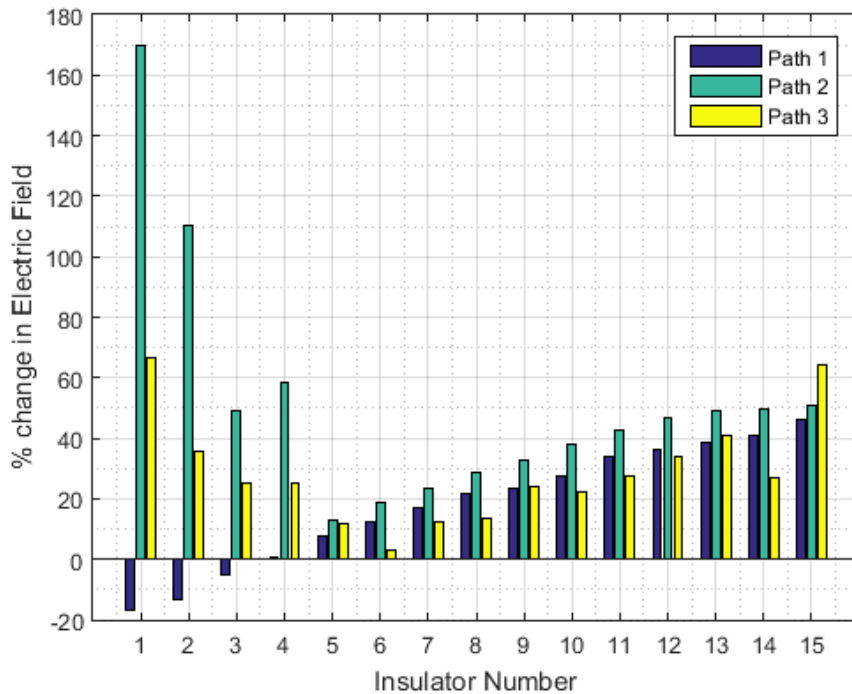


Figure 6.15. Percentage change in maximum electric field due contamination

### 6.2.3 Glass insulator (B) -15 units string

Similarly, for the case of glass insulator, fifteen units string was assembled with same PATHs and pollution profiles used in 6.2.1 as shown in Figure 6.16.

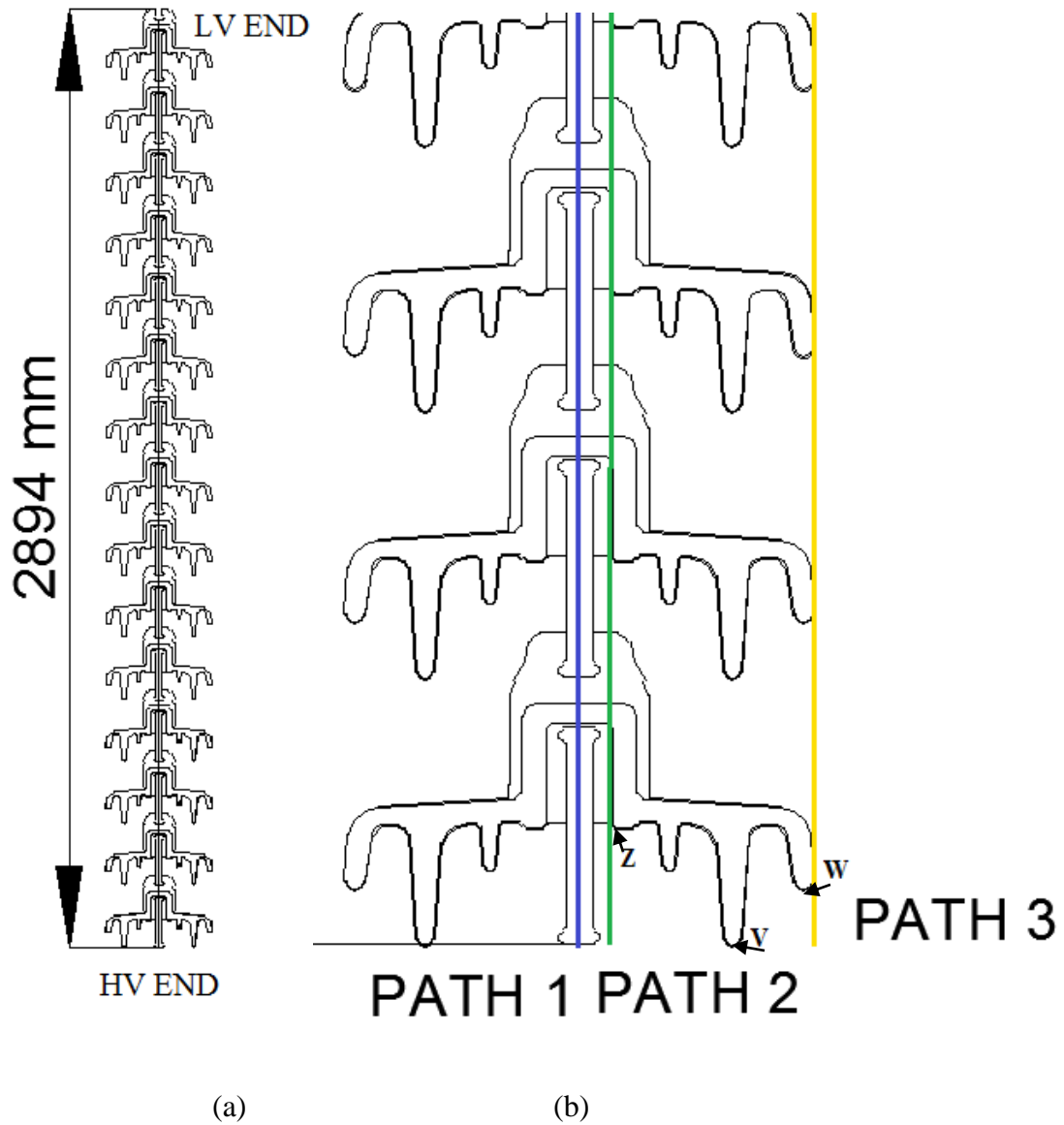
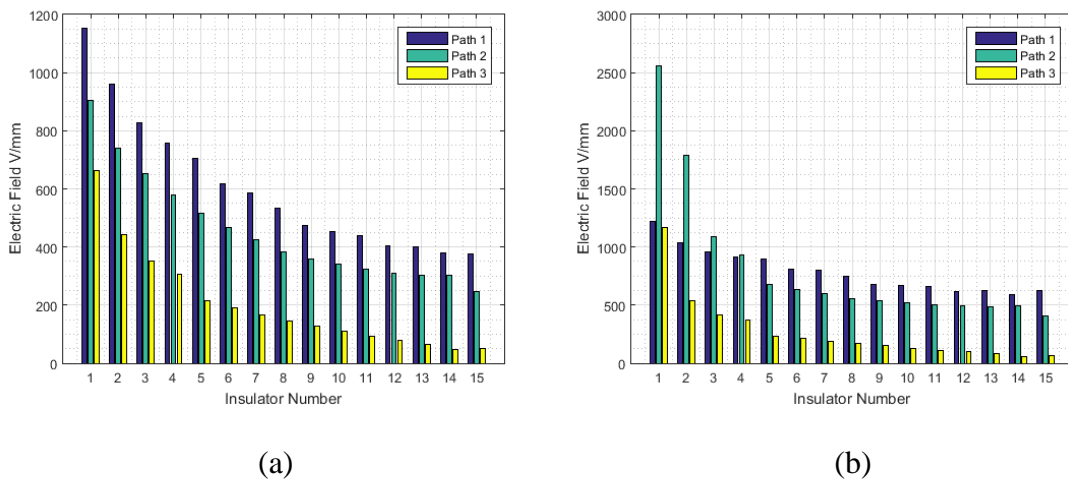


Figure 6.16. Fifteen units string of insulator (B). a) Complete string. b) Considered paths

For comparison, the bar chart in Figure 6.17 (a and b) shows the maximum electric field values for each insulator unit, under clean and contaminated conditions. It is quite clear from Figure 6.17 (b) that each insulator has been affected by the pollution profile, especially the first four contaminated insulators at pollution junction (PATH 2), which also supports our previous conclusion, about looking carefully at this specific region when selecting HV insulators.



**Figure 6.17. Maximum electric field comparison of the three paths. a) clean. b) contaminated**

Figure 6.18 was calculated according to equation (6.1). It shows the percentage change in maximum electric field values due to contaminated conditions as compared to clean case. Similar to porcelain insulator (A), all insulator units have suffered from electric field increase, especially at PATH 2 for the first four insulators with percentages of 183%, 142%, 68% and 61%, respectively. Whereas for the rest of insulator's string, the increases were between 30% and 69%.

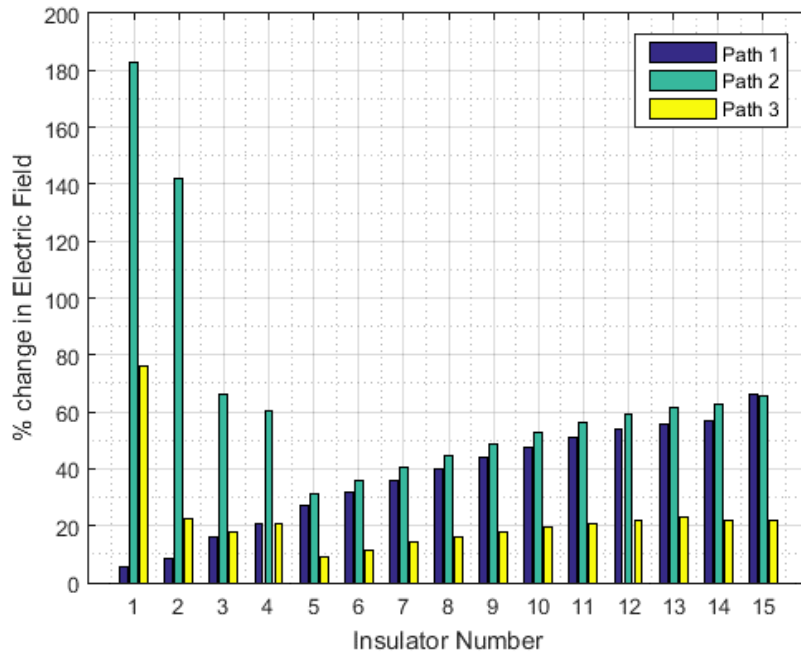


Figure 6.18. Percentage change in maximum electric field due contamination

## 6.2.4 SiR insulators (C-E)

### - The 15 kVDC Insulator (C)

For three sheds SiR insulator (C), different pollution scenarios have been investigated according to Table 5.5, and illustrated in Figure 6.19. As it can be seen from Figure 6.20, the non-uniform pollution scenario has affected the electric field distribution by causing some sharp pulses in certain areas. As for water droplets case, Figure 6.21, this contamination scenario has a clear effect on increasing the electric field distribution. However, Figure 6.22 shows that electric field profile has reached the highest disturbance under combined contamination, as compared to the previous scenarios. On the other hand, Figure 6.23 shows how each pollution scenario has affected the voltage profile. It can be seen that voltage profile is lower at the second shed in case of non-uniform pollution and combined water-pollution as compared to the clean and non-uniform water droplets cases.

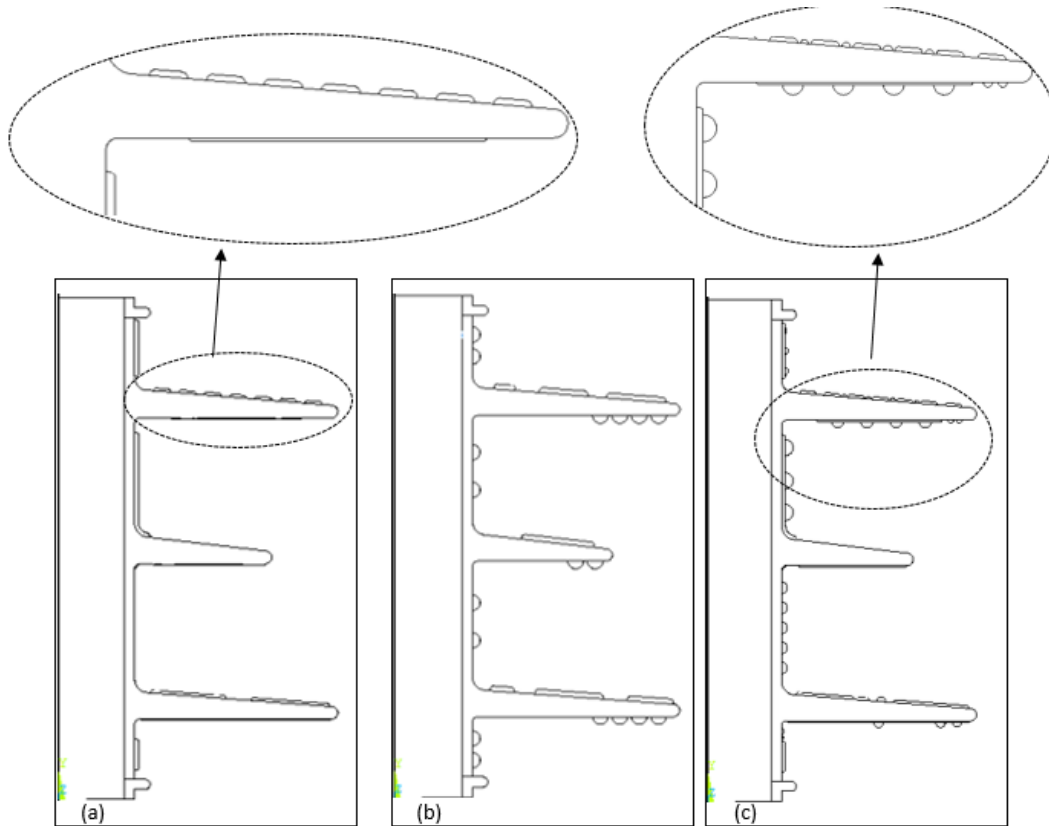


Figure 6.19. SiR insulator (C). a) non-uniform pollution (S2). b) non uniform water droplet (S3). c) non-uniform water+pollution (S4)

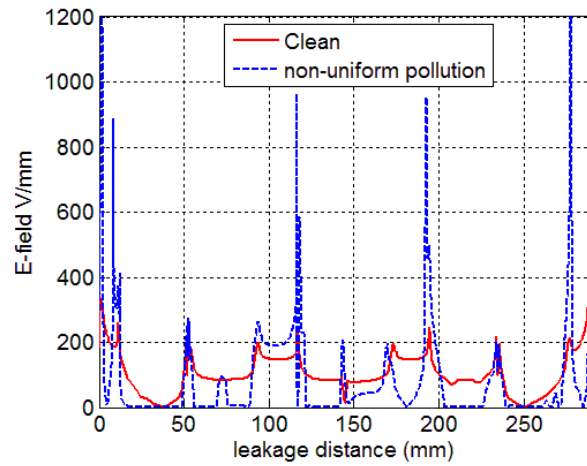


Figure 6.20. Electric field distribution of insulator (C) under non-uniform pollution

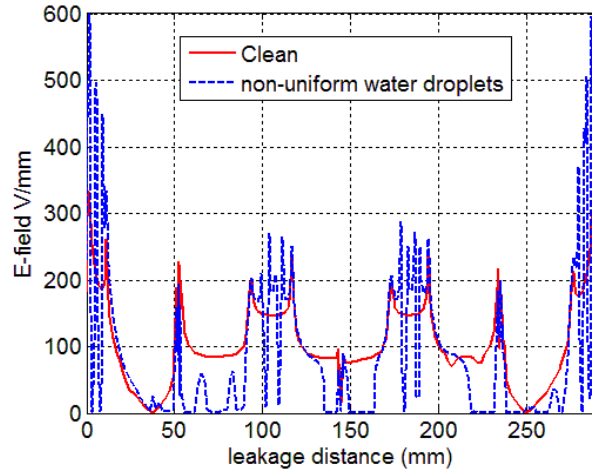


Figure 6.21. Electric field distribution of insulator (C) under non-uniform water droplets

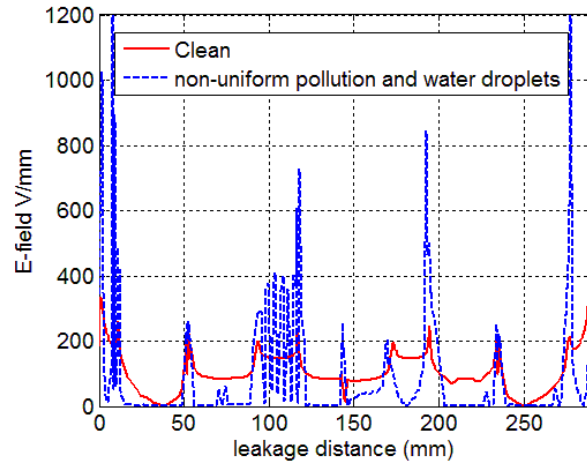


Figure 6.22. Electric field distribution of insulator (C) under combined pollution

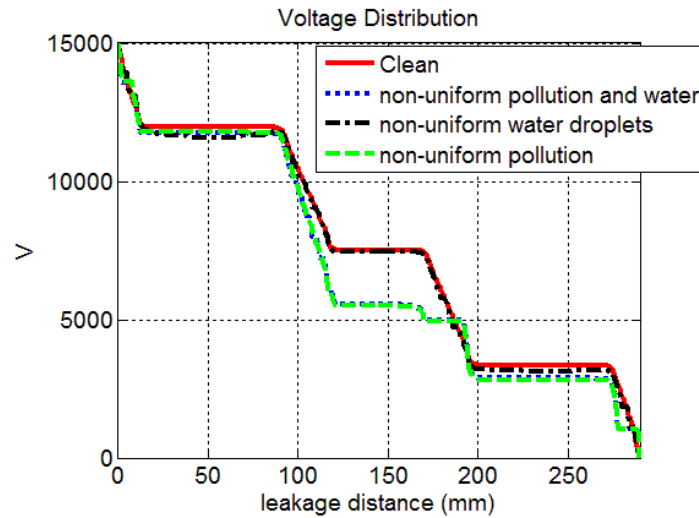


Figure 6.23. Voltage distribution of insulator (C)

- **300 kVDC Insulator (D)**

As for insulator (D), which has 55 sheds, a heavy contamination layer with resistivity of 277.3  $\Omega$  cm was considered, and applied on the first four sheds close to HV end. Figure 6.24 shows electric field distribution along insulator's surface, for both clean and contaminated conditions. The effect of contamination layer clearly appears near HV end, where it reaches a maximum value of 1080 V/mm as opposite to 675.5 V/mm for clean insulator. This corresponds to an increase of 59%. The non-uniformity in the voltage clearly appears near HV end, where the contamination layer is located as shown in Figure 6.25.

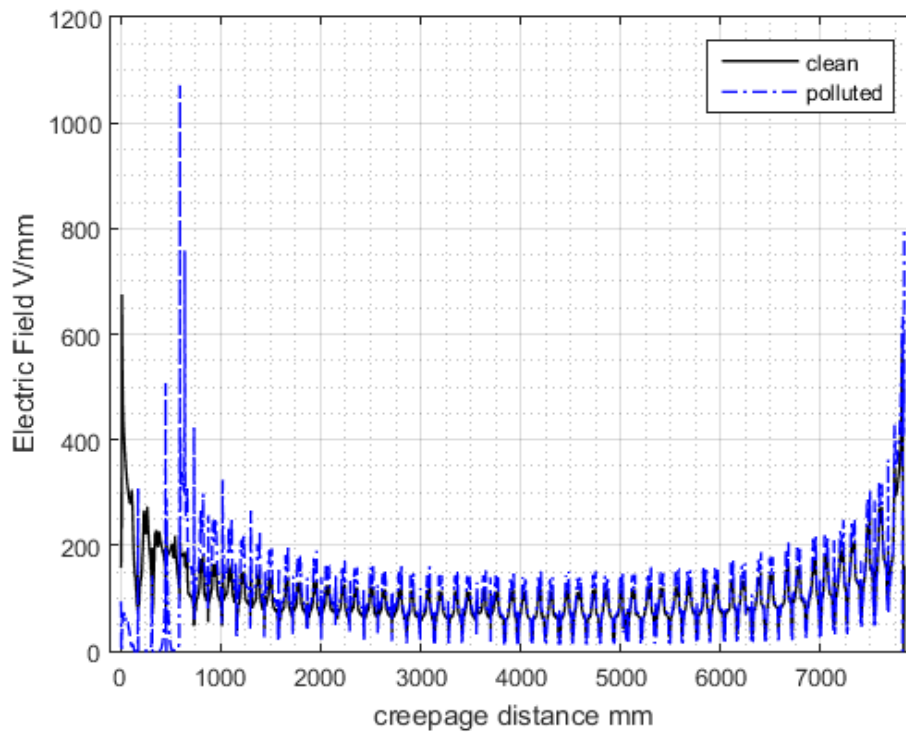


Figure 6.24. Electric field distribution along insulator's (D) surface

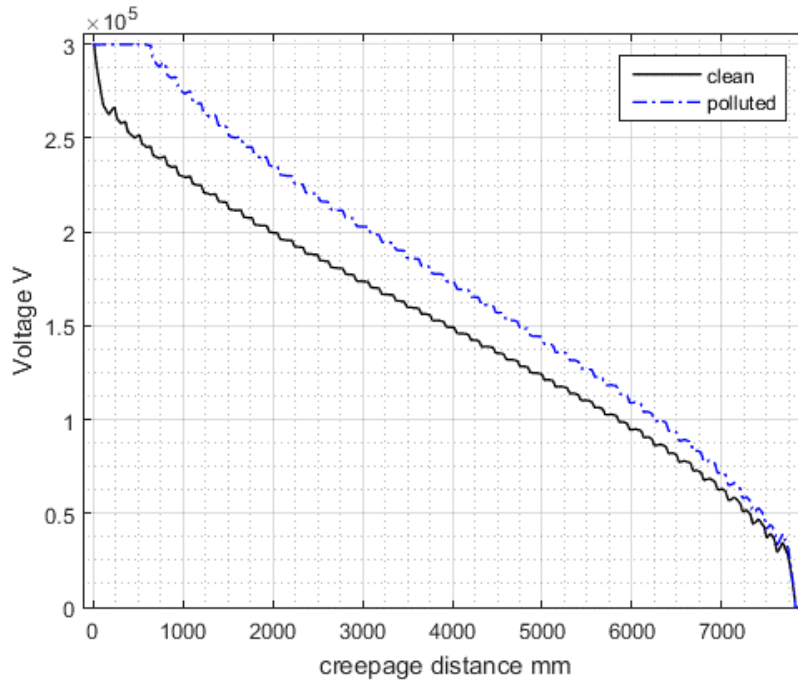


Figure 6.25. Voltage distribution along insulator's (D) surface

- **500 kVDC Insulator (E)**

Similarly for insulator (E), which has 117 sheds, the same contamination layer used in insulator (D) was considered. Figure 6.26 shows the electric field profiles of both clean and contaminated conditions. It can be seen that maximum electric field has reached a value of 912.5 V/mm as compared to 675 V/mm for clean case. Which can be read as an increase of 40.38%. The corresponding voltage distribution shown in Figure 6.27, shows the non-uniformity in voltage near HV end, where the contamination layer is located.

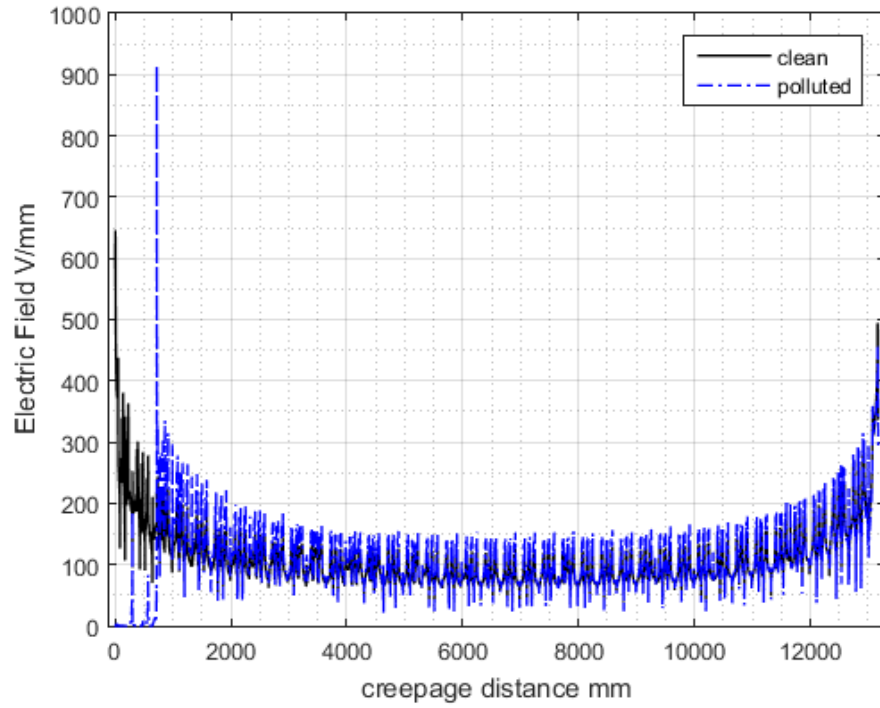


Figure 6.26. Electric field distribution along insulator's (E) surface

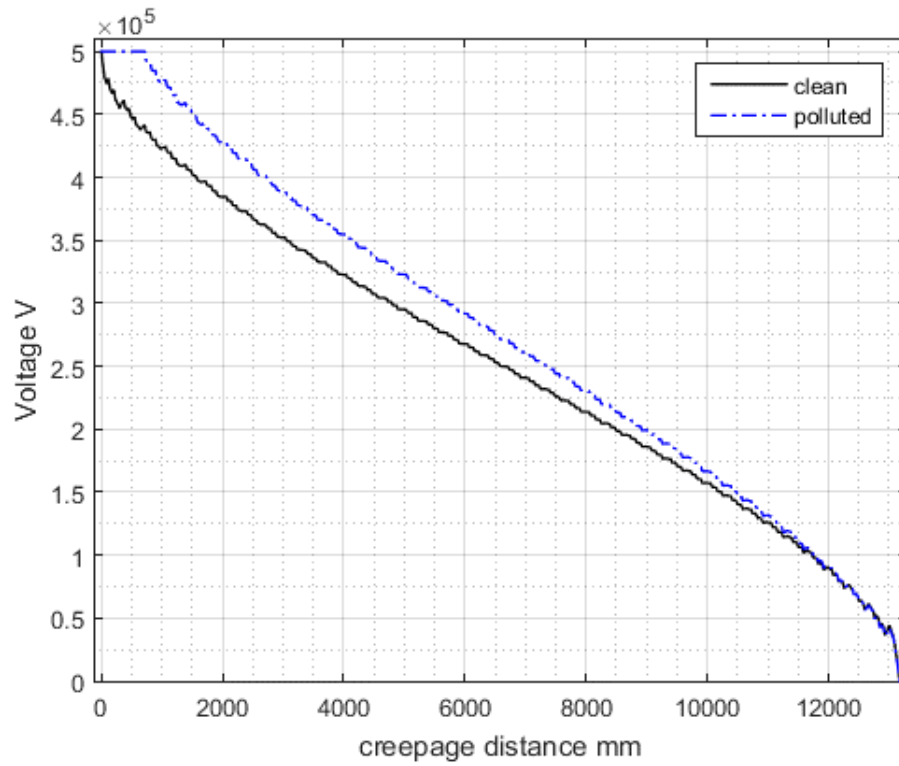


Figure 6.27. Voltage distribution along insulator's (E) surface

### **6.3 Enhancement of electric field profiles using control devices**

To demonstrate the effect of electric field control devices on contaminated insulators, corona ring and arc horn devices were used. In some cases, a combination between Arc horn and corona ring, besides different configurations were investigated on SiR insulator (D).

The governing equations given in (3.7 and 3.8) are solved while minimizing the objective function given in (4.1). It is well known that the electric field is very high in the near vicinity of the HV end fitting. Therefore, we focused on checking for maximum electric field in that area then minimizing it. The upper and lower limits of optimization domains for corona ring and Arc horns are given in Table 6.1 and Table 6.2, respectively. To make fair comparison with previous work reported in the literature, these limits were determined based on previous optimization work reported before for AC insulators in the references [7], [9] and [45].

**Table 6.1. Upper and lower limits of optimized corona ring parameters**

<b>Insulators (15 units-A &amp; B) 200 kVDC</b>	<b>D (mm)</b>	<b>R (mm)</b>	<b>H (mm)</b>
Lower limit	50	285	-100
Upper limit	100	490	450
<b>Insulator (D) 300 kVDC</b>	<b>D (mm)</b>	<b>R (mm)</b>	<b>H (mm)</b>
Lower limit	35	130	60
Upper limit	45	160	280
<b>Insulator (E) 500 kVDC</b>	<b>D (mm)</b>	<b>R (mm)</b>	<b>H (mm)</b>
Lower limit	35	150	30
Upper limit	52	200	400

**Table 6.2. Upper and lower limits of optimized Arc Horn parameters**

<b>Insulators (15 units-A &amp; B) 200 kVDC</b>	<b>X (mm)</b>	<b>Y (mm)</b>
Lower limit	290	20
Upper limit	540	590

### **6.3.1 Porcelain insulator (A- 15 units)**

Under contaminated conditions. Two electric field control devices were used, which are Corona ring and Arc horn. The proposed algorithm has been used to optimize these control devices. The optimizing domain were subjected to the limits in Table 6.1 and Table 6.2 for corona ring and arc horn, respectively. Convergence of the objective function  $J$  versus number of iterations when using Corona ring device is shown in Figure 6.28.

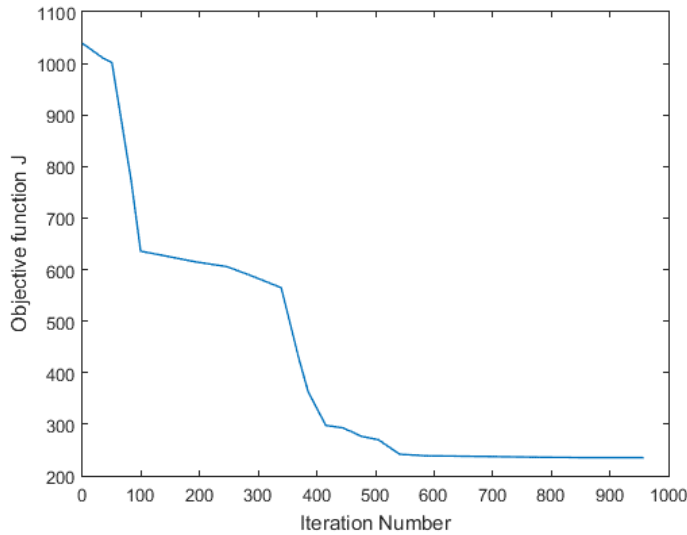


**Figure 6.28. Variation of  $J$  with Iteration number**

The optimal parameters converged to be:  $[D, R, H] = [100, 442.85, 153.6]$  mm for Corona ring and  $[X, Y] = [350, 580]$  mm for Arc horn. For both control devices, electric field and voltage profiles along PATH 1 are shown in Figure 6.29 and Figure 6.30, respectively. On comparing the electric fields, a maximum value of 962.4 V/mm near the HV end is obtained under no control, while in the presence of optimized Corona ring, the maximum electric field has been reduced to 734.5 V/mm, and 715 V/mm when using Arc horn. This corresponds to 23.6% and 25.7% reduction in electric field for corona ring and Arc horn, respectively. On the other hand, Figure 6.31 and Figure 6.32, show the electric field and voltage profiles along PATH 2. The maximum electric field had reached a value of 2659 V/mm, under no control and 1964 V/mm when corona ring is used and 1603 V/mm when using the Arc horn. This corresponds to an electric field reduction of 26.13% for corona ring and 39.7% due to Arc horn. Lastly along PATH 3, the electric field and voltage profiles were very much affected by the corona ring as compared to the Arc horn case, Figure 6.33

and Figure 6.34. The value of maximum electric field was 814.7 V/mm with no control and 312.1 V/mm with corona ring and 342 V/mm when using the Arc horn. Thus, the amount of electric field reduction has reached 61.69% and 58% for Corona ring and Arc horn, respectively. The corresponding electric field and voltage contours are displayed in Appendix A.1.

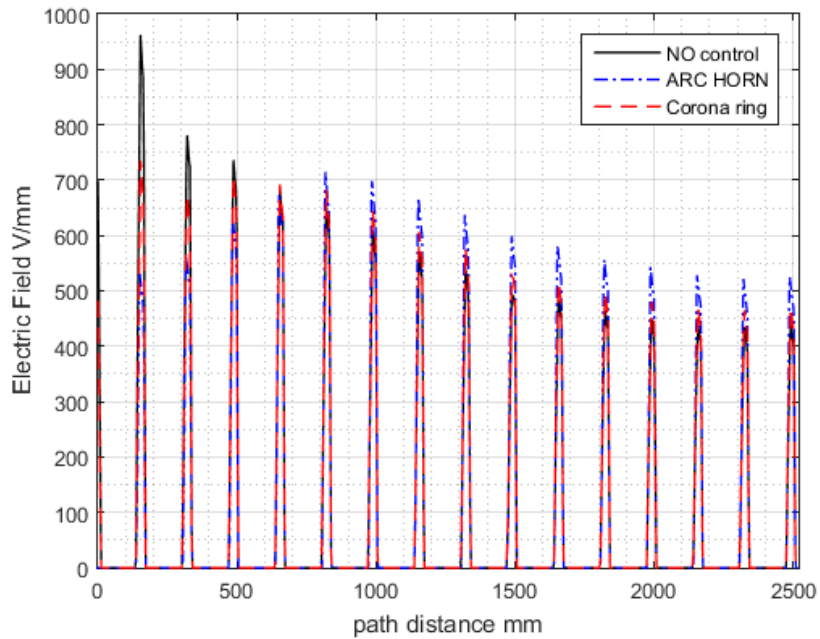


Figure 6.29. Electric field of PATH 1 along the string (A-15) with control devices under contaminated conditions

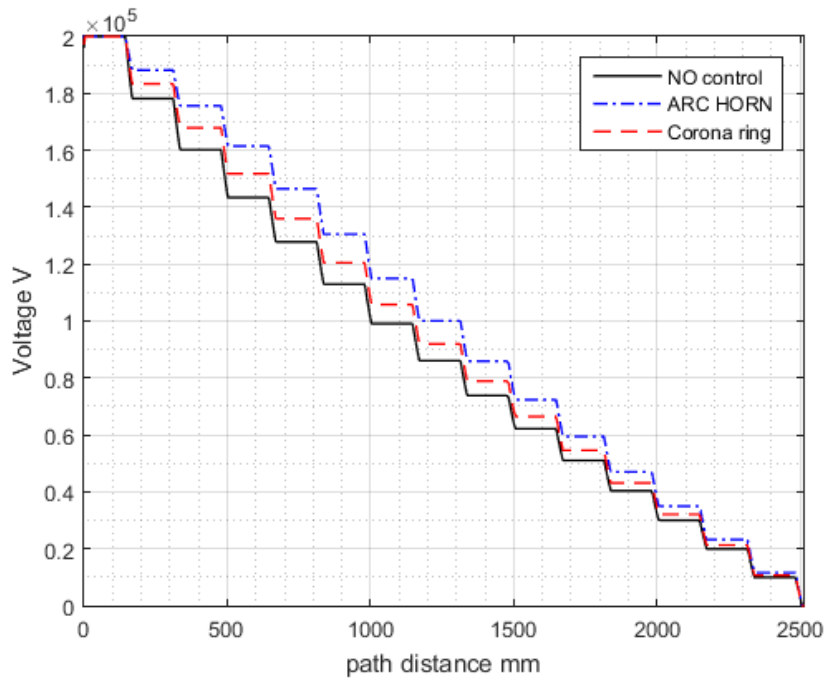


Figure 6.30. Voltage distribution of PATH 1 along the string (A-15) with control devices under contaminated conditions

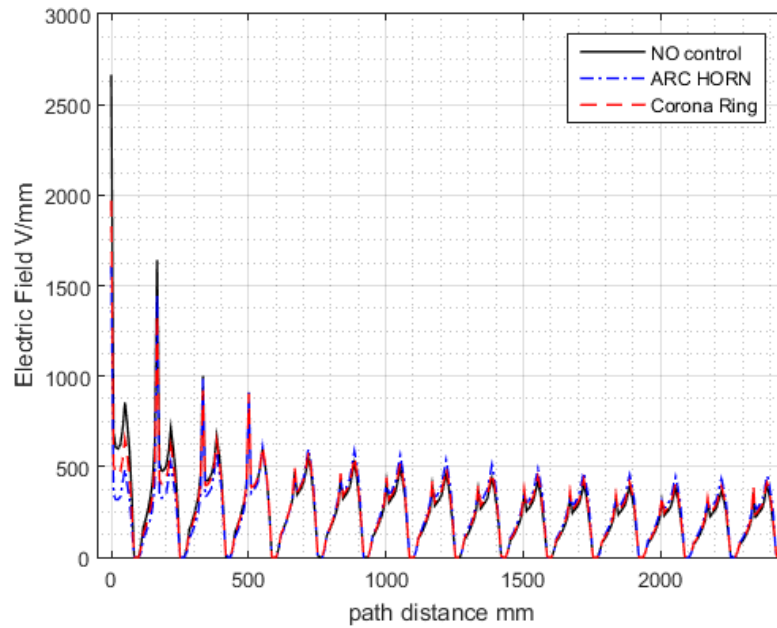


Figure 6.31. Electric field of PATH 2 along the string (A-15) with control devices under contaminated conditions

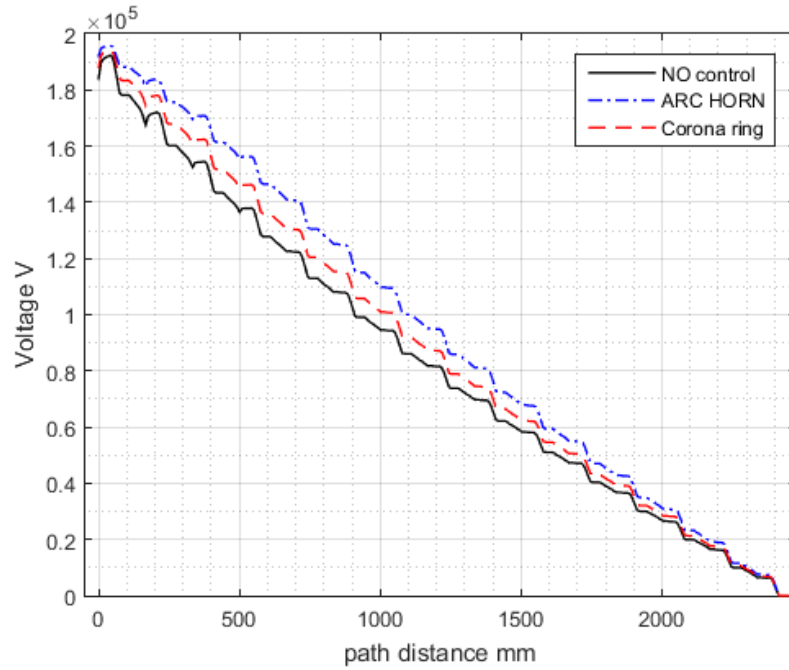


Figure 6.32. Voltage Distribution of PATH 2 along the string (A-15) with control devices under contaminated conditions

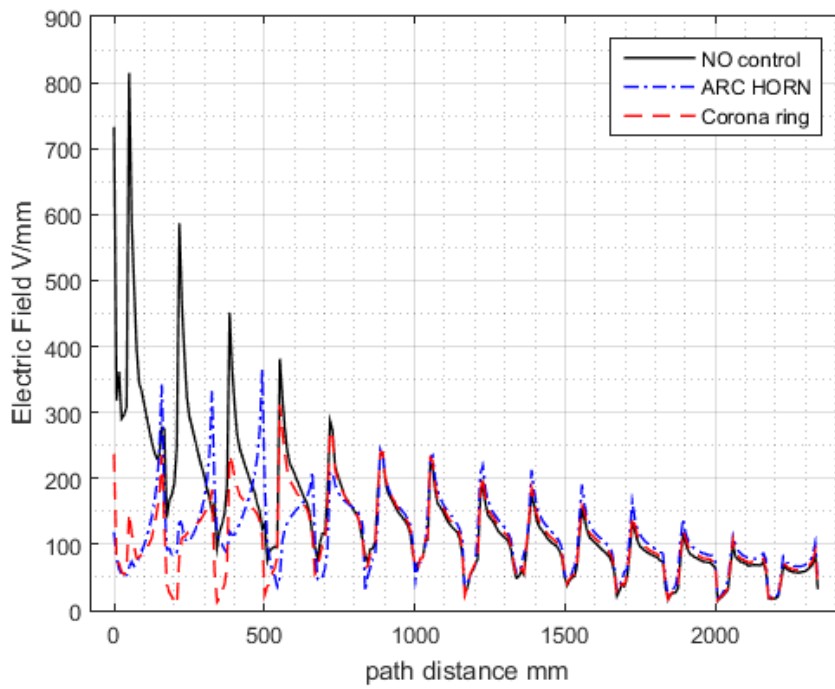
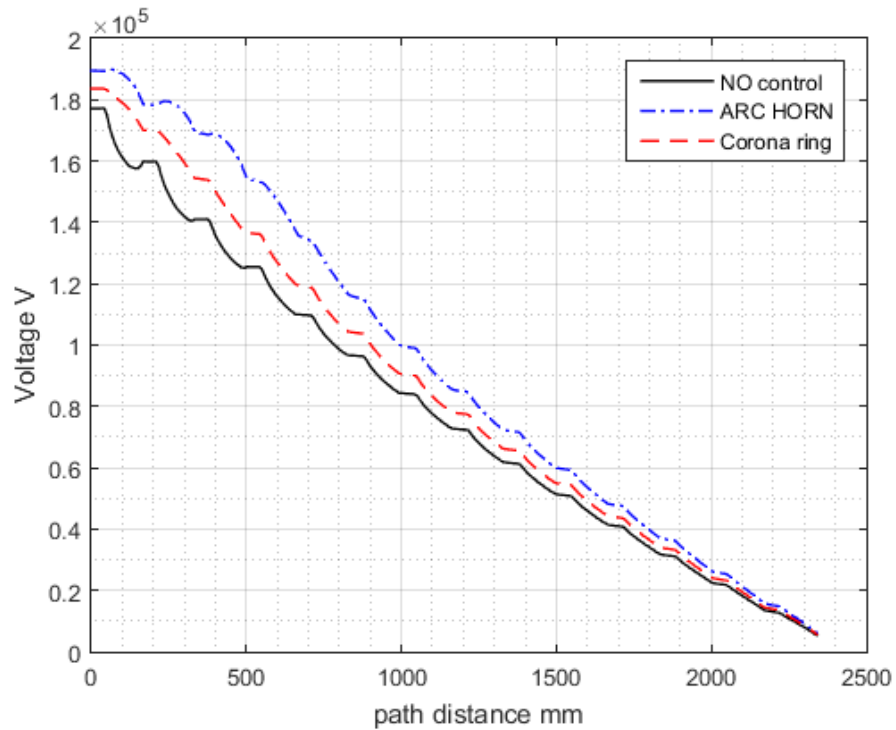
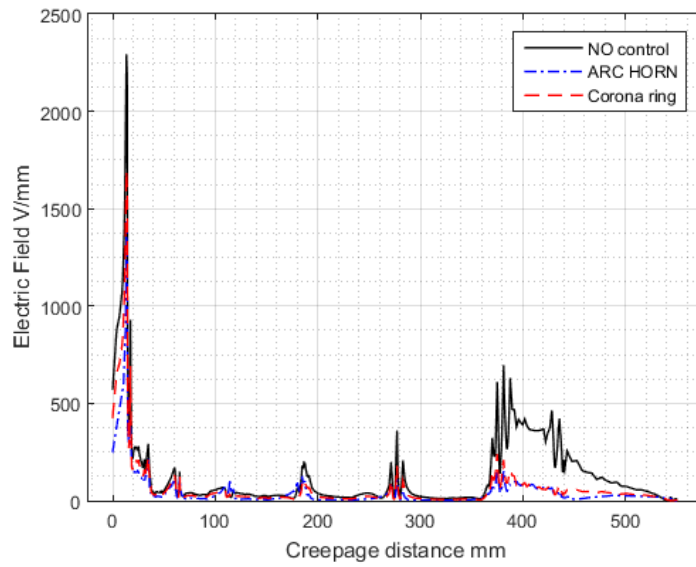


Figure 6.33. Electric field of PATH 3 along the string (A-15) with control devices under contaminated conditions



**Figure 6.34. Voltage Distribution of PATH 3 along the string (A-15) with control devices under contaminated conditions**

It is worth to mention that the electric field profile, along the first contaminated insulator surface, has been reduced dramatically when using both devices and relatively lower when using the Arc horn, as shown in Figure 6.35. This came as a results of having more uniform voltage profile as demonstrated in Figure 6.36.



**Figure 6.35. Electric field along the surface of the first insulator (A) with control devices under contaminated conditions**

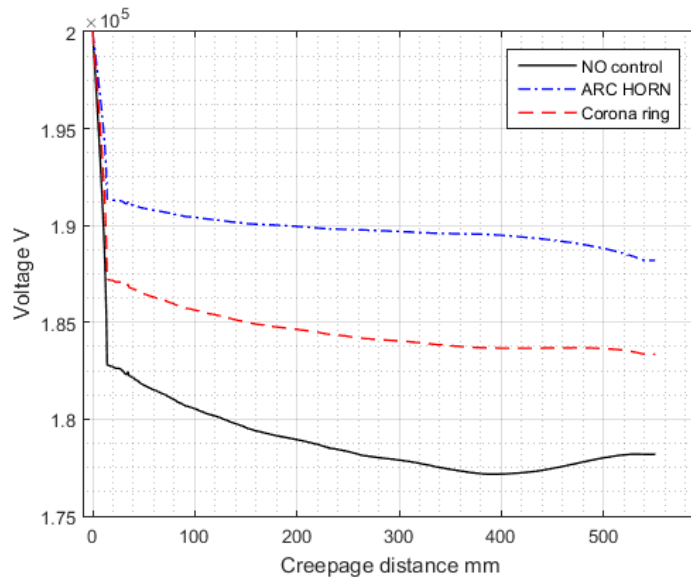


**Figure 6.36. Voltage Distribution along the surface of the first insulator (A) with control devices under contaminated conditions**

Figures (6.37 -6.39) clearly show the maximum electric field comparison on the PATHs 1, 2 and 3 between the control devices. These values when compared to the case where no control device is used, show an enormous reduction in the electric field values especially

near HV end. The bar charts in Figure 6.40 and Figure 6.41 were calculated using equation (6.2).

$$\% \text{ Percentage change in } E_{max} = \frac{E_{controlled} - E_{no\ control}}{E_{no\ control}} * 100 \quad (6.2)$$

The results show the amount of electric field reduction due to corona ring and Arc horn on each unit of the string. It is worth mentioning that 82.03% and 58% reduction in electric field is obtained along PATH 3, due to Corona ring and Arc horn, respectively. In addition to a reduction of 26.14% and 39.7% along PATH 2, besides 23.68% and 44.5% along PATH 1, owed to Corona ring and Arc horn, respectively. On the other hand, units 6 to 15 experience a slight increase in the electric field which is in the acceptable range for both control devices. Moreover, String efficiency is a very helpful indicator which describes the improvement of HV insulator strings. In order to calculate the string efficiency, equation (6.3) given below is used.

$$\% \text{ String Efficiency } \eta = \frac{\text{Voltage accross the string}}{(n) * \text{Voltage accross unit near HV end}} \quad (6.3)$$

Where  $n$  is the number of string's unit.

As a result, the string efficiency has been improved from 61.16% when no control is used, to 80.321% and 83.85% when using corona ring and Arc horn, respectively.

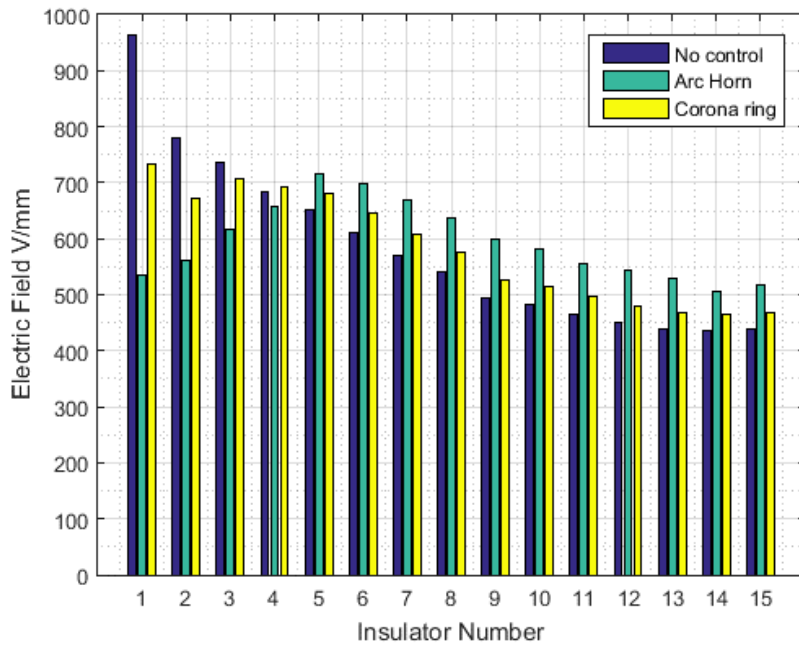


Figure 6.37. Maximum electric field comparison along PATH 1, when using control devices under contaminated conditions

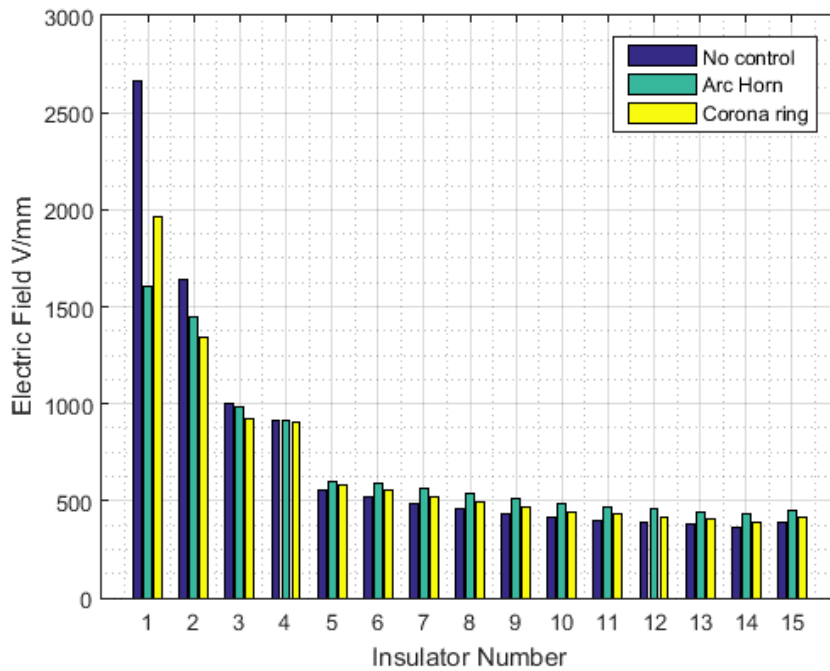


Figure 6.38. Maximum electric field comparison along PATH 2, when using control devices under contaminated conditions

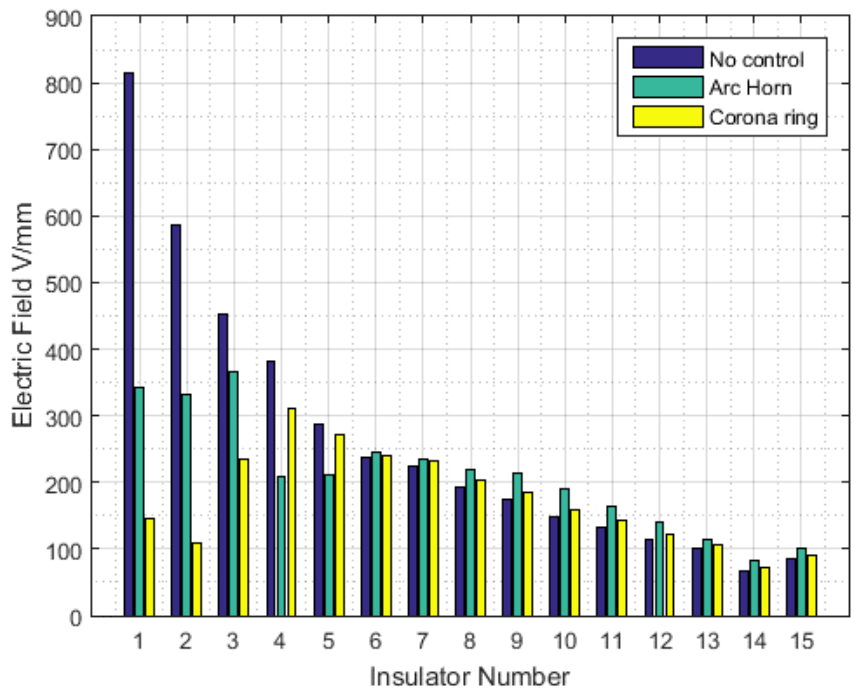


Figure 6.39. Maximum electric field comparison along PATH 3, when using control devices under contaminated conditions

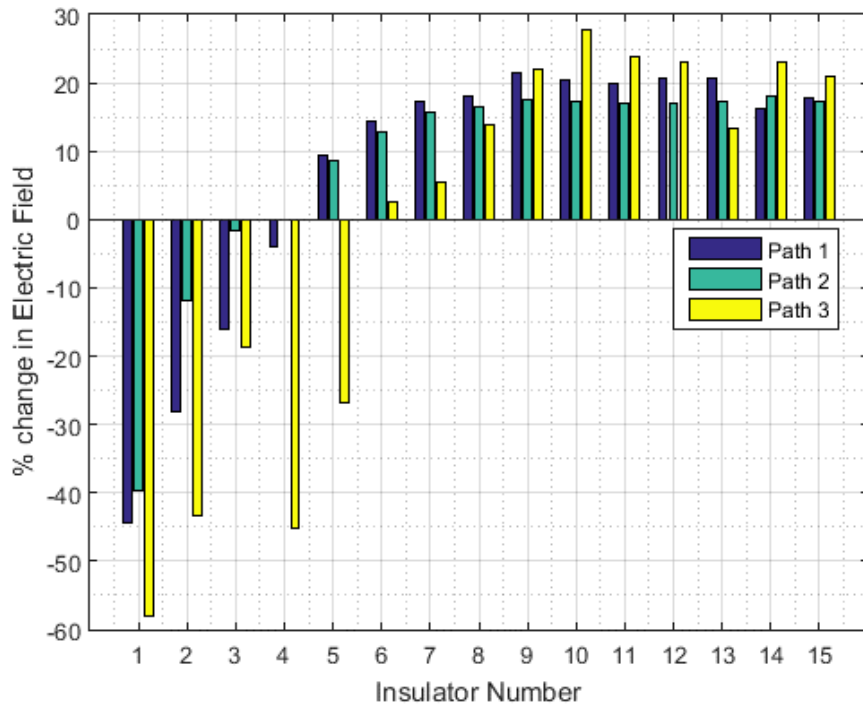


Figure 6.40. Percentage change in the maximum electric field due to Arc Horn for insulator (A) under contaminated conditions.

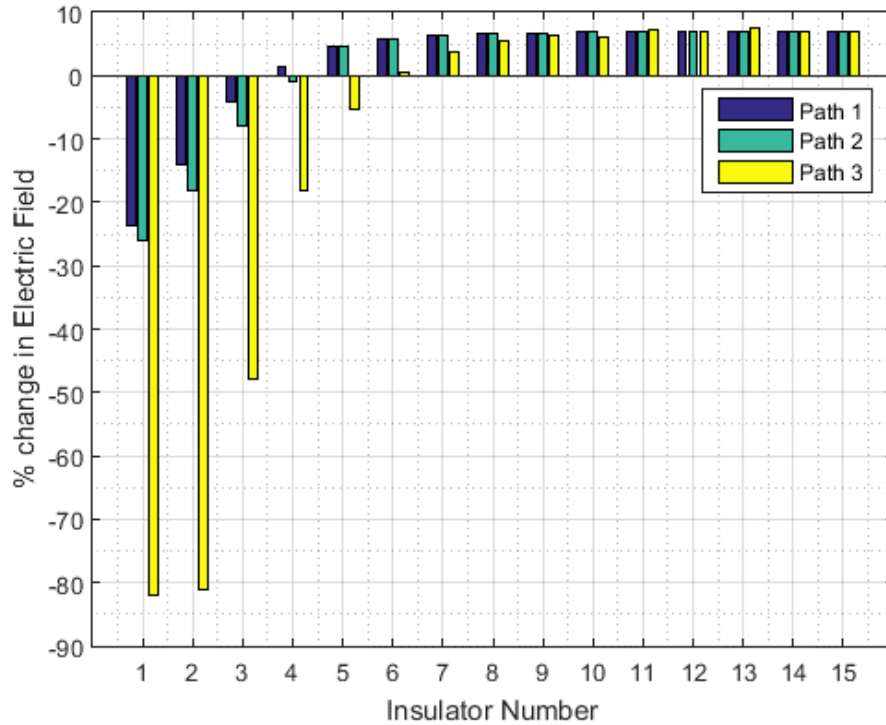


Figure 6.41. Percentage change in the maximum electric field due to corona ring for insulator (A) under contaminated conditions.

### 6.3.2 Glass insulator (B- 15 units)

Similarly for the case of Glass insulator, the same analysis has been made under contaminated conditions, with both electric field control devices Corona ring and Arc horn. The optimized parameters for each device subjected to the limits in Table 6.1 and Table 6.2, have converged to:  $[D, R, H] = [100, 433, 109.6]$  mm for Corona ring, and  $[X, Y] = [300, 567.2]$  mm for Arc horn. The corresponding electric field and voltage contours are displayed in Appendix A.2.

First of all, it is worth to mention that the electric field profile along the first contaminated insulator surface, has been reduced dramatically when using both devices and relatively

lower when using the Arc horn, as shown in Figure 6.42. This came as a results of having more uniform voltage profile as demonstrated in Figure 6.43.

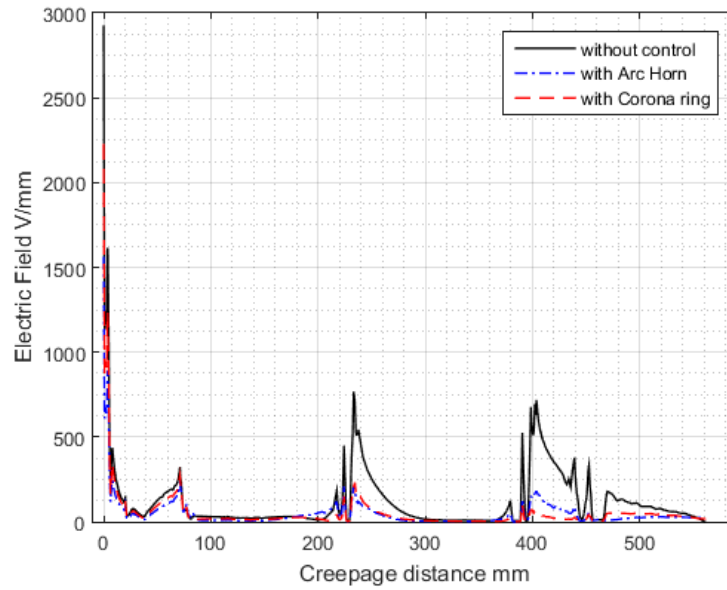


**Figure 6.42. Electric field along the surface of the first insulator (B) with control devices under contaminated conditions**

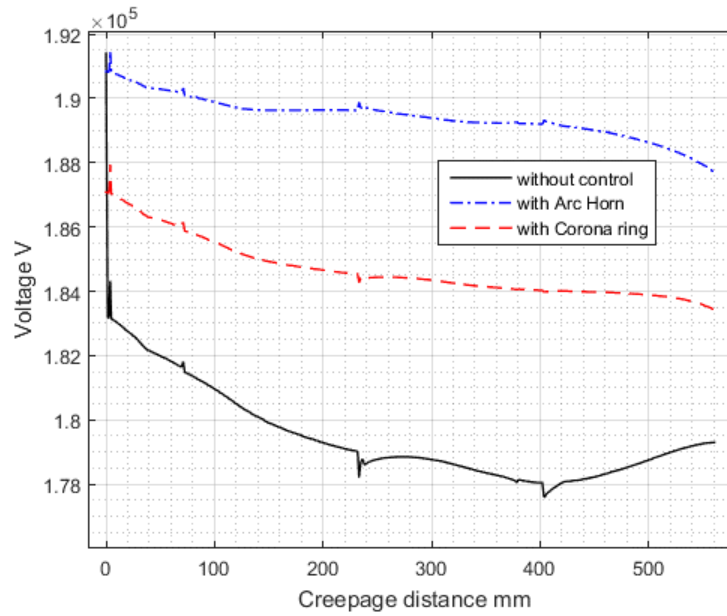


**Figure 6.43. Voltage distribution along the surface of the first insulator (B) with control devices under contaminated conditions**

Figures (6.44 - 6.46) clearly show the maximum electric field comparison on the PATHS 1, 2 and 3 when using corona ring and Arc Horn. These values when compared to the case where no control device is used, show an enormous reduction in the electric field values especially near HV end. On comparing the electric fields along PATH 1, a maximum value of 1220 V/mm near HV end is obtained under no control, while in the presence of optimized Corona ring, the maximum electric field has been reduced to 976.5 V/mm, and 966 V/mm when using the Arc horn. This corresponds to 20 % and 21 % reduction in electric field for corona ring and Arc horn, respectively, along PATH 2 on the other hand, the maximum electric field had reached a value of 2562 V/mm, under no control and 1953 V/mm when corona ring is used and 1369 V/mm when using the Arc horn. This corresponds to an electric field reduction of 26.35 % for corona ring and 48.37 % due to Arc horn. Lastly along PATH 3, the value of maximum electric field was 1166 V/mm with no control and 309.8 V/mm with corona ring and 341 V/mm when using the Arc horn. Thus, the amount of electric field reduction has reached 73.4 % and 70.75 % for Corona ring and Arc horn, respectively.

The bar charts in Figure 6.46 and Figure 6.47 were calculated using equation (6.2). The results show the amount of electric field reduction due to corona ring and Arc horn on each unit of insulator string. It is worth mentioning that 87% and 76.6 % reduction in electric field is obtained along PATH 3, due to Corona ring and Arc horn, respectively. In addition to a reduction of 26% and 46.57% along PATH 2, besides 20% and 40.61% along PATH 1, owed to Corona ring and Arc horn, respectively. On the other hand, units 6 to 15 experience a slight increase in electric field which is in the acceptable range for both control

devices. In addition, the string efficiency has been improved from 64.412 % where no control is used, to 80.3% and 84.3 % when using corona ring and Arc horn respectively.

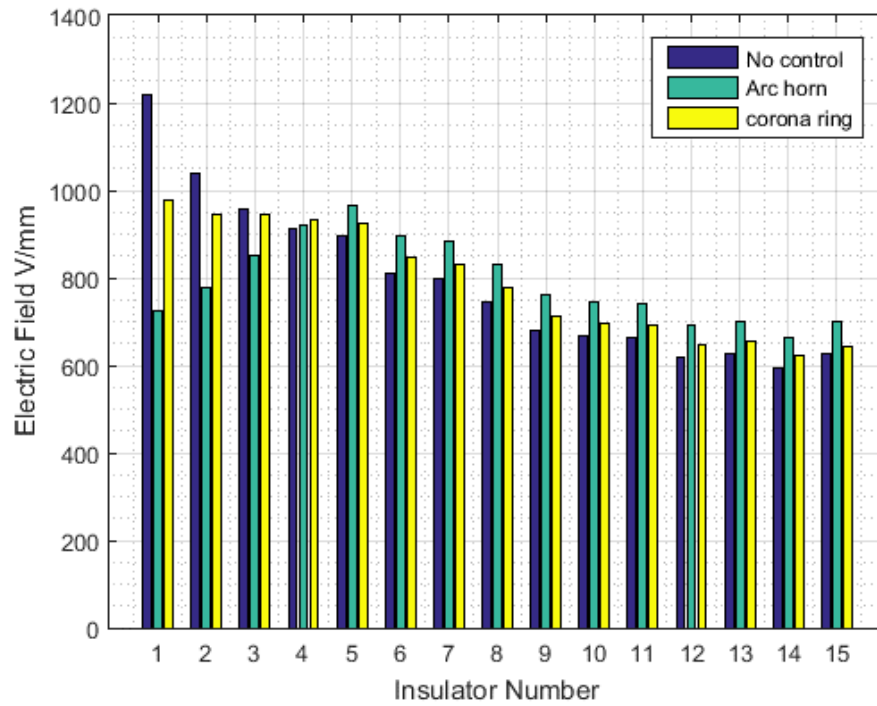


Figure 6.44. Maximum electric field comparison of PATH 1 with control devices under contaminated conditions

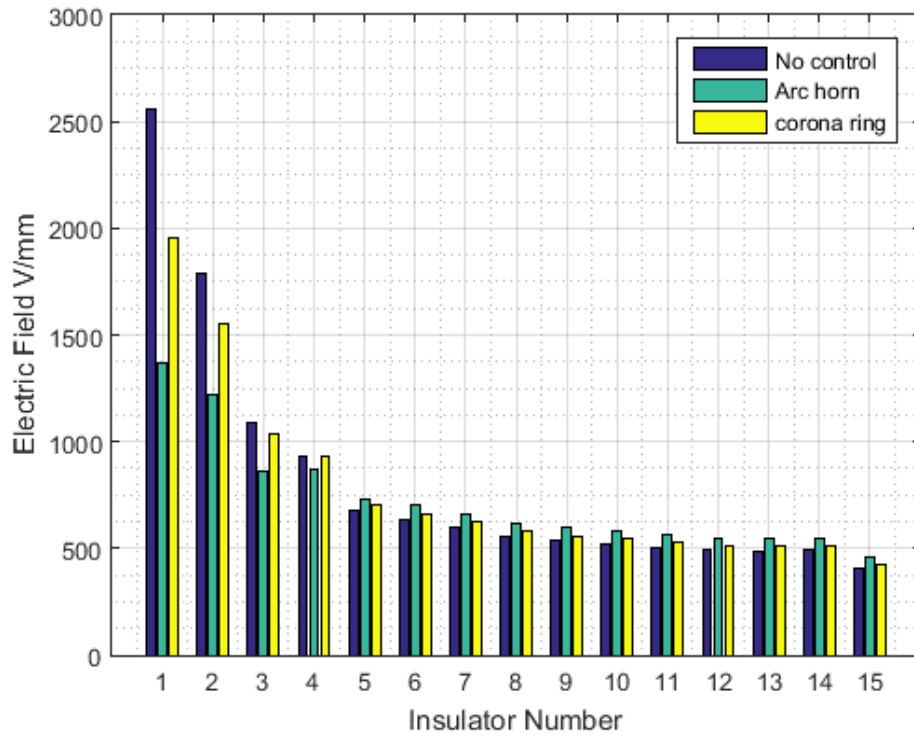


Figure 6.45. Maximum electric field comparison of PATH 2 with control devices under contaminated conditions

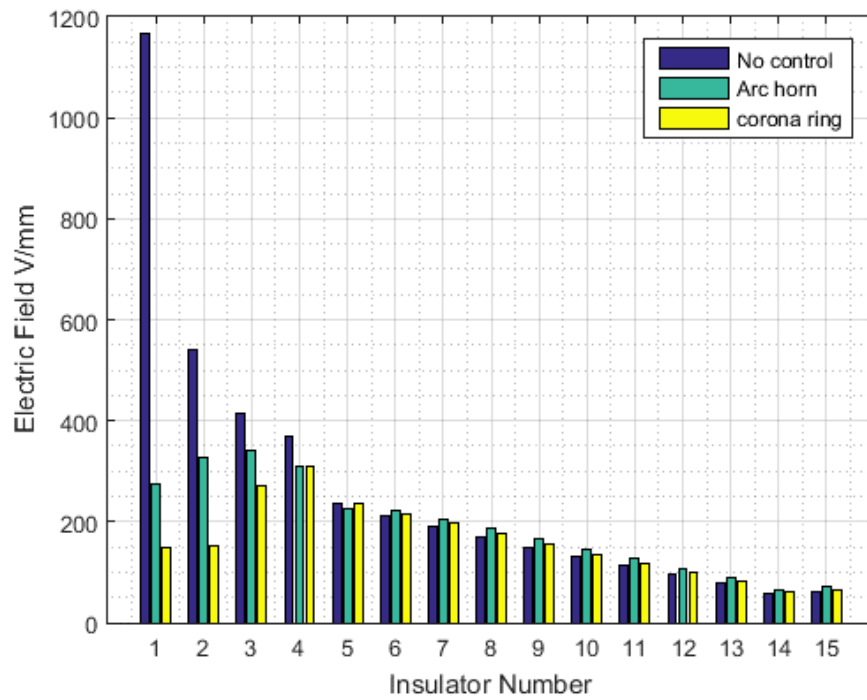


Figure 6.46. Maximum electric field comparison of PATH 3 with control devices under contaminated conditions

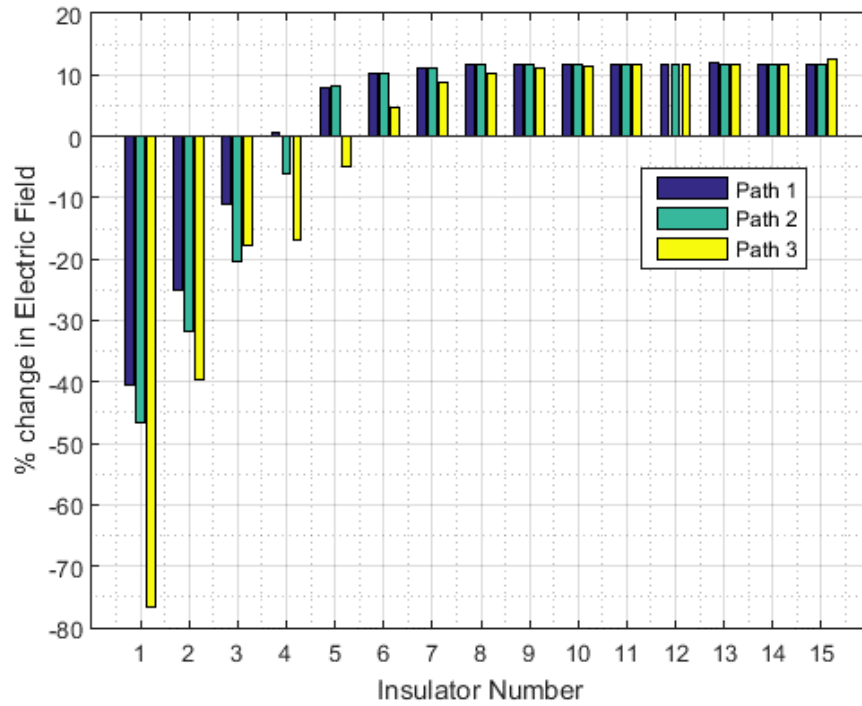


Figure 6.47. Percentage change in the maximum electric field due to Arc horn for insulator (B).

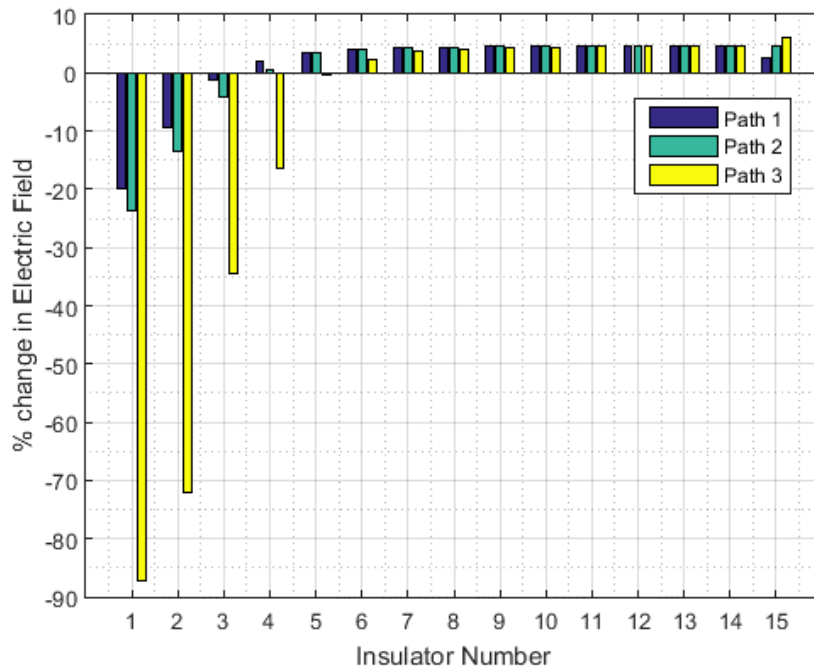


Figure 6.48. Percentage change in the maximum electric field due to corona ring for insulator (B).

For completeness, the results of strings efficiencies for both insulators A and B, are summarized in Table 6.3. It is quite clear from the table how control devices can significantly improve the string efficiencies even under contaminated conditions.

**Table 6.3. Summary of insulator’s string efficiencies**

%String efficiency $\eta$ at polluted conditions	Without control	With corona ring	With Arc Horn
Porcelain insulator (A-15)	61.16%	80.321%	83.85%
Glass insulator (B-15)	64.41%	80.3%	84.3%

As a conclusion, based on the string efficiencies and the obtained results, Arc horn control device appears to work relatively better than corona ring under contaminated conditions for both porcelain and glass insulators.

### **6.3.3 Comparison between Porcelain (A-15) and Glass (B-15) insulators**

Furthermore, since both insulators (A and B) were subjected to the same contamination condition and stressed by same voltage, we can compare the electric fields of both insulators. For example, under Arc Horn control, the electric field profiles of both insulators A and B along PATH 2 was plotted in Figure 6.49. The figure shows that glass insulator (B) show a lower electric field profile as compared to porcelain insulator (A), given the same contamination condition.

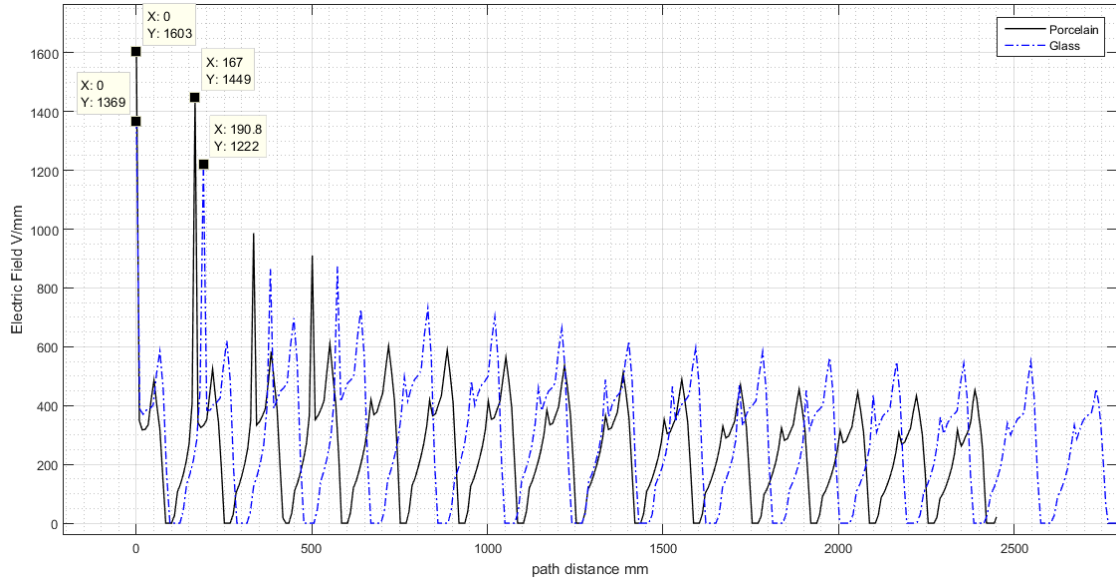


**Figure 6.49. Comparing Glass and Porcelain Insulators**

Moreover, Table 6.4 shows a quick comparison between glass and porcelain insulators, under the influence of electric field control devices. Results show that glass insulator has obtained higher percentage of reduction as compared to porcelain insulator when using the Arc horn. On the other hand, both insulators have rather same percentage of reduction when using corona ring.

**Table 6.4. %Percentage Reduction in the maximum electric field Along PATH 2 for both insulators**

	Porcelain insulator (A-15)	Glass insulator (A-15)
Corona Ring	26.13%	26.35%
Arc Horn	39.7%	48.37%

### 6.3.4 SiR insulator (D)

For the case of SiR insulator (D), single corona ring has been considered to be optimized near the HV end. The optimization has result in the following parameters [D, R, H] = [45, 135, 280] mm. the electric field and voltage distribution are shown in Figure 6.50 and Figure 6.51. For better comparison between the no control case and the corona ring case, Figure 6.52 clearly shows how the corona ring has considerably minimized the electric field near the polluted area. Where the maximum electric field near HV end has been reduced form 1071 V/mm to 343 V/mm which corresponds to 67.97% reduction.

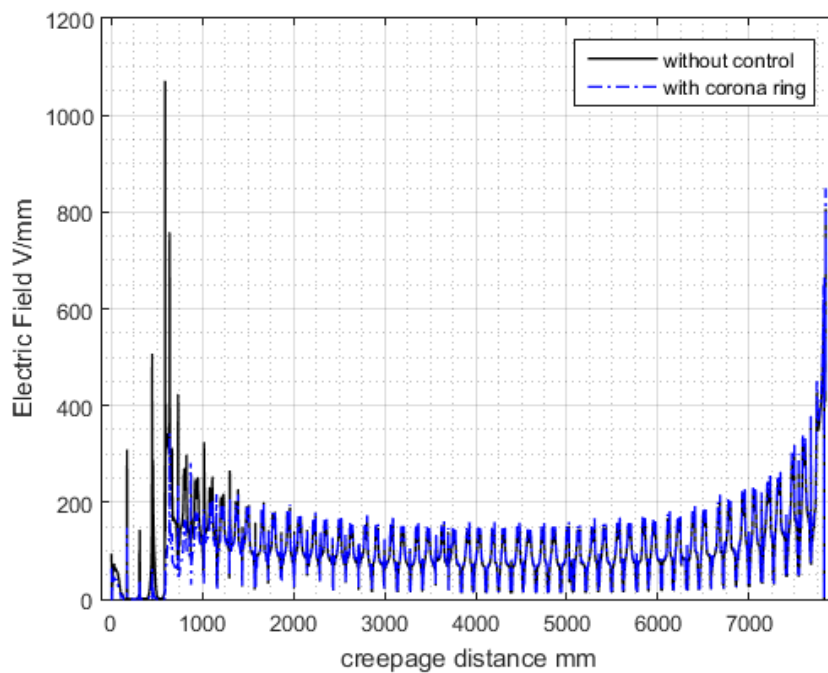


Figure 6.50. Electric field distribution along insulator's (D) surface with corona ring

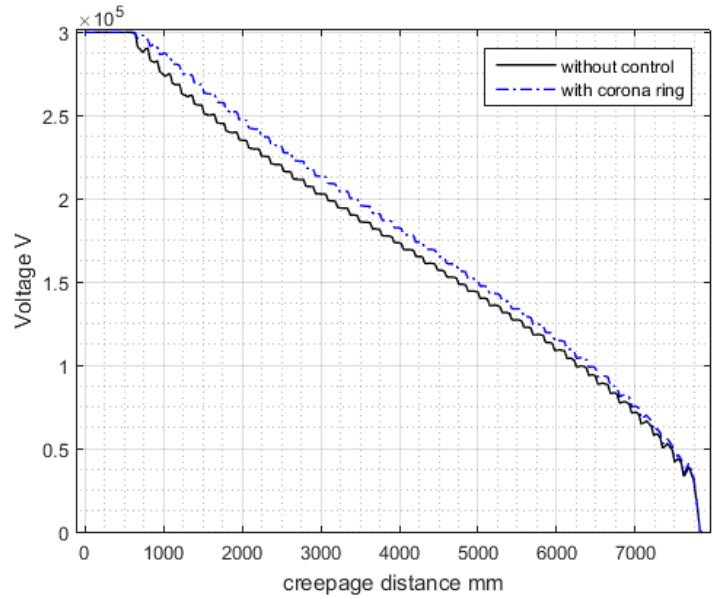


Figure 6.51. Voltage distribution along insulator's (D) surface, in the presence of corona ring

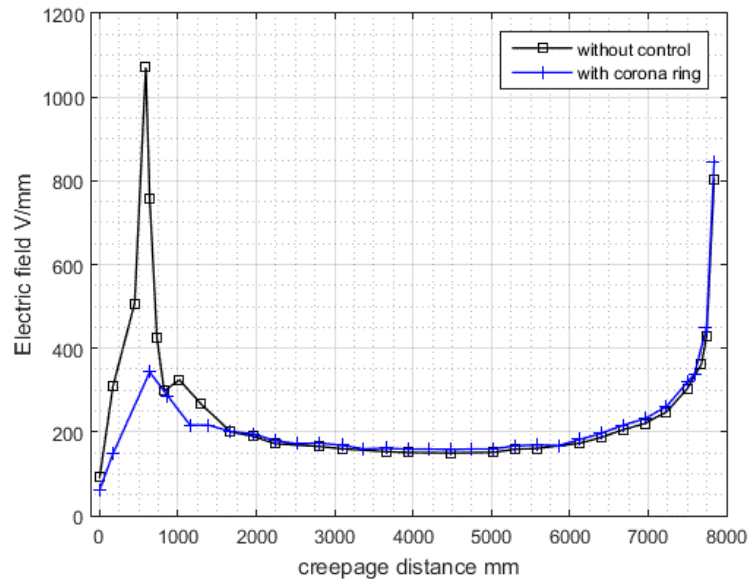


Figure 6.52. Electric field distribution along insulator's (D) surface with corona ring (Selected points)

Furthermore, in addition to single corona ring near the HV end, four different electric field control devices configuration have been considered, which are: single arc horn near the HV end, double corona rings near HV and LV ends, double arc horns near HV and LV ends and combined corona ring and arc horn near HV and LV ends, respectively. The

optimization problem has been solved using the same algorithm with respect to the limits in Table 6.1 and Table 6.5. Convergence example of the objective function  $J$  versus iteration number in the case of double arc horn configuration is shown in Figure 6.53.

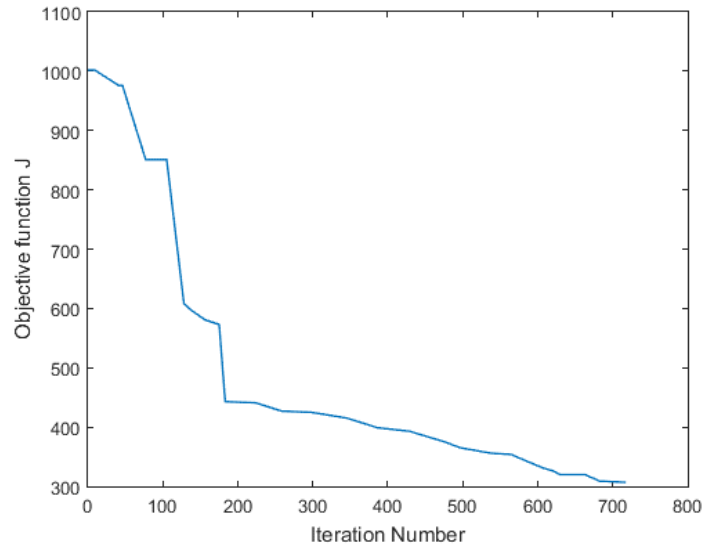


Figure 6.53. Objective function  $J$  versus Iteration number for double arc horns devices

The values of optimal parameters for each configuration are listed in Table 6.6 and displayed on Figure 6.54.

Table 6.5. upper and lower limits of optimized parameters of insulator (D)

<b>Lower Arc horn</b>	X (mm)		Y (mm)
upper limits	330		400
lower limits	120		66
<b>Upper Arc horn</b>	X' (mm)		Y' (mm)
upper limits	245		2233
lower limits	90		2065
<b>Upper Corona ring</b>	D' (mm)	R' (mm)	H' (mm)
upper limits	45	160	2265
lower limits	35	128	1975

Table 6.6. Optimal positions of electric field control devices

Device/ optimal position	Unit (mm)					
	D	R or X	H or Y	D'	R' or X'	H' or Y'
Single corona ring	45	135.0	280	-	-	-
Single arc horn	-	140.9	400	-	-	-
Double corona ring	45	130.3	280	35.05	138.9	2262
Double arc horn	-	143.18	400	-	147.9	2233
Corona ring and arc horn	45	135.0	280	-	112.78	2233

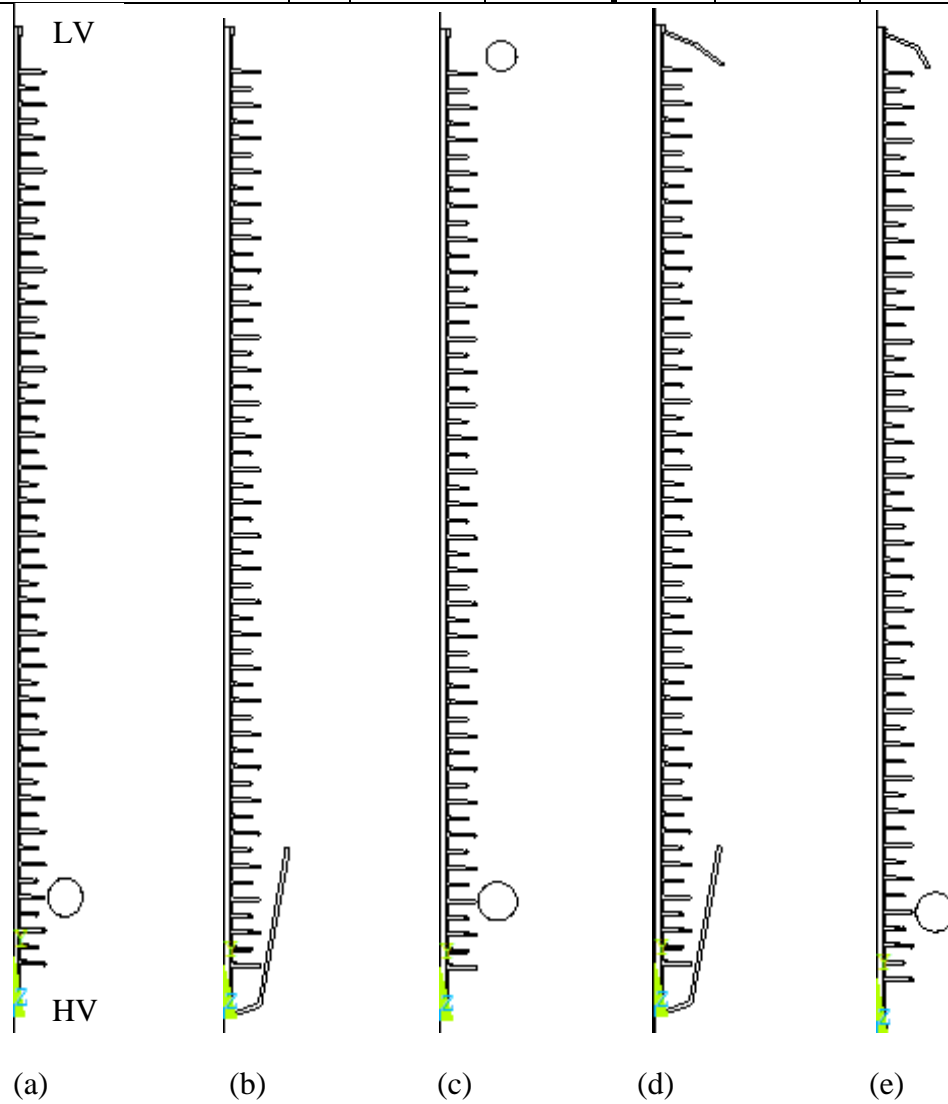


Figure 6.54. Different electric field control devices configurations, a) single corona ring, b) single arc horn, c) double corona rings, d) double arc horns, e) corona and arc horn

The corresponding electric field and voltage contours for each control configuration are displayed in Figure 6.55 and Figure 6.56. On the other hand, Figure 6.57 shows the electric field distribution with respect to each control device arrangement. It is quite clear that all of the control configurations have considerably reduced the maximum electric field near the polluted HV end. However, for the cases of single corona ring and single arc horn, the electric field near the LV side has slightly increased as compared to the no control case, while it has been controlled by other configurations.

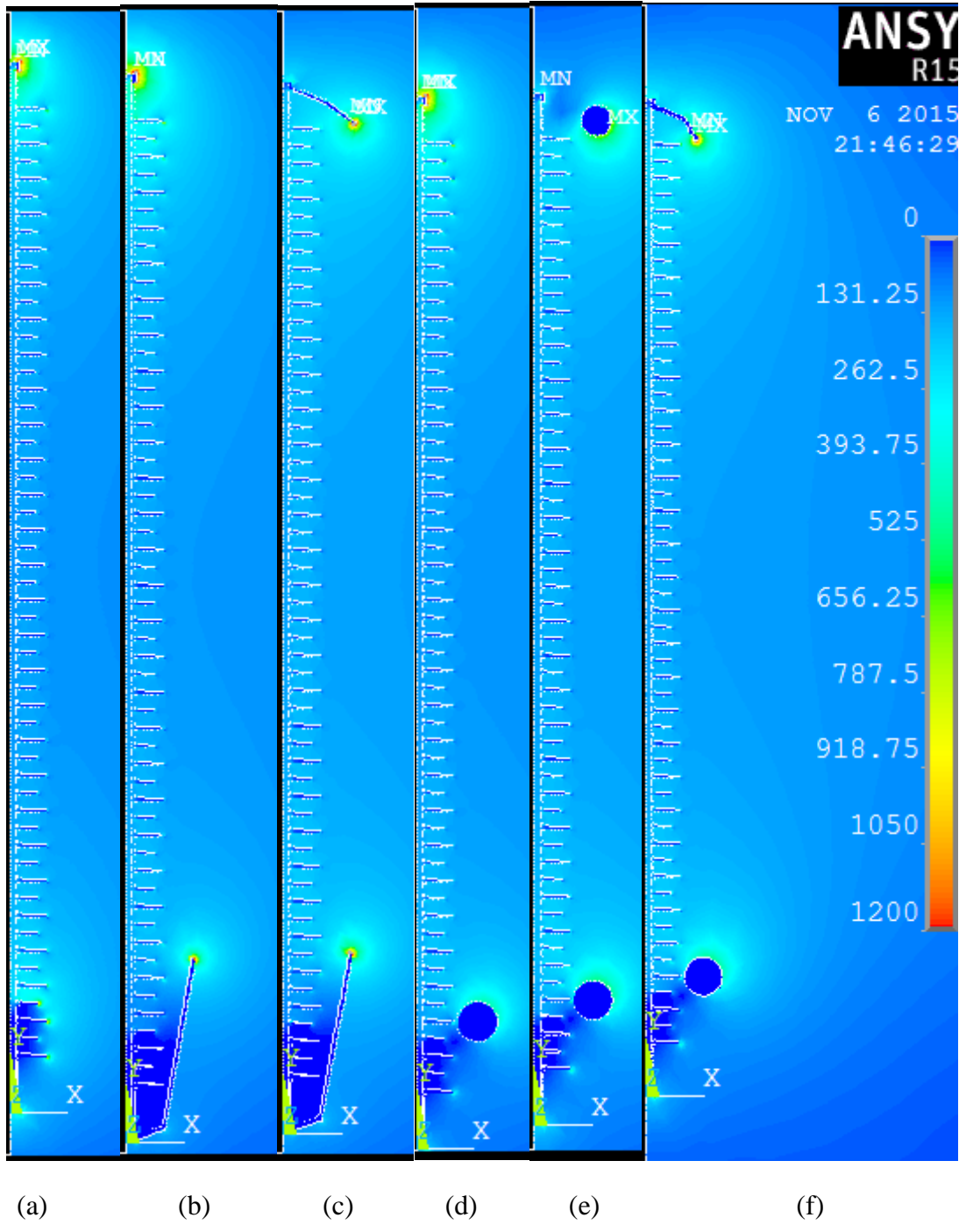


Figure 6.55. Insulator (D) Electric field contours; a) without control, b) with single arc horn, c) with double arc horns, d) with single corona ring, e) with double corona ring, f) with combined corona ring and arc horn

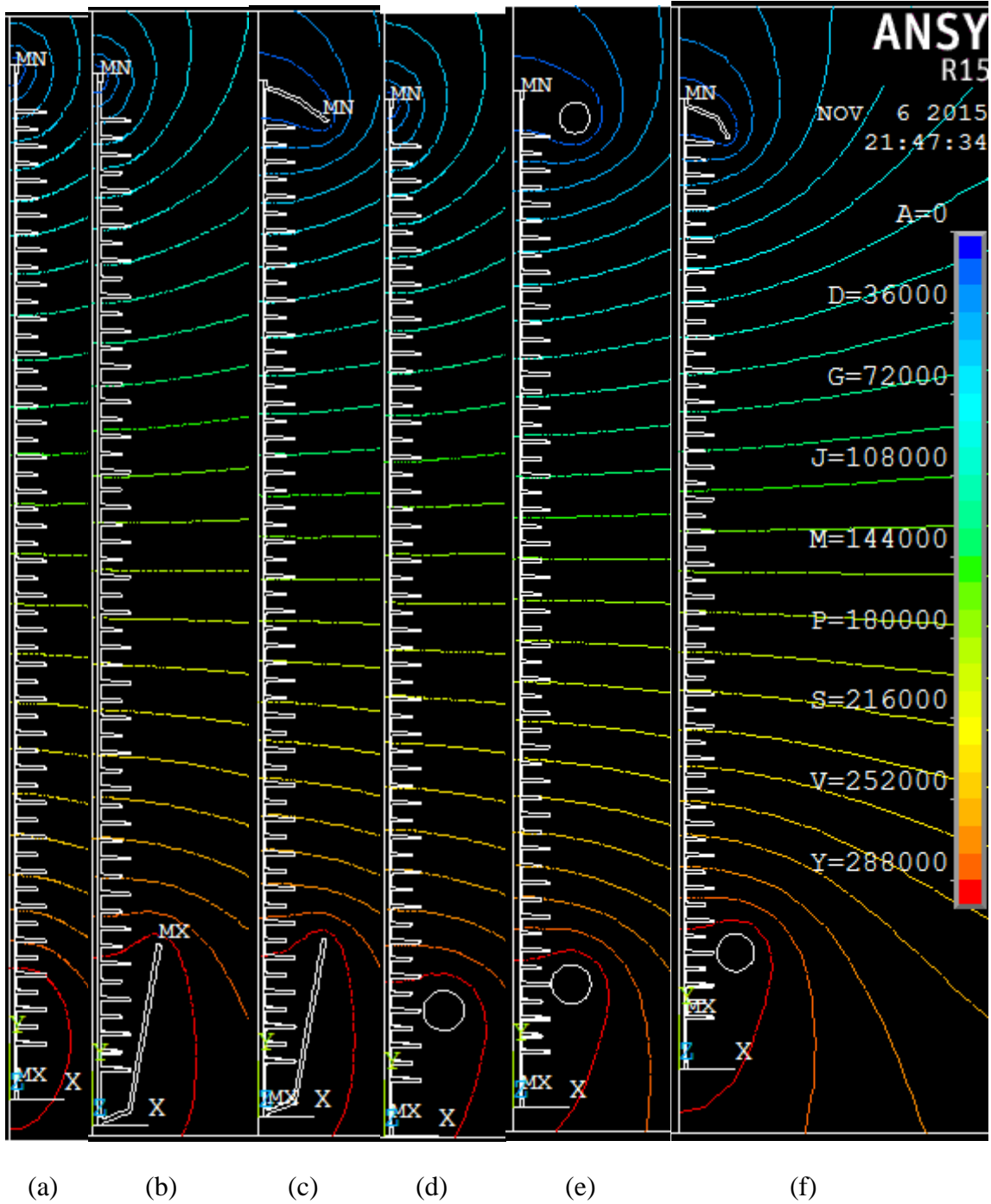
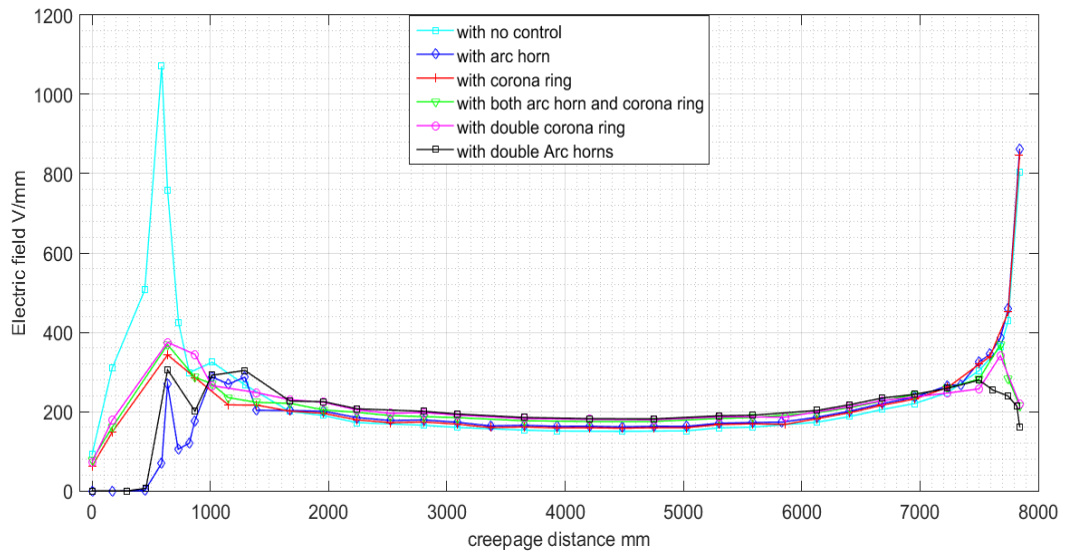


Figure 6.56. Insulator (D) Voltage contours; a) without control, b) with single arc horn, c) with double arc horns, d) with single corona ring, e) with double corona ring, f) with combined corona ring and arc horn



**Figure 6.57. Electric field distributions for different control devices**

The bar charts in Figure 6.58 shows the maximum electric field near both HV and LV ends. The percentage reduction of maximum electric field was calculated according to (6.4), and the results were given in Figure 6.59.

$$\% \text{ Percentage reduction in } E_{max} = \frac{E_{no \text{ control}} - E_{with \text{ control}}}{E_{no \text{ control}}} * 100 \quad (6.4)$$

As appears from the graph, the double arc horn configuration has recorded about 305.3 V/mm near HV end and 161.9 V/mm near LV end, corresponding to 71.49% and 79.87% reduction respectively. The corona ring and arc horn configuration has 65.56% and 73.42% reduction in the HV and LV ends respectively. The double corona ring scheme has reached a reduction of 65.02% and 72.66% near HV and LV ends respectively. As a result, the Double arc horn configuration has provided the lowest electric field profile on both ends as compared to the others. Nevertheless, all of the control arrangements namely (double corona rings, double arc horn and corona+ arc horn) are close to each other with no significant difference. The single arc horn scheme on the other hand has the lowest electric

field profile among all other configurations from the HV side with 269 V/mm corresponding to 74.88% reduction.

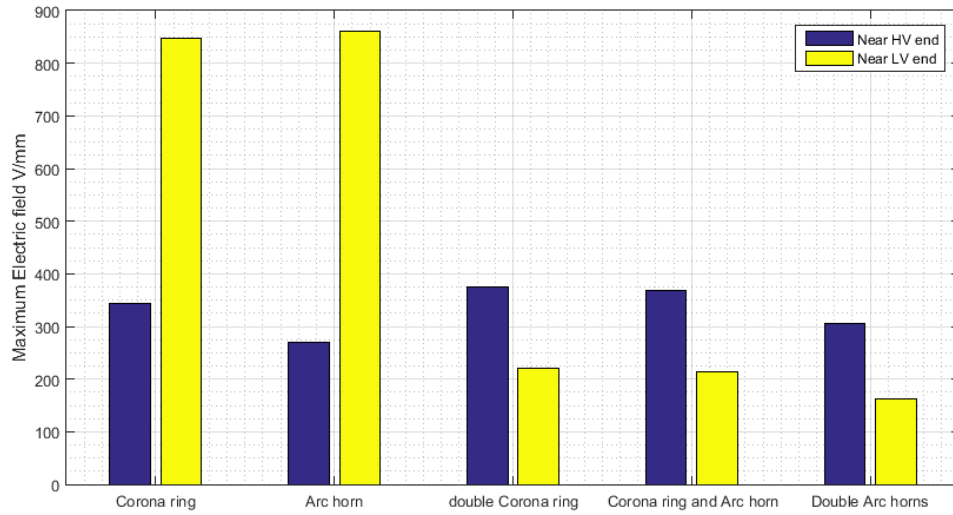


**Figure 6.58. Maximum electric field comparison for different control devices**

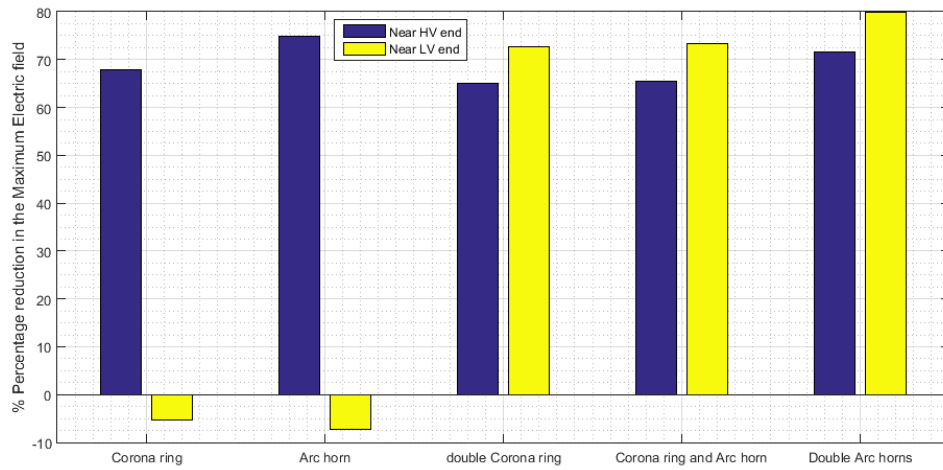


**Figure 6.59. Percentage reduction in Maximum electric field for different control devices**

### 6.3.5 Insulator (E) 500 kVDC

Similar to the previous insulators, single corona ring has also been considered near the HV end of insulator (E). The optimization has result in the following parameters [D, R, H] = [52, 158.1, 400] mm. the electric field and voltage distribution are shown in Figure 6.60 and Figure 6.61. Figure 6.62 clearly shows how the corona ring has considerably minimized the electric field near the polluted area. Where the maximum electric field has been reduced form 914.6 V/mm to 286.9 V/mm which corresponds to 68.63%. The corresponding electric field and voltage contours are shown in Appendix 3

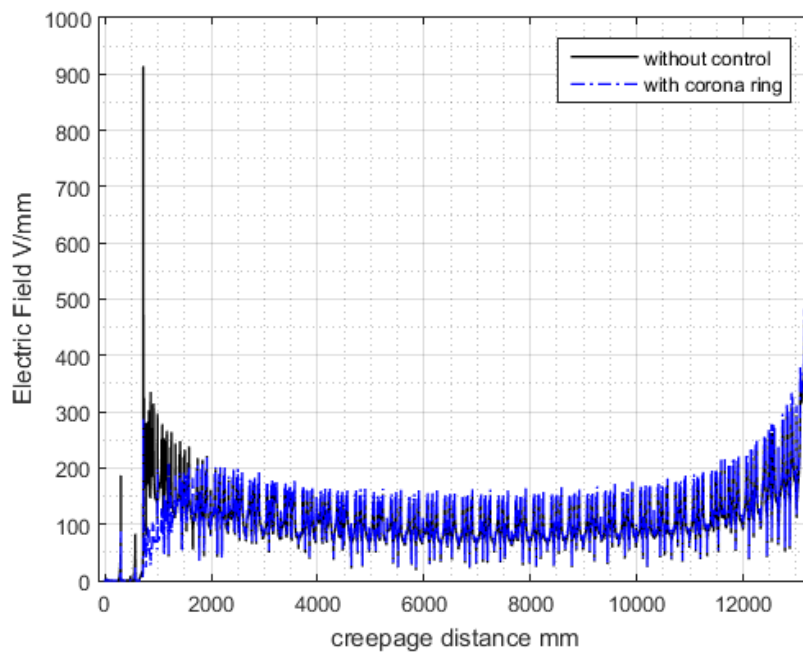


Figure 6.60. Electric field distribution along insulator's (E) surface with corona ring

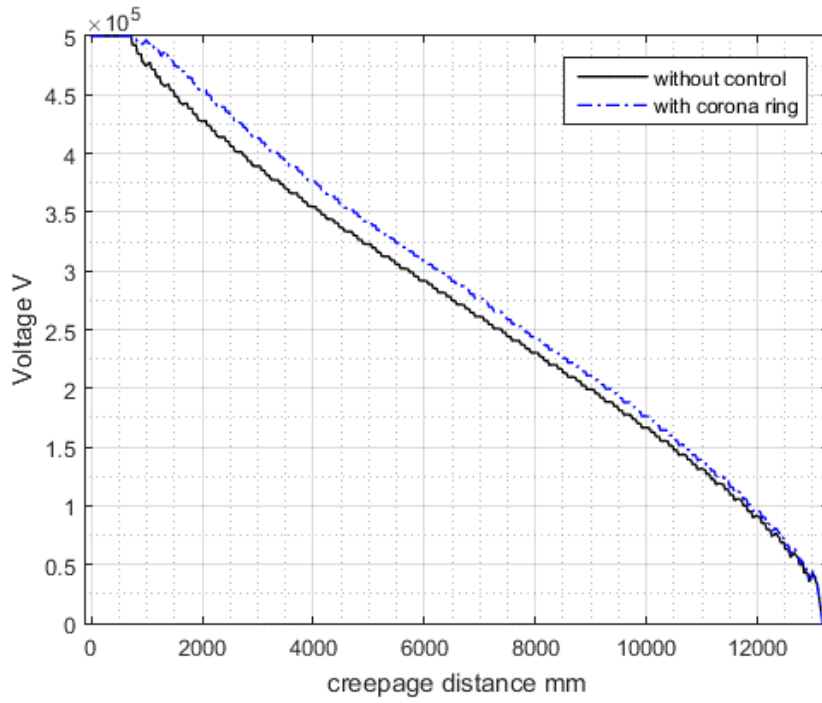


Figure 6.61. Voltage distribution along insulator's (E) surface, in the presence of corona ring

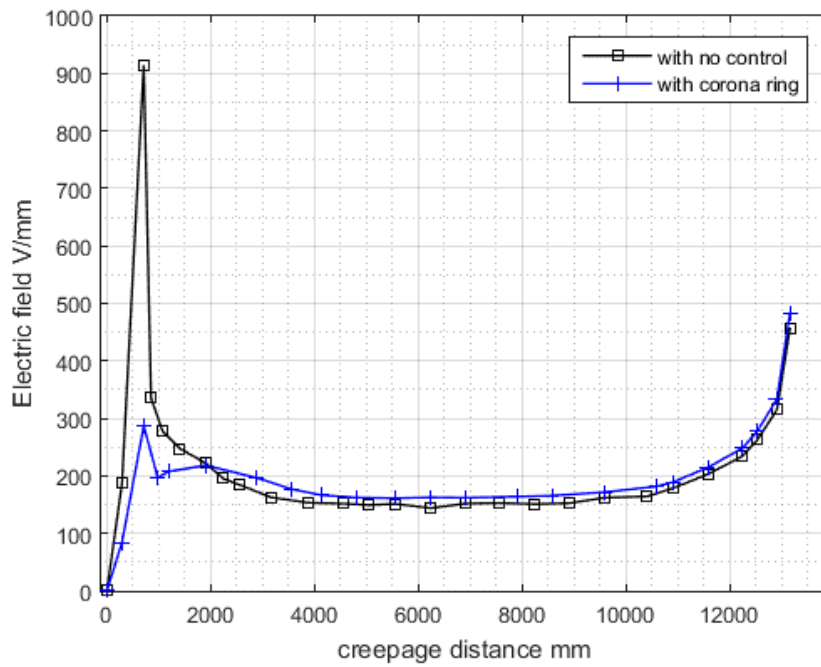


Figure 6.62. Electric field distribution along insulator's (E) surface with corona ring (Selected points)

## 6.4 Effect of using corona ring device on AC and DC electric fields

To demonstrate the effect of corona ring device on DC stressed insulators as compared to the AC's, fifteen unit of porcelain insulator (A) was tested under AC voltage with and without control, and compared to the results in case of DC voltage. The electric field was taken from PATH 2 considered earlier. The results in Figure 6.63 clearly shows the different between DC and AC electric fields. Where the DC electric field appears to have higher values near the HV end as compared to the AC. After introducing the electric field control device, Figure 6.64 shows the percentage improvement in the electric field profile. The bar chart comparison shows that when controlling the electric field under DC, the percentage reduction has reached 27%, while under AC it reached around 20%. This is a clear indication that DC electric field can be controlled just as good as or even better than AC.

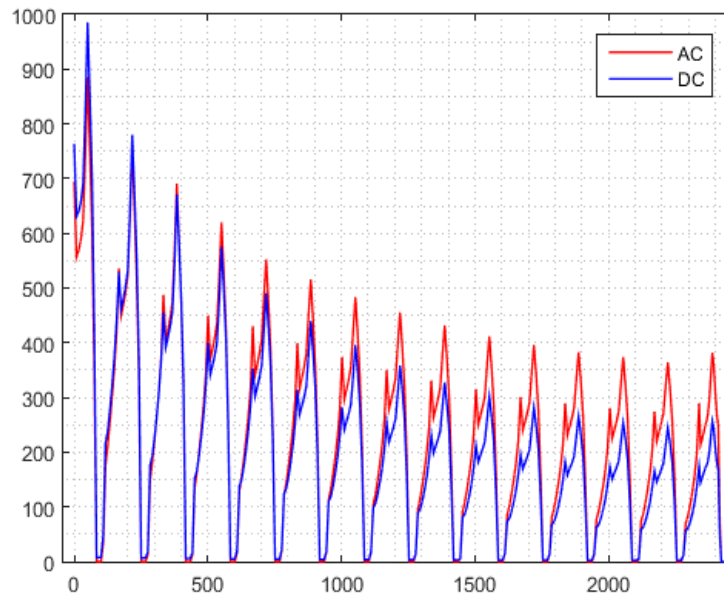


Figure 6.63. AC and DC electric field comparison along PATH 2

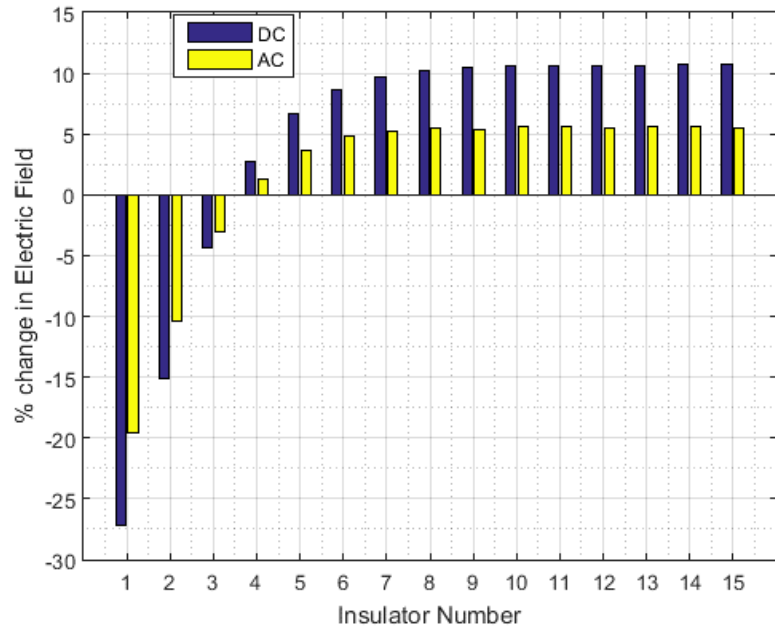


Figure 6.64. Percentage change comparison between AC and DC electric fields in the presence of corona ring

# CHAPTER SEVEN

## CONCLUSIONS AND RECOMMENDATIONS

### 7.1 Conclusions

To the best knowledge of the investigator, this is the first reported work that evaluates the electric field and voltage profiles of different HVDC insulators namely Porcelain, Glass and SiR, under clean and contaminated conditions when using electric field control devices. The electric field and voltage distributions around these insulators are quantified using FEM. The dimensions of the electric field control devices were optimized using the MATLAB<sup>TM</sup> tool (PSO) to minimize the maximum electric field around those insulators. Thus, the main Thesis's findings can be summarized as follows:

- A comprehensive literature review has been accomplished on contaminated HVDC insulators problem, covering both experimental and simulation work.
- Six different types of insulators have been investigated, including; porcelain, glass and four types of SiR insulators.
- For all the aforementioned insulators, electric field and voltage distribution have been quantified using the FEM technique in ANSYS<sup>TM</sup> software stressed by DC voltage, under clean and contaminated conditions.
- Comparison of a single unit of porcelain insulator stressed by AC and DC voltages, shows that DC electric field is higher than the AC field, confirming what has been reported in the literature.

- On a single unit of insulator (A) and insulator (C), the effect of three different pollution scenarios have been studied, namely water droplets, non-uniform pollution and combined water droplets and pollution. The results revealed that both insulators were severely affected by the combined contamination followed by the case of non-uniform pollution, and non-uniform water droplets.
- In the case of fifteen units string (insulators (A) and (B)), the most affected region by the contamination was found to be at the pollution junction, with maximum electric field percentage increase of 170% and 183% respectively.
- Under contaminated fifteen unit string of insulators A and B, Arc horn and corona ring control devices were tested. The Arc horn device has shown a lower electric field profiles, more uniform voltage profiles and higher string efficiencies as compared to the corona ring's.
- For SiR insulators (D) and (E), they were subjected to a heavy contamination layer near the HV end which has result in an increase of the maximum electric field of 59% and 40.38% respectively.
- For contaminated SiR insulator (D), extensive analysis has been made in order to find the optimal control device configuration. Five different control configurations were investigated. The results reveal that double Arc Horns configuration provides the lowest electric field profile with reduction of 71.49% and 79.87% in the HV and LV ends respectively, as compared to the other investigated configurations.
- Finally, the results show that the electric field control device (corona ring) has performed even better under DC stress as compared to AC, which indicates the high potential of using HVDC.

## 7.2 Future work

The problem of HVDC contaminated insulators is far from being completed by only relying on limited numbers of case studies and software packages. Thus, in order to comprehensively study the problem, the following aspects may be addressed as well:

- Building a complete 3-D model of HVDC insulators is necessary to completely include the effect of the ground tower, the ground, the line itself, non- uniform contamination, 3-d water droplets.
- More software packages should be used to implement the same problem such as (MAXWELL-3D<sup>TM</sup>, COLOMB<sup>TM</sup> and OPERA-3D<sup>TM</sup>) and choosing the most suitable ones.
- Regarding the optimization process, different optimization techniques could be also used for the same problem, the best technique should be chosen based on the speed of convergence and optimal solution results.
- Experimental setups can be done by referring to the part in the literature review, to confirm the software and the experimental results.
- The effect of space charge on the electric field and voltage profiles can be investigated.

## References

- [1] L. Maraaba, Z. Al-Hamouz and H. Al-Duwaish, "Prediction of the Levels of Contamination of HV Insulators Using Image Linear Algebraic Features and Neural Networks," *Arabian Journal for Science and Engineering*, vol. 40, no. 9, pp. 2609-2617, 2015.
- [2] A. Z. El Dein, "Optimal arrangement of Egyptian overhead transmission lines' conductors using genetic algorithm," *Arabian Journal for Science and Engineering*, vol. 39, no. 2, pp. 1049-1059, 2014.
- [3] B. Marungsri, W. Onchantuek, A. Oonsivilai and T. Kulworawanichpong, "Analysis of electric field and potential distributions along surface of silicone rubber insulators under various contamination conditions using finite element method," *World Academy of Science, Engineering and Technology*, pp. 1353-1363, 27 May 2009.
- [4] W. L. Vosloo and J. P. Holtzhausen, "The electric field of polluted insulators," in *6th Africon Conference, Africa*, 2002.
- [5] R. Boudissa, A. Bayadi and R. Baersch, "Effect of pollution distribution class on insulators flashover under AC voltage," *Electric Power Systems Research*, vol. 10, no. 4, pp. 176-182, 2013.
- [6] Z. Aydogmus, "A neural network-based estimation of electric fields along high voltage insulators," *Expert Systems with Applications*, vol. 36, no. 4, pp. 8705-8710, 2009.
- [7] A. Hassanvand, H. Illias and H. Mokhlis, "Effects of corona ring dimensions on the electric field distribution on 132 kV glass insulator," in *Power Engineering and Optimization Conference, Malaysia*, 2014.
- [8] D. Azizi, A. Gholami and A. Siadatan, "Corona Ring Optimization for Different Cases of Polymer Insulators Based on its Size and Distance," *Journal of Artificial Intelligence in Electrical Engineering*, vol. 1, no. 2, pp. 1-7, 2012.
- [9] M. Natarajan, V. Basharan, K. G. Pillai, M. R. Velayutham and W. I. M. Silluvairaj, "Analysis of Stress Control on 33-kV Non-ceramic Insulators Using Finite-element Method," *Electric Power Components and Systems*, vol. 43, no. 5, pp. 566-577, 2015.

- [10] H. Wang and M. A. Redfern, "The advantages and disadvantages of using HVDC to interconnect AC networks," in Universities Power Engineering Conference, United Kingdom, 2010.
- [11] A. Al-Arainy, M. Qureshi and N. Malik, Fundamentals of High Voltage Engineering, Riyadh, Saudi Arabia: King Saud University Press, 2005.
- [12] A. Al-Arainy, N. Malik and S. AL-Guhwainem, Fundamentals of Electrical Power Engineering, Riyadh, Saudi Arabia: King Saud University Press, 2005.
- [13] EEP, "Electrical Engineering Portal," [Online]. Available: <http://electrical-engineering-portal.com/ceramic-porcelain-and-glass-insulators>. [Accessed 13 12 2015].
- [14] taocijueyuanzi, [Online]. Available: <http://www.taocijueyuanzi.com/dgvrdrh/xgfdtrh/index.html>. [Accessed 13 12 2015].
- [15] "hivoltinsulators," Dalian Hivolt Power System Co.,Ltd, [Online]. Available: [http://www.hivoltinsulators.com/Products/Composite\\_Insulator/2012/1012/Dead%20End%20composite%20insulator.html](http://www.hivoltinsulators.com/Products/Composite_Insulator/2012/1012/Dead%20End%20composite%20insulator.html). [Accessed 21 12 2015].
- [16] L. Qisheng, W. Lai, S. Zhiyi, L. Yansheng, K. Morita, R. Matsuoka and S. Ito, "Natural contamination test results of various insulators under DC voltage in an inland area in China," in Properties and Applications of Dielectric Materials, china, 1991.
- [17] K. Ishikawa, H. Kageyama, Y. Yamada, R. Matsuoka, S. Ito and K. Sakanishi, "Investigation of single unit flashovers in HVDC insulator strings," Power Delivery, IEEE Transactions, vol. 11, no. 4, pp. 1888-1894, 1996.
- [18] A. Karn, S. Potivejkul, N. Pattanadech and P. Yutthagowith, "Behavior comparison of corona inception and flashover voltage between HVAC and HVDC insulator," in Power Engineering Conference, IPEC , 2005.
- [19] J. M. Seifert, W. Petrusch and H. Janssen, "A comparison of the pollution performance of long rod and disc type HVDC insulators," IEEE Trans. Dielectr., vol. 14, no. 1, pp. 125-129, 2007.

- [20] X. Jiang, J. Yuan, L. Shu, Z. Zhang, J. Hu and F. Mao, "Comparison of DC pollution flashover performances of various types of porcelain, glass, and composite insulators," *IEEE Trans. Dielectr.*, vol. 23, no. 2, pp. 1183-1190, 2008.
- [21] V. Muralidhara, B. Ramachandra, N. Vasudev, P. V. Nambudiri and K. N. Ravi, "Study of Thermal-runaway tests on Insulators subjected to DC voltages," in *High Voltage Engineering and Application, ICHVE*, Chongqing, China., 2008.
- [22] Z. Zhang, X. Jiang, Y. Chao, L. Chen, C. Sun and J. Hu, "Study on DC pollution flashover performance of various types of long string insulators under low atmospheric pressure conditions," *Power Delivery, IEEE Transactions*, vol. 25, no. 4, pp. 2132-2142, 2010.
- [23] G. Heger, H. J. Vermeulen, J. P. Holtzhausen and W. L. Vosloo, "A comparative study of insulator materials exposed to high voltage AC and DC surface discharges," *IEEE Trans. Dielectr.*, vol. 17, no. 2, pp. 513-520, 2012.
- [24] I. J. Seo, J. Y. Koo, J. K. Seong, B. W. Lee, Y. J. Jeon and C. H. Lee, "Experimental investigation on the DC breakdown of silicone Polymer composites employable to 500kV HVDC insulator," in *Electric Power Equipment-Switching Technology (ICEPE-ST)*, china, 2011.
- [25] J. Y. Heo, H. G. Cho and L. Y. Soon, "A comparison of AC and DC surface discharges characteristics for silicone rubber," in *Condition Monitoring and Diagnosis (CMD)*, Bali, Indonesia, 2012.
- [26] L. Yang, Y. Hao, L. Li and Y. Zhao, "Comparison of pollution flashover performance of porcelain long rod, disc type, and composite UHVDC insulators at high altitudes," *IEEE Trans. Dielectr.*, vol. 19, no. 3, pp. 1053-1059, 2012.
- [27] A. Abbasi, A. Shayegani and K. Niayesh, "Pollution performance of HVDC SiR insulators at extra heavy pollution conditions," *IEEE Trans. Dielectr.*, vol. 21, no. 2, pp. 721-728, 2014.
- [28] A. Abbasi, A. Shayegani and K. Niayesh, "Contribution of Design Parameters of SiR Insulators to Their DC Pollution Flashover Performance," *Power Delivery, IEEE Transactions*, vol. 29, no. 4, pp. 1814-1821, 2014.
- [29] Z. Zhang, D. Zhang, J. You, J. Zhao, X. Jiang and J. Hu, "Study on the DC Flashover Performance of Various Types of Insulators With Fan-Shaped

- Nonuniform Pollution," *Power Delivery, IEEE Transactions*, vol. 30, no. 4, pp. 1871-1879, 2015.
- [30] R. Sundararajan and R. S. Gorur, "Effect of insulator profiles on dc flashover voltage under polluted conditions," *IEEE Trans. Dielectr.*, vol. 1, no. 1, pp. 124-132, 1994.
- [31] R. Sundararajan and R. S. Gorur, "Dynamic arc modeling of pollution flashover of insulators under dc voltage," *Electrical Insulation, IEEE Transactions*, vol. 28, no. 2, pp. 209-218, 1993.
- [32] Y. Xiuke, L. Yanbing, Y. Cunzhan, W. Jiaxun and L. Liyang, "Numerical calculation of electric field and potential distribution for HVDC insulator," in *Power and Energy Engineering Conference, Asia-Pacific*, 2012.
- [33] Y. Xiuke, Y. Liming, Y. Cunzhan, L. Yuepeng, Y. Tiejun, Z. Yidong and W. Jiayin, "Electric-field analysis for HVDC insulators considering space charge," in *Electrical Machines and Systems (ICEMS)*, Busan, Korea, 2013.
- [34] P. H. Pretorius, A. C. G. Britten, T., N. Mahatho, N. Parus and J. P. Reynders, "Electric field modelling of HVDC glass insulators preliminary findings from insulation strength studies," in *Power Engineering Society Conference and Exposition, Africa*, 2012.
- [35] R. Kumar and R. S. Gorayan, "Electric field around HVDC insulator string for various contamination levels," in *National Power Systems Conference IIT(BHU)*, Varanasi, 2012.
- [36] J. He and R. Gorur, "Charge simulation based electric field analysis of composite insulators for HVDC lines," *IEEE Trans. Dielectr. Electr. Insul*, vol. 21, no. 6, pp. 2541-2548, 2014.
- [37] W. H. Hayt, *Engineering Electromagnetics*, New York: McGraw Hill, 2006.
- [38] P. Kohnke, *ANSYS mechanical APDL theory reference*, 2012.
- [39] C. Kim, J. Jang, X. Huang, P. Jiang and H. Kim, "Finite element analysis of electric field distribution in water treed XLPE cable insulation (1): The influence of geometrical configuration of water electrode for accelerated water treeing test," *Polymer testing*, vol. 26, no. 4, pp. 482-488, 2007.

- [40] R. P. Canale and S. C. Chapra, Numerical methods for engineers, New York: Mc Graw Hill, 1998.
- [41] J. Kennedy and R. Eberhart, "Particle swarm optimization," in IEEE International Conference on Neural Networks, Perth, WA, 1995.
- [42] D. P. Rini, S. M. Shamsuddin and S. S. Yuhaniz, "Particle swarm optimization: technique, system and challenges," International Journal of Computer Applications, vol. 14, no. 1, pp. 19-26, 2011.
- [43] Q. Bai, "Analysis of particle swarm optimization algorithm," Computer and information science , vol. 3, no. 1, pp. 180-184, 2010.
- [44] L. Maraaba, Image processing based contamination level monitorings oh HV insulators, Dahrn: King Fahad University for Petroleum and Minerals, 2013.
- [45] "Hubbell Power Systems, INC," hubbell power systems, [Online]. Available: <http://www.hubbellpowersystems.com/insulators/sub/deadends/quadrisil/corona.asp>. [Accessed 12 5 2015].

# APPENDIX

## A.1 Insulator (A) Contours

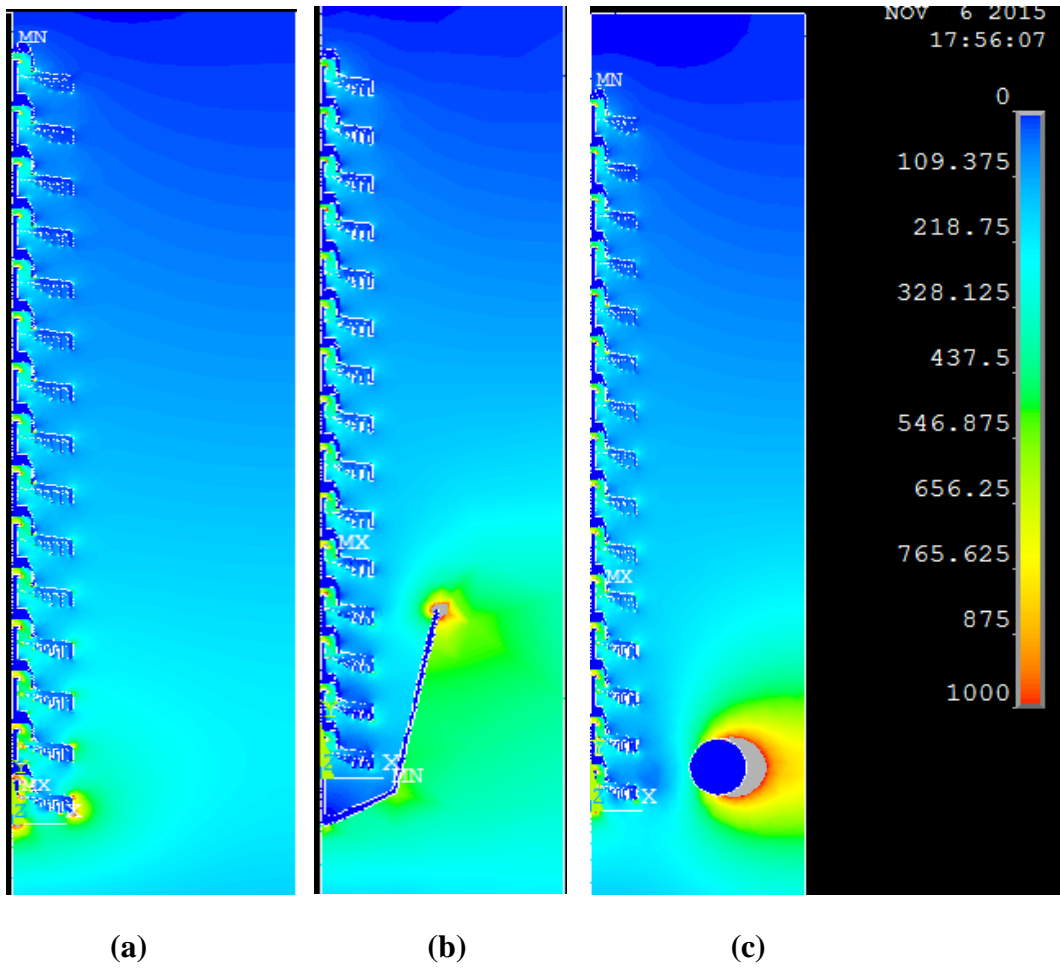
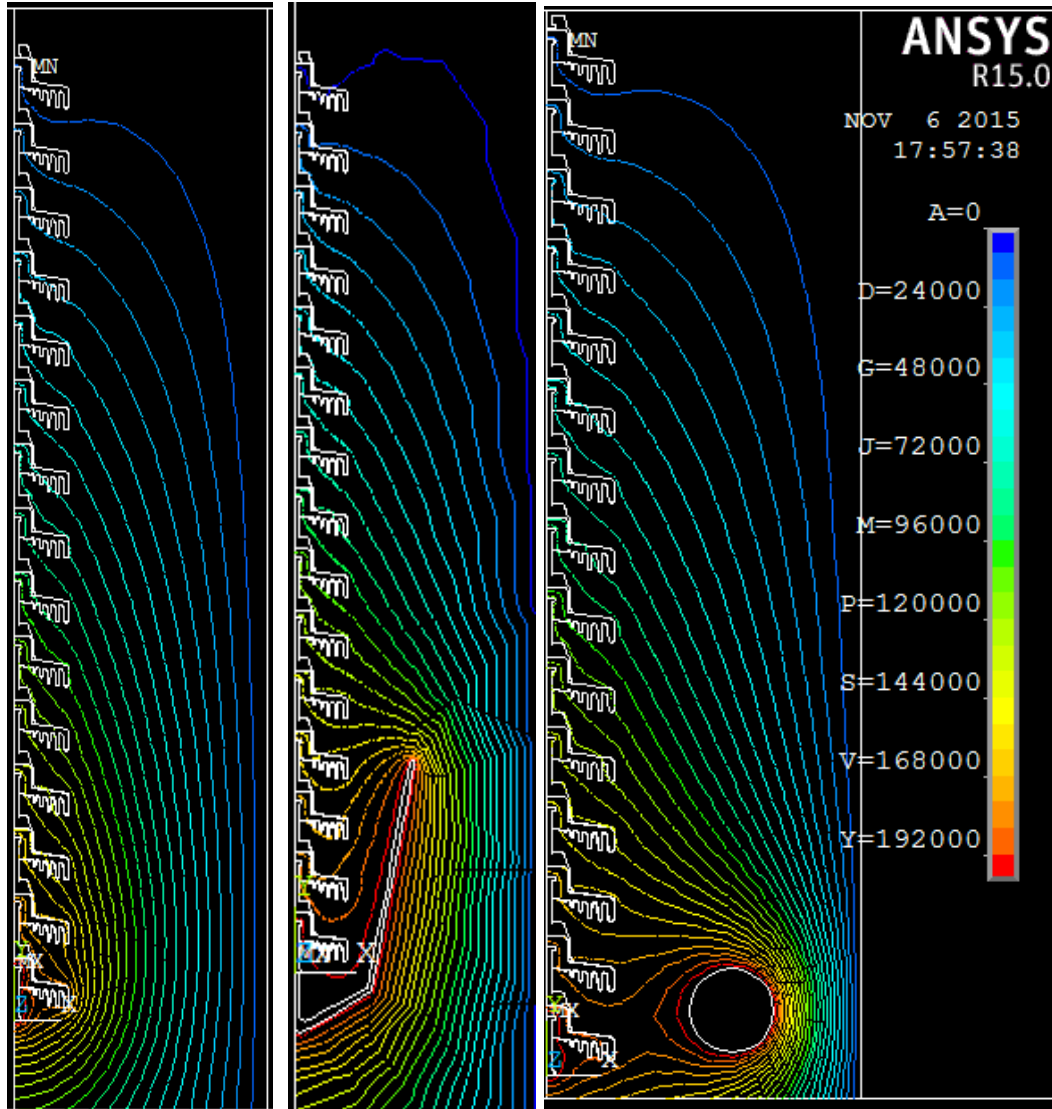


Figure A. 1. Insulator (A- 15 units) Electric field contours; a) without control, b) with Arc horn, c) with corona ring



(a)

(b)

(c)

Figure A. 2. Insulator (A- 15 units) Voltage contours; a) without control, b) with Arc horn, c) with corona ring

## A.2 Insulator (B) Contours

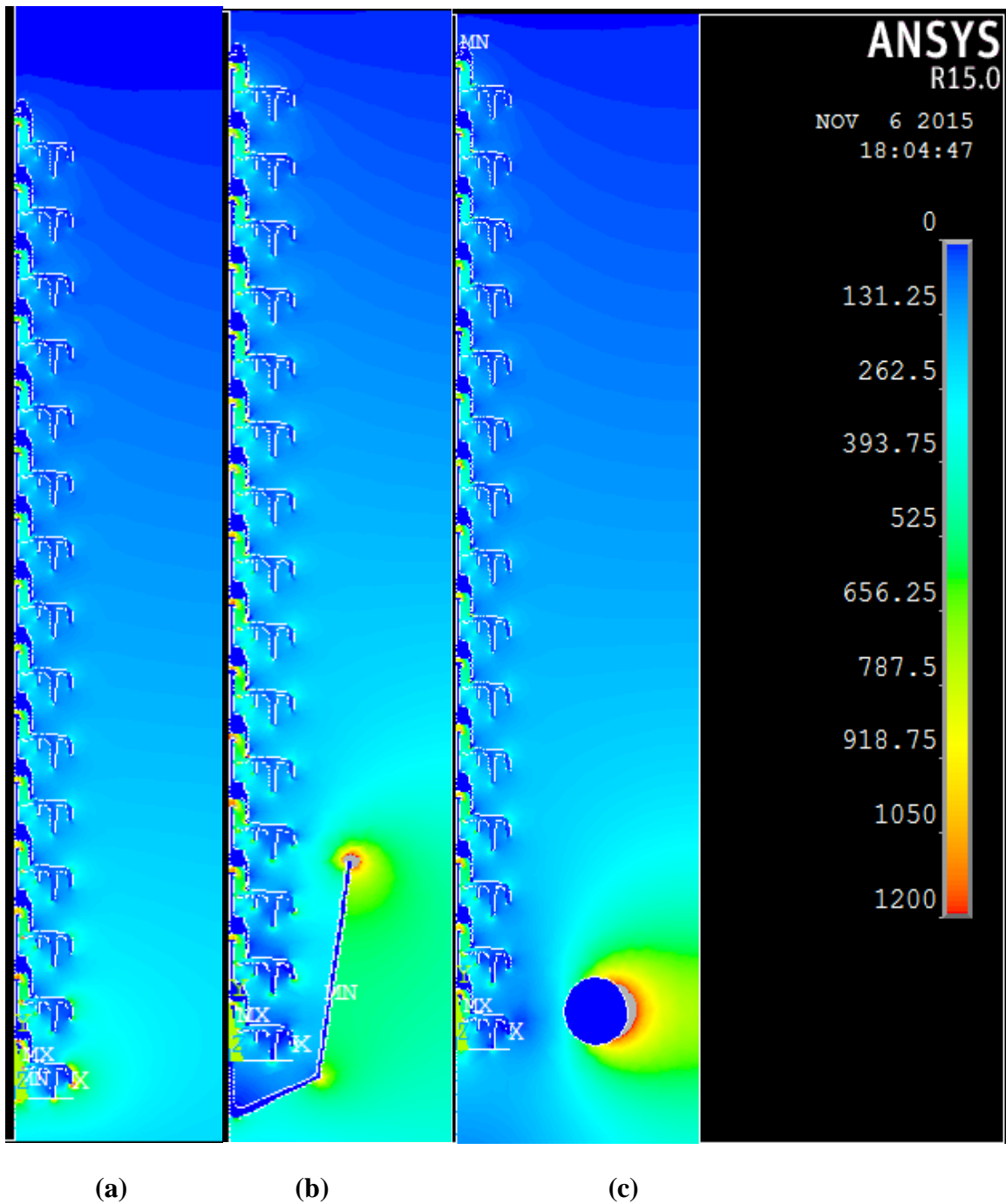


Figure A. 3. Insulator (B- 15 units) Electric field contours; a) without control, b) with Arc horn, c) with corona ring

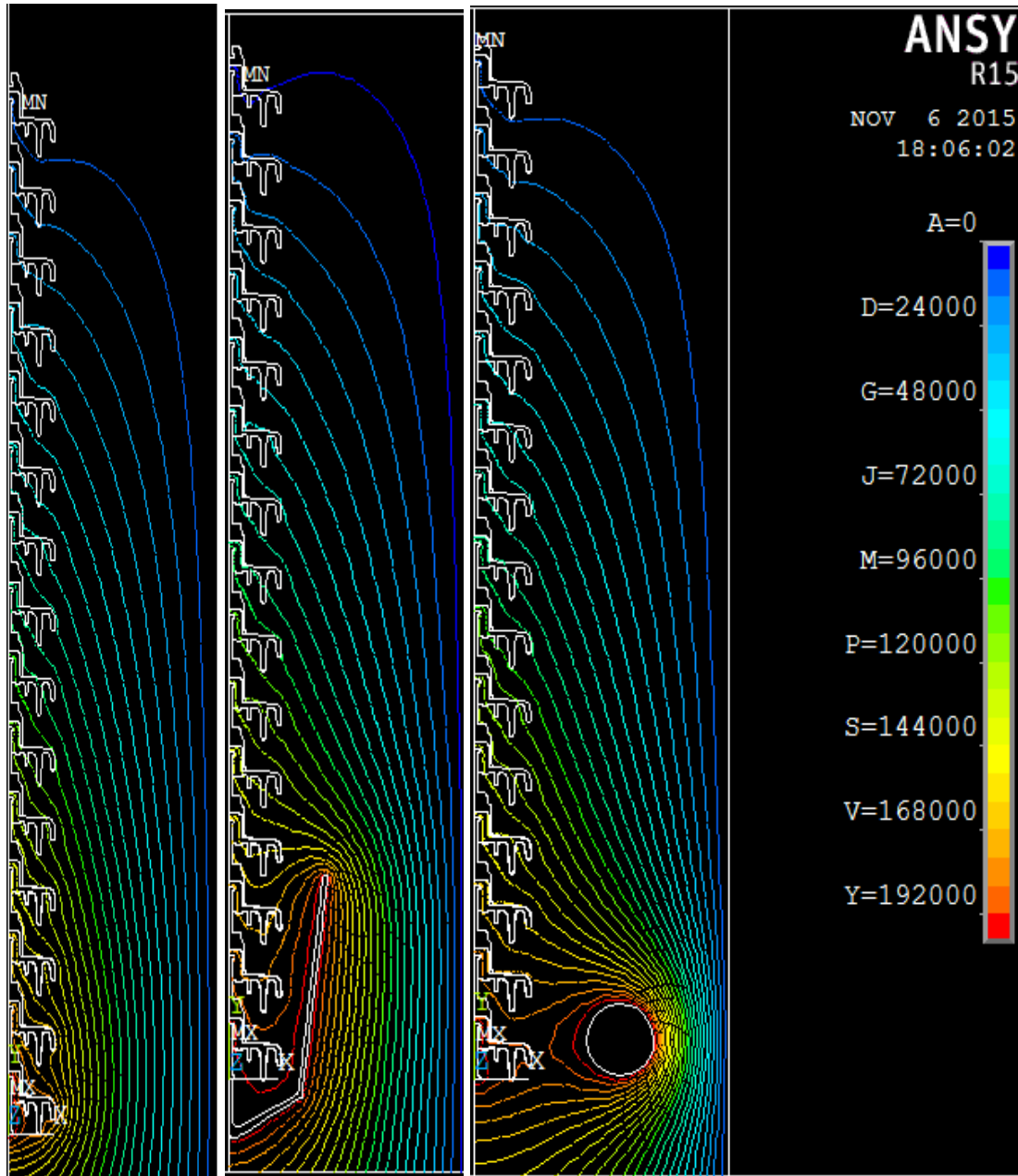


Figure A. 4. Insulator (B- 15 units) Voltage contours; a) without control, b) with corona ring

### A.3 Insulators (E) Contours

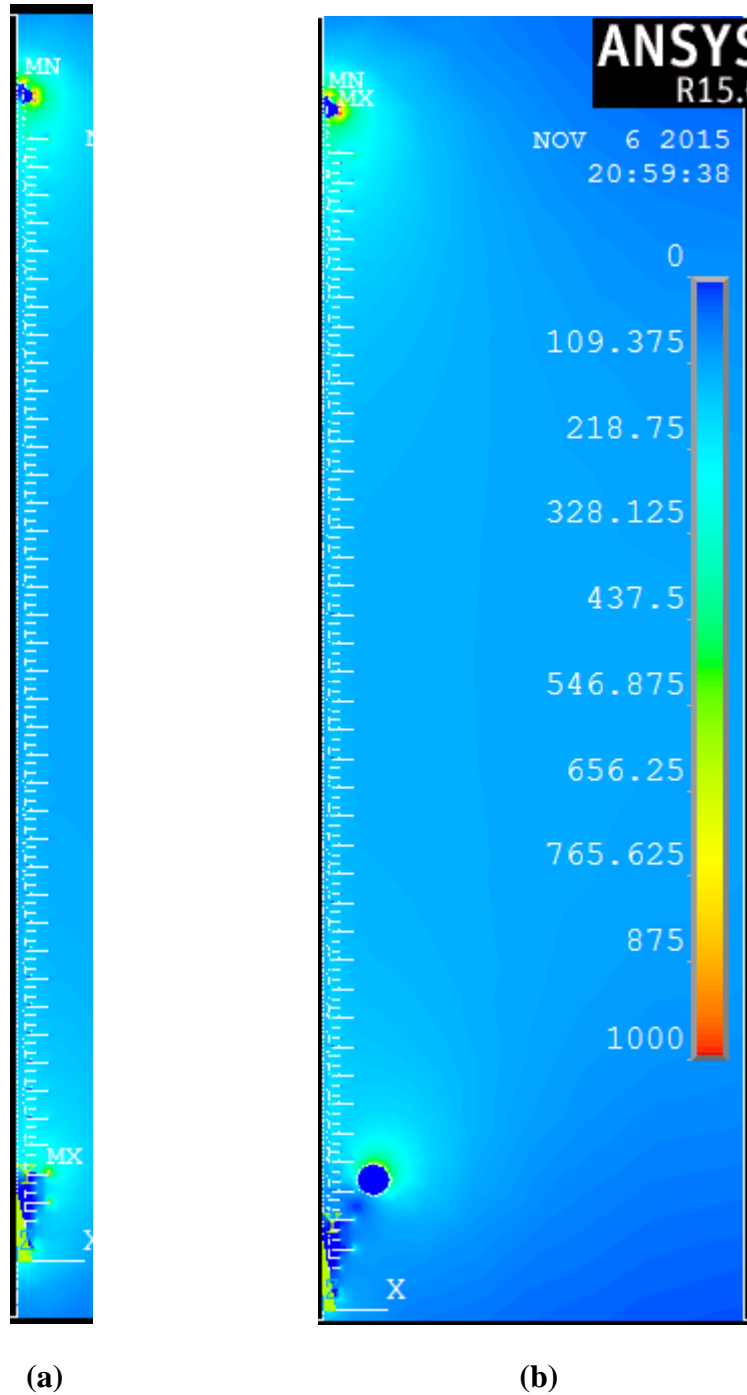
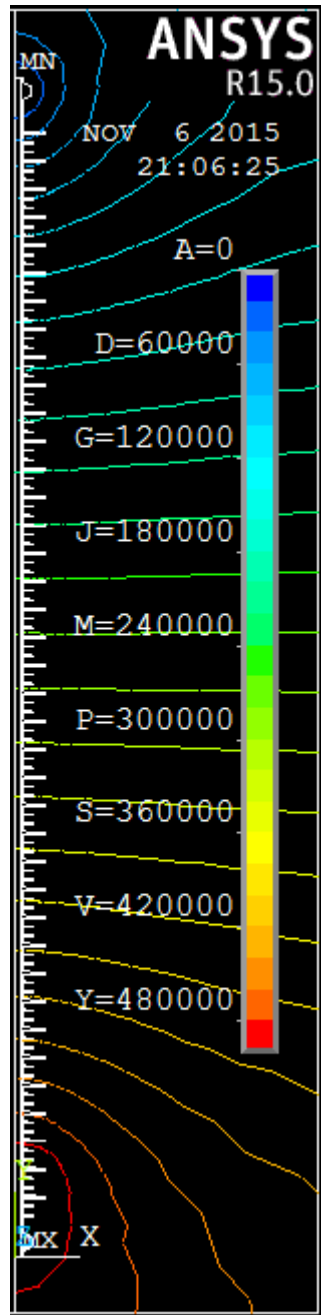
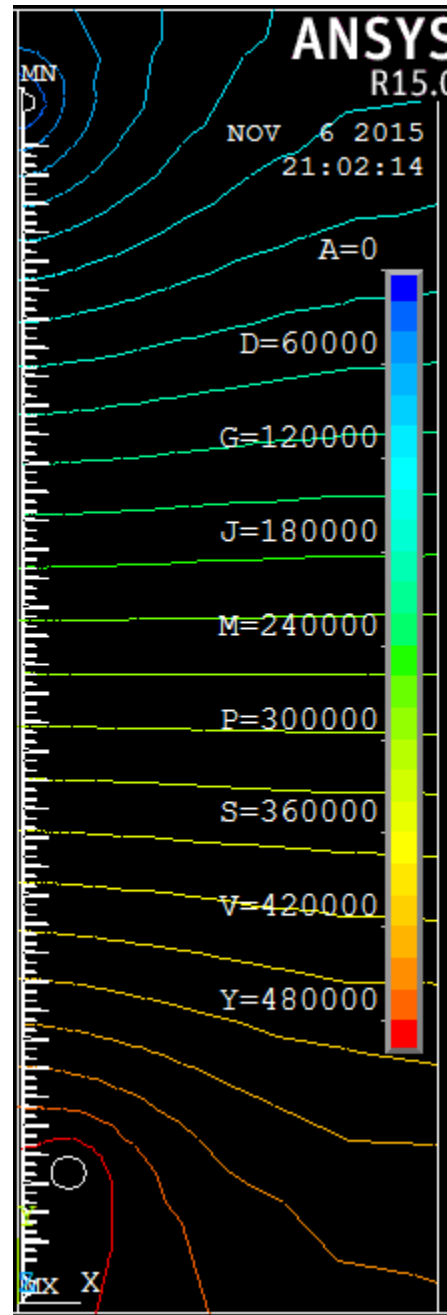


Figure A. 5. Insulator (E) Electric field contours; a) without control, b) with corona ring



(a)



(b)

Figure A. 6. Insulator (E) Voltage contours; a) without control, b) with corona ring

## VITAE

Name : TAISIR HUSAM TUFFAHA

Nationality : JORDANIAN

Date of Birth : 12/24/1990

Email : abu\_husam90@hotmail.com

Address : Saudi Arabia – Riyadh - Solymania

Academic Background : Bachelor Degree in Electrical Power Engineering from King Saud University with first honor, Saudi Arabia in 2013.

Working Experience : Worked as a researcher in Saudi Aramco chair of Research at King Saud University 2014. I was involved in renewable energy research and published the following journal paper:

- Tuffaha, T. H., et al. "Comparative Study of Different Hill Climbing MPPT through Simulation and Experimental Test Bed." *Research Journal of Applied Sciences, Engineering and Technology* 20.7 (2014): 4258.

Then I worked as a research assistant at King Fahad University for Petroleum and Minerals in electrical engineering department until august 2015. I was involved in lab teaching activities beside other administration work.

Workshops : I have provided MATLAB™ workshops in advanced levels, as a part of my duties in IEEE KFUPM branch .